

COPENHAGEN UNIVERSITY

PHD THESIS

**Aspects of Majorana Bound States  
in One-Dimensional Systems  
with and without  
Time-Reversal Symmetry.**

*Konrad Wölms*

supervised by  
Karsten Flensberg

August 31, 2015



# Contents

<b>1</b>	<b>Introduction</b>	<b>7</b>
<b>2</b>	<b>Background</b>	<b>9</b>
2.1	Topological Phases of Matter . . . . .	9
2.2	Topological Quantum Computation . . . . .	10
2.2.1	Gates in Classical and Quantum Computing . . . . .	11
2.2.2	Braiding and a Finite Set of Gates . . . . .	12
2.3	Majorana Bound States . . . . .	13
2.3.1	Kitaev Chain . . . . .	13
2.3.2	Time-Reversal-Invariant Kitaev Chain . . . . .	16
2.4	Bosonization and Luttinger Liquids . . . . .	18
2.4.1	Translation into Bosons . . . . .	21
2.4.2	Klein Factors and Spin and Charge Sectors . . . . .	26
2.5	Renormalization Group Theory . . . . .	27
2.5.1	The Renormalization Group Idea, Phase Transitions and Fixed Points . . . . .	27
2.5.2	Scaling Operators and Scaling Dimension . . . . .	28
2.5.3	Continuous Renormalization and Flow Equations . . . . .	29
<b>3</b>	<b>Braiding in Class DIII</b>	<b>31</b>
3.1	Time-Reversal Symmetry and Majorana Fermion Operators . . . . .	31
3.2	The Adiabatic Theorem and Berry Phases . . . . .	33
3.3	Relation between Fock Space States and Operators . . . . .	36
3.3.1	Connection to BdG States . . . . .	39
3.4	Local Mixing . . . . .	41
3.4.1	Analytical Toy Model . . . . .	41
3.4.2	Numerical Demonstration of Local Mixing . . . . .	44
3.4.3	Sufficient Conditions for the Absence of Local Mixing . . . . .	48
3.5	Braiding of Kramers pairs of Majorana Bound States . . . . .	52
3.5.1	Toy Model . . . . .	55
3.5.2	Numerical Simulation . . . . .	59
3.6	Summary . . . . .	61
<b>4</b>	<b>Topologically Non-Trivial DIII Phase Through Interactions</b>	<b>63</b>
4.1	Fixed-Point System and Perturbations . . . . .	63

4.2	Superconducting Pairing and Interactions . . . . .	68
4.2.1	Systems with Initial Triplet Pairing . . . . .	70
4.3	Operator Product Expansion and Flow Equations . . . . .	72
4.3.1	Symmetry of the OPE Coefficients . . . . .	75
4.3.2	Combining Flow Equations for Different Fixed Points . . . . .	76
4.4	Flow Equations and their Solutions . . . . .	77
4.4.1	Flow Equations Close to $K_s = K_c = 1$ . . . . .	78
4.4.2	General Flow Equations . . . . .	82
4.5	Summary . . . . .	83
4.A	Conformal Spin . . . . .	83
<b>5</b>	<b>Environmental Coulomb Blockade</b>	<b>87</b>
5.1	Superconductor-Luttinger Liquid Junction . . . . .	87
5.1.1	Normal-Reflection Fixed Point . . . . .	89
5.1.2	Andreev-Reflection Fixed Point . . . . .	91
5.2	Coupling to an Electric Environment . . . . .	92
5.2.1	Normal-Reflection Fixed Point . . . . .	96
5.2.2	Andreev-Reflection Fixed Point . . . . .	96
5.3	Special Environments . . . . .	96
5.3.1	Metallic Dot with a Quantum Point Contact Drain . . . . .	97
5.3.2	Two Majorana Bound States Coupled via a Metallic Dot . . . . .	99
5.4	Summary . . . . .	102
<b>6</b>	<b>Conclusion</b>	<b>105</b>

### **Acknowledgements**

I would like to thank my supervisor Karsten Felsberg, my collaborators Ady Stern, Erez Berg, Yuval Oreg and Arbel Haim, and my colleagues Erikas Gaidamauskas, Gediminas Krišankas, Kim Lind Pedersen and Samuel Sánchez for many helpful discussions. Furthermore I would like to thank my friends Samuel Sánchez and Jörg Behrmann for their help in proofreading this thesis.



# 1 Introduction

In recent years there has been a lot of interest in topological phases of matter. Unlike conventional phases of matter, topological phases are not distinguished by symmetries, but by so-called topological invariants which have more subtle physical implications. It comes therefore as no surprise that for a long time only a few topological phases were studied and those that were, were not studied in the full topological context, which is only known now. One of the topological phases that has been known for a very long time is the quantum Hall effect. The quantum Hall effect is a topological phase in two-dimensions without any symmetries. Even though the bulk of a quantum Hall system is insulating, it exhibits gapless edge modes. It is therefore different from other insulating two-dimensional materials. It was soon realized after the discovery of the quantum Hall effect, that there is a quantized invariant (topological invariant) associated with the quantum Hall effect [48], but only much later such invariants were found and studied in other systems.

By now other topological systems are also being studied from an experimental and theoretical point of view [7]. There exist topological phases in any number of dimensions. One of the topological phases that received a lot of attention in recent years, is the one-dimensional topological superconducting phase, without time-reversal symmetry [5]. Similar to the quantum Hall effect, this phase exhibits edge excitations, which are zero-dimensional for one-dimensional systems. For this particular phase the edge excitations are called Majorana bound states and they are interesting in themselves. There has been a lot of effort in detecting Majorana bound states in the lab. One reason is that these excitations provide evidence that a system is indeed in a topological phase. It is therefore required to have unambiguous experimental evidence for the presence Majorana bound states, which in turn requires a good theoretical understanding of the physics associated with Majorana bound states. In particular for the most common experimental methods that are used to study them, the signature of Majorana bound states in the measurement still has to be understood better. An example would be the frequently performed tunnel probe measurement on Majorana bound states [26, 40, 41]. A second reason why Majorana bound states are interesting is their potential application to a certain quantum computation scheme. This scheme, called topological quantum computation, relies on the braiding of so-called non-abelian anyons in order to perform computations [18]. Majorana bound states are the simplest example of such non-abelian anyons. No other non-abelian anyons have been realized experimentally yet, which puts further focus on the study of Majorana bound states. Additionally to probing Majorana bound states, their use in topological quantum computation also requires them to be manipulated. This also poses an interesting problem for both experimentalists and theorists [25, 27].

We can summarize the challenges presented so far as being related to generating a topological phase, probing Majorana bound states and manipulating them. These challenges are actually important beyond the intensively studied topological phase of one-dimensional superconducting systems without time-reversal symmetry. In particular they are very important for the closely related phase of one-dimensional topological superconductors with time-reversal symmetry. This phase also exhibits Majorana bound states, and we will study some of its aspects in this thesis. We will discuss some issues related to obtaining this topological phase and how electron-electron interactions may help in achieving this. We will also discuss issues related to using this phase and its edge states for topological quantum computation, by calculating the result of an exchange of two such edge states. Finally we will return to the broken time-reversal-symmetry case and discuss aspects related to tunnel probing Majorana bound states.

## 2 Background

In this chapter we introduce the background needed for understanding this thesis. We will point out for which of the following chapters the specific theories are relevant. Most of the background is either general to Majorana bound states or relevant to several of the following chapters.

We begin by introducing the concept of topological phases of matter and we state some of the existing classification for these phases. In particular we will introduce the classes that we will focus on. These will be the ones that exhibit phases with Majorana bound states. Afterwards we will introduce the key ideas of topological quantum computation. Specifically its primary idea and how it is related to Majorana bound states. This will be important for chapter 3 where we study whether braiding of Kramers pairs of Majorana bound states is suited for topological quantum computation. Thereafter we will introduce more concrete models for systems that exhibit Majorana bound states. In that context we will emphasize the most important properties of Majorana bound states, which will be needed for the rest of this thesis. Hereafter we will give a brief summary of bosonization and Luttinger liquids, which we use to study one-dimensional interacting systems. It will by no means be a complete introduction to bosonization, and we will skip some of the details in order to focus on the aspects that will be relevant for later calculations. Bosonization will be needed in chapter 4 and 5. Finally we introduce the renormalization group idea and explain how it can be used to study systems. This will again be important in chapter 4 and 5.

### 2.1 Topological Phases of Matter

For a long time it was believed that phase transitions in physics are always connected to a change of symmetry in the physical system. This idea was due to Landau and was very successful in describing phase transitions. Examples are, when a non-magnetic phase goes over into a ferromagnetic one it breaks rotational symmetry or when a liquid becomes a crystal it breaks continuous translational symmetry.

It was eventually realized that there can be phases and phase transitions that cannot be classified according to symmetries and symmetry breaking. Most of these so-called topological phases are strongly interacting and their ground states exhibit long-range entanglement. This is for instance reviewed in [49]. We will not be concerned with topological phases in their full generality, but with a subset called topological insulators and topological superconductors. Those systems are usually only weakly interacting, they have a band gap in their electronic excitation spectrum and they always belong to certain symmetry classes. Within each symmetry class there are topologically distinct phases.

There usually exist gapless excitations at the boundary between two such topological phases or at the system boundary of a topological phase to vacuum. Majorana bound states, which we will study in this thesis, are such edge excitations.

The question arises which symmetries one should consider when classifying topological insulators and superconductors. One of the first topological classifications [44] used time-reversal symmetry  $\mathcal{T}$ , particle-hole symmetry  $\mathcal{P}$  and chiral symmetry  $\mathcal{C} = \mathcal{TP}$ . Those symmetries were chosen because they are not broken by disorder. The resulting symmetry classes were previously known in the context of random matrix theory and are known as Altland-Zirnbauer classes [3]. The topological phases of each symmetry class are classified according to a mathematical group, such that each element of the group corresponds to a distinct topological phase. It was later realized by Kitaev [36] that there is a certain periodicity to the classification with respect to the dimensionality of the system. Therefore the classification is often called “the periodic table of topological insulators and superconductors”. Table 2.1 shows this periodic table up to dimensionality three. Subsequently there was and is a lot of work on classifying topological phases with respect to other symmetries, for instance the space group symmetries of crystals [45].

We will only be concerned with the original classification. Even more specifically, out of the symmetry classes from table 2.1 we are interested in the classes that have topological phases with Majorana bound states. Those are the classes BDI, D and DIII in one dimension and the classes D and DIII in two dimensions. In this thesis we focus on the one-dimensional classes, but some of the results in chapter 3 can easily be generalized to two dimensions. One-dimensional systems are sometimes referred to as wires, and we will also use this nomenclature.

In every topological class one of the topological phases is called the trivial phase. These are the ones that do not exhibit edge excitations on boundaries to the vacuum. For the one-dimensional system, which we will consider, this means that the trivial phases do not have Majorana bound states at the ends of the one-dimensional wires. Other topological phases are referred to as non-trivial. Often one also refers to topologically non-trivial phases simply as topological phases and to topologically trivial phases as non-topological phases. It has been an experimental and theoretical challenge to engineer topologically non-trivial phases from existing materials. Chapter 4 is related to this in that we will study how to get a non-trivial phase for systems of class DIII.

## 2.2 Topological Quantum Computation

In this section we will explain the main idea behind topological quantum computation. Before we can do this, we have to explain the origin of the problem which topological quantum computation tries to overcome. For this purpose we will briefly compare bits and qubits.

Class	$\mathcal{T}$	$\mathcal{P}$	$\mathcal{C}$	$d = 1$	$d = 2$	$d = 3$
A	0	0	0	0	$\mathbb{Z}$	0
AIII	0	0	1	$\mathbb{Z}$	0	$\mathbb{Z}$
AI	1	0	0	0	0	0
BDI	1	1	1	$\mathbb{Z}$	0	0
D	0	1	0	$\mathbb{Z}_2$	$\mathbb{Z}$	0
DIII	-1	1	1	$\mathbb{Z}_2$	$\mathbb{Z}_2$	$\mathbb{Z}$
AII	-1	0	0	0	$\mathbb{Z}_2$	$\mathbb{Z}_2$
CII	-1	-1	1	$\mathbb{Z}$	0	$\mathbb{Z}_2$
C	0	-1	0	0	$\mathbb{Z}$	0
CI	1	-1	1	0	0	$\mathbb{Z}$

Tab. 2.1: The table shows the topological classification of different symmetry classes [36].  $\mathcal{T}$ ,  $\mathcal{P}$  and  $\mathcal{C}$  denote time-reversal symmetry, particle-hole symmetry and chiral symmetry respectively. An entry of zero in the symmetry columns means that the symmetry is absent. For  $\mathcal{T}$  and  $\mathcal{P}$  the entries  $\pm 1$  are the square of the symmetry operator. For  $\mathcal{C}$  the entry 1 only means that chiral symmetry is present.

### 2.2.1 Gates in Classical and Quantum Computing

A classical computer is based on bits. A bit can be in one of two states, denoted by 0 or 1. When the computer operates on bits the only operations it can perform is to flip the bit from  $0 \rightarrow 1$  or from  $1 \rightarrow 0$  or not to flip the bit. Such an operation is called a gate. Whether or not to flip a bit may depend on the state of the bit itself and on the state of other bits. The only errors that can occur when working with classical bits are that a bit gets flipped that should not have been flipped, or that a bit that should have been flipped does not get flipped. These errors still have to be dealt with, but the fact that there are only a finite number of them simplifies the situation.

We now consider a quantum computer, which is made out of qubits instead of bits. Qubits are two-level quantum systems, which take states in a two-dimensional Hilbert space. This means that if we choose a basis  $|0\rangle$ ,  $|1\rangle$  for this Hilbert space, then the qubit can be in any one of the states

$$\{a|0\rangle + b|1\rangle \mid a, b \in \mathbb{C}, |a|^2 + |b|^2 = 1\}. \quad (2.1)$$

A lot of the computational power of quantum computers arises from this multitude of possible states, but there are also new problems associated with it. In order to understand these problems it is helpful to visualize the state of an individual qubit on the Bloch sphere. Every point on the sphere corresponds to a possible state of the qubit. One can see that a sphere represents the possible qubit states (2.1) as follows. First of all as long

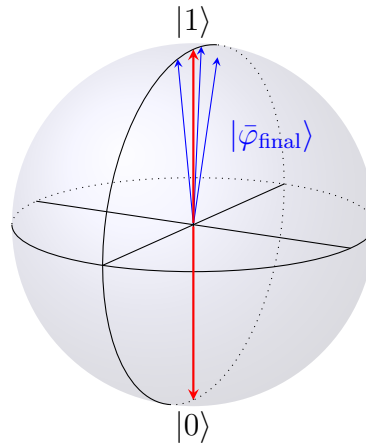


Fig. 2.1: Every point on the surface of the Bloch sphere represents a possible state of the qubit. This increases the room for error because when performing an operation which should map the initial state  $|\varphi_{\text{initial}}\rangle = |0\rangle$  onto the final state  $|\varphi_{\text{final}}\rangle = |1\rangle$  (both red) one has many states close to  $|\varphi_{\text{final}}\rangle$  where one could end up instead. The blue arrows are some examples for these erroneous final states  $|\bar{\varphi}_{\text{final}}\rangle$ .

as we only consider one qubit, its overall phase is of no physical significance. We use this freedom to always choose  $a$  to be real. The condition in (2.1) then reads

$$|a|^2 + |b|^2 = (\text{Re } a)^2 + (\text{Re } b)^2 + (\text{Im } b)^2 = 1 \quad (2.2)$$

and therefore the three real parameters  $\text{Re } a$ ,  $\text{Re } b$  and  $\text{Im } b$  lie on the surface of a sphere. This illustrates not only that the qubit can be in infinitely many states, but also that there are always states that are arbitrarily close to each other. This causes problems for gates. If we consider a gate that transform a state  $|\varphi_{\text{initial}}\rangle$  into a state  $|\varphi_{\text{final}}\rangle$ , anything that results in a different final state is an error and we end up with a final state  $|\bar{\varphi}_{\text{final}}\rangle$  in that case. Opposed to the binary case of the classical bits this does not only include our gate not doing anything, but it also includes infinitely many other errors. Even if our gate is approximately doing what it is supposed to do, there are many other states close to the final state  $|\varphi_{\text{final}}\rangle$ . Therefore a slight error or imperfection in operating the qubit can lead to an error. This is illustrated in figure 2.1. Said another way, there are infinitely many gates that can potentially be applied to a single qubit and this makes it challenging to operate a physical system such that it performs exactly the desired gate. Because even small errors can accumulate after performing several gates it is important to find ways to reduce these errors.

### 2.2.2 Braiding and a Finite Set of Gates

There has been a lot of work on how to prevent errors in quantum gate operations. One of the approaches is topological quantum computation, which was first proposed

by Kitaev [35]. The main idea is that we return from having infinitely many possible gates to having a small number of them that are well distinguished. This way a small perturbation will not change the outcome of a gate. The general mathematical details of how to achieve this are beyond the scope of this thesis, but we will sketch the general idea here and explain some problem-specific details in chapter 3.

Topological quantum computation is based on certain two-dimensional particles called anyons. In a system with a certain number of anyons, there will be a Hilbert space associated with these anyons. This will be the Hilbert space used for topological quantum computation. Qubits will be subspaces of this Hilbert space. A property of anyons is that we can perform operations on this Hilbert space and therefore on the qubits by braiding the anyons. Braiding the anyons means that we move them around each other such that initially and finally there are always anyons at the same positions, even though they may have exchanged position throughout the braiding process. This is called braiding because when visualized in (2+1) dimensions the paths of the anyons, called world lines, form braids. This is illustrated in figure 2.2. One can classify the braids according to their topology, which means according to which braids can be continuously deformed into each other. An example of topologically equivalent braids is given in figure 2.2 b). The most important property of braiding is that the transformation on the Hilbert space only depends on the topology of the braids and not on the details of the path. This means that there is only one gate per braid. This may still leave us with infinitely many gates, but one can show that all braids can be generated from a relatively small subset. The braids in themselves are inherently robust to small perturbations, because if the braiding path is only altered locally the topology of the braid does not change. This is illustrated in figure 2.2 b).

In chapter 3 we will study whether Kramers pairs of Majorana bound states can be used as anyons and therefore for topological quantum computation. In order to answer this question we will investigate the requirements listed here, namely whether there is a finite set of transformations that only depend on the braiding topology and not on the braiding path.

## 2.3 Majorana Bound States

We will now review the most important properties of Majorana bound states in the context of simple toy models. We start by describing the Kitaev chain [34], which is the simplest model with Majorana bound states.

### 2.3.1 Kitaev Chain

The Kitaev chain is the simplest example of a topological system in class D. It consists of a one-dimensional chain of spinless fermions. Later we will discuss the generalization to the time-reversal invariant case, for which spin will be important. Therefore we will

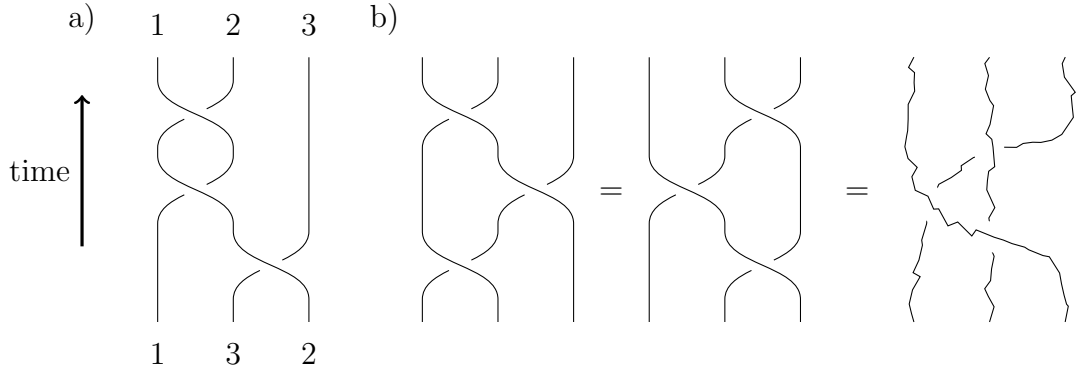


Fig. 2.2: In (a) the general idea behind braiding of anyons is illustrated. The numbers represent the different anyons. The anyons change positions as a function of time in such a way that they eventually return to the initial positions, but not necessarily to their own ones. In (b) the equivalence of braids is illustrated. This results in an inherent robustness against perturbations because even the perturbed paths on the right still form the same braid topologically. (Note that the disordered component in the time direction is not physical and is only in the picture for illustrative purposes).

start with a spin-polarized chain instead of a spinless one. The Hamiltonian of the Kitaev chain is

$$H = \sum_i t(c_{i\uparrow}^\dagger c_{i+1\uparrow} + \text{h.c.}) + \mu c_{i\uparrow}^\dagger c_{i\uparrow} + \Delta(c_{i\uparrow}^\dagger c_{i+1\uparrow}^\dagger + \text{h.c.}). \quad (2.3)$$

The special feature of this Hamiltonian that makes it hard to realize in practice is the superconducting pairing, which is of p-wave type.

There is a special point in parameter space for the Hamiltonian (2.3). This point is  $\mu = 0$ ,  $t = \Delta$ . It is of particular interest because it exhibits most clearly the Majorana bound states as edge excitations, as we will review shortly. Because of that it is a good starting point for constructing other toy models based on the Kitaev chain.

In order to see why there is something special about the mentioned point in parameter space, one should write the Hamiltonian in terms of Majorana fermions. At this point this is a purely mathematical decomposition, because every fermionic operator can always be written as the sum of two Majorana fermions of the form

$$c_{i\uparrow} = \frac{1}{2}(\chi_{i\uparrow a} + i\chi_{i\uparrow b}), \quad (2.4)$$

where the Majorana fermions  $\chi_{i\uparrow a}, \chi_{i\uparrow b}$  are hermitian operators that satisfy

$$\begin{aligned}\chi_{i\uparrow a}^2 &= 1, \\ \chi_{i\uparrow b}^2 &= 1, \\ \{\chi_{i\uparrow a/b}, \chi_{j\uparrow a/b}\} &= 2\delta_{ij}, \\ \{\chi_{i\uparrow a/b}, \chi_{j\uparrow b/a}\} &= 0.\end{aligned}\tag{2.5}$$

In terms of Majorana fermions the Hamiltonian takes the form

$$H = \frac{i}{2} \left[ \sum_{i=1}^N -\mu \chi_{i\uparrow a} \chi_{i\uparrow b} + (t + \Delta) \chi_{i\uparrow b} \chi_{i+1\uparrow a} + (-t + \Delta) \chi_{i\uparrow a} \chi_{i+1\uparrow b} \right].\tag{2.6}$$

We now note that at the special point  $\mu = 0, t = \Delta$ , the Hamiltonian takes the particularly simple form

$$H = i \sum_{i=1}^{N-1} t \chi_{i\uparrow b} \chi_{i+1\uparrow a}.\tag{2.7}$$

The remarkable thing is that the two Majorana fermions  $\chi_{1\uparrow a}$  and  $\chi_{N\uparrow b}$  do not appear in the Hamiltonian and therefore commute with it. This indicates a ground state degeneracy. We can think about this ground state degeneracy in terms of the fermion  $d = \frac{1}{2}(\chi_{1\uparrow a} + i\chi_{N\uparrow b})$ , so that one ground state is the one where the  $d$ -fermion is absent and in the other one it is present. Even though we can think about the ground state degeneracy in terms of the fermion there is something special about its Majorana fermion constituents, namely that they are localized on opposite ends of the wire. This gives a certain reality to the mathematical decomposition (2.4) in the sense that one is now able to interact with individual unpaired Majorana fermions. We will refer to these unpaired Majorana fermions as Majorana bound states. They have many interesting properties. For example Majorana bound states are equal superpositions of electrons and holes, because they are of the form  $\chi_{1\uparrow a} = d + d^\dagger$  and  $\chi_{N\uparrow b} = i(d^\dagger - d)$  and  $d$  and  $d^\dagger$  are zero-energy fermions in a superconductor.

So far we have only discussed one particular set of parameters for which the system is inside the topological phase. For other parameters inside the topological phase the Majorana bound states are not perfectly localized. Instead they are exponentially localized at opposite ends of the wire. This means that Majorana bound states at the ends of a sufficiently long wire are still decoupled. This is the situation that is most relevant for the rest of the thesis. In particular we will always assume that the systems are long enough such that Majorana bound states are decoupled and can therefore be studied independent of each other.

It is instructive to compare the Hamiltonian (2.7) with the Hamiltonian of the systems for the parameter values  $t = \Delta = 0$  and  $\mu \neq 0$ . The latter takes the form

$$H = \frac{i}{2} \sum_{i=1}^N \mu \chi_{i\uparrow a} \chi_{i\uparrow b}.\tag{2.8}$$

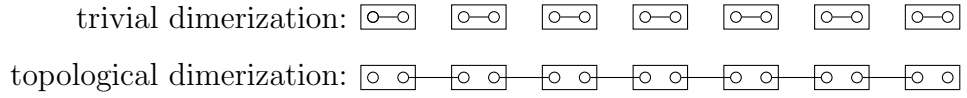


Fig. 2.3: The figure illustrates the trivial-dimerization parameter point corresponding to (2.8) and the topological-dimerization parameter point corresponding to (2.7). The rectangles denote the original fermions, the circles the Majorana fermions in which the electrons were decomposed and the lines correspond to couplings in the Hamiltonian. The topological-dimerization parameter point is inside the topological phase and has an unpaired Majorana fermion at each end of the wire.

Even though this Hamiltonian is very similar to (2.7) it does not have unpaired Majorana fermions at the ends. This is an example for a parameter point inside the topologically trivial phase. The difference between this parameter point and the one in the topological phase discussed previously is illustrated in figure 2.3. Because in both cases the Hamiltonian only consists out of uncoupled quadratic Majorana-fermion terms, we will call these points in parameter space topological-dimerization point and trivial dimerization-point respectively.

### Difference Between Majorana Fermions and Majorana Bound States

Because this subtle point will be important throughout the thesis let us summarize the difference between Majorana fermions and Majorana bound states. Majorana fermions, sometimes also referred to as Majorana operators, result from the mathematical decomposition of an ordinary fermion, also called complex fermion. They are related to an ordinary fermion through (2.4) and they have the properties (2.5). Even though all complex fermions can always be written in terms of Majorana fermions, this generally bears no physical significance. In particular Majorana fermions are not related to the Hamiltonian of any system.

Majorana bound states are also Majorana fermions. But on top of that, they are related to the Hamiltonian of the system, in particular they commute with it. Majorana bound states are therefore system specific. They are usually localized at the phase boundary between topological phases. As such they can be moved adiabatically by changing the position of the phase boundary. This can be used to adiabatically exchange them, resulting in braiding operations which are known to exhibit non-abelian statistics [29].

### 2.3.2 Time-Reversal-Invariant Kitaev Chain

We will now introduce the time-reversal-invariant version of the Kitaev chain. This is the simplest toy model for topological systems in class DIII, which we study extensively in this thesis.

In order to obtain a time-reversal-invariant model we consider both spin directions. That way the time-reversal-invariant version of equation (2.3) takes the form

$$H = \sum_{i,\sigma} t(c_{i\sigma}^\dagger c_{i+1\sigma} + \text{h.c.}) + \mu c_{i\sigma}^\dagger c_{i\sigma} + \sigma \Delta (c_{i\sigma}^\dagger c_{i+1\sigma}^\dagger + \text{h.c.}), \quad (2.9)$$

where the  $\sigma$  prefactor is 1 for  $\uparrow$  and  $-1$  for  $\downarrow$ .

If one now considers the topological-dimerization point in parameter space, one is left with two Majorana bound states at each end of the wire, namely  $\chi_{1\uparrow a}, \chi_{1\downarrow a}$  and  $\chi_{N\uparrow b}, \chi_{N\downarrow b}$  respectively. This implies a fourfold ground state degeneracy, instead of just a twofold one, because two distinct fermions can be formed out of the Majorana bound states.

Similar to the time-reversal-broken Kitaev chain, there is a certain robustness to the edge states, such that away from the topological-dimerization point in parameter space there are still two Majorana bound states localized at each end, as long as the wire is long enough.

A major difference to the time-reversal-broken Kitaev chain is that our Majorana bound states are now strictly speaking not unpaired, because there are always two of them localized at the same end of the wire. These two Majorana bound states are actually Kramers partners. This prevents them from coupling and acquiring a finite energy, even if the spin-up and spin-down chains are coupled. Nonetheless, nothing prevents us from forming local fermions out of the Majorana bound states and their Kramers partners. They take the form

$$\begin{aligned} d_R &= \frac{1}{2}(\chi_{1\uparrow a} + i\chi_{1\downarrow a}), \\ d_L &= \frac{1}{2}(\chi_{N\uparrow b} + i\chi_{N\downarrow b}). \end{aligned} \quad (2.10)$$

The local fermions fulfill the usual fermionic anti-commutation relations. But they actually behave quite differently from normal fermions under time-reversal symmetry. In particular we note that they do not seem to have Kramers partners, since there is only one at each end of the wire. If one explicitly calculates how the corresponding states transform under time-reversal symmetry one finds that time-reversal symmetry actually flips the occupation number of this local fermion. In other words the Kramers partner of an occupied state is an empty state. This is known as a parity anomaly and it implies that there has to be another such local fermion somewhere in the system such that total parity is conserved under time-reversal symmetry.

For most of our studies we adopt a local point of view for DIII systems. Sometimes we will describe the edge excitations in terms of local fermions and sometimes in terms of a Kramers pair of Majorana bound states. The former has the advantage that it is more intuitive to think about the states. The latter has the advantage that it is easier to check for time-reversal symmetry or construct time-reversal-symmetric models.

## 2.4 Bosonization and Luttinger Liquids

In this section we will summarize the most important bosonization results and techniques that we will use throughout the rest of this thesis. Bosonization is a technique used for one-dimensional problems, that maps their low-lying degrees of freedom to a free bosonic field theory. We will apply this to fermions. The advantage of bosonization is that it allows to treat certain types of interactions exactly. Interactions which cannot be treated exactly will then be studied in the context of renormalization group theory which we will introduce in the next section.

One main goal of this section is to remind the reader about some of the most important aspects of one-dimensional electronic systems in their original and bosonized form. The other goal of this section is to set up a dictionary for how to translate fermions into the bosonic theory. This is by no means a complete introduction. Out of the many relevant details for bosonization we will only present those which are beneficial for later discussions. This section mostly follows a review by Sénéchal [46], but sticks to the conventions used in [21], except that we will treat the high energy cutoff differently as we will explain below. Another goal of this section is to introduce complex coordinates for the  $(1+1)$ -dimensional free bosonic theory. Those will turn out to be useful for some of the conformal-field-theory techniques that we use in chapter 4.

We consider a one-dimensional electronic Hamiltonian which is diagonal in  $k$ -space. Ignoring spin for the moment such a Hamiltonian takes the form

$$H = \sum_k \epsilon(k) c^\dagger(k) c(k). \quad (2.11)$$

We only want to describe the low-energy degrees of freedom of this system and therefore we linearize the dispersion relation around the two Fermi points. Simultaneously we introduce a cutoff  $\Lambda$  such that our linear approximation is valid for energies in the interval  $[-\Lambda, \Lambda]$ . This is illustrated in figure 2.4. The approximate Hamiltonian takes the form

$$\begin{aligned} H = & \sum_{-\Lambda < v_F k < \Lambda} (v_F k) c^\dagger(k + k_F) c(k + k_F) \\ & + \sum_{-\Lambda < v_F k < \Lambda} (-v_F k) c^\dagger(k - k_F) c(k - k_F). \end{aligned} \quad (2.12)$$

We now define position-space operators for right- and left-moving electrons. To lighten the notation we will not include the ranges for  $k$  explicitly, but they are always in an interval around zero, describing the linearized region around the Fermi points. The right- and left-moving operators take the form

$$\begin{aligned} \psi(x) &= \frac{1}{\sqrt{L}} \sum_k e^{ikx} c(k + k_F), \\ \bar{\psi}(x) &= \frac{1}{\sqrt{L}} \sum_k e^{ikx} c(k - k_F). \end{aligned} \quad (2.13)$$

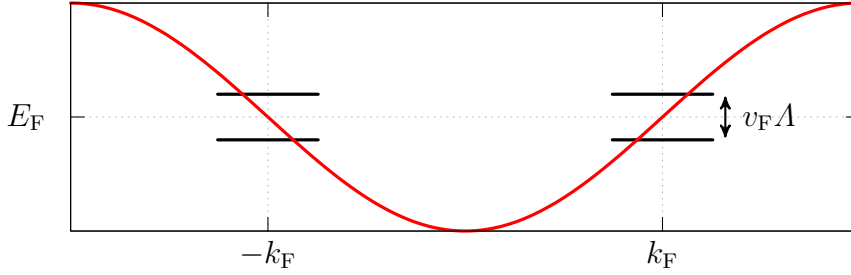


Fig. 2.4: The figure shows an example for a dispersion relation. For low energies only the linearized part of the dispersion close to the Fermi momenta is relevant. Such a description is necessarily only valid in an energy interval around the Fermi energy, as indicated in the picture.

Here  $L$  is the system size which is always assumed to be large enough such that we can go from sums to integrals via  $\sum_k \rightarrow \frac{L}{2\pi} \int dk$ . The fields  $\psi, \bar{\psi}$  are fermionic fields that fulfill

$$\begin{aligned} \{\psi(x), \psi^\dagger(x')\} &= \delta(x - x'), \\ \{\bar{\psi}(x), \bar{\psi}^\dagger(x')\} &= \delta(x - x'), \\ \{\psi(x), \bar{\psi}(x')\} &= 0. \end{aligned} \quad (2.14)$$

In terms of the left- and right-moving operators and in the continuum limit we can write the Hamiltonian as

$$H = iv_F \int dx \left[ -\psi^\dagger(x) \partial_x \psi(x) + \bar{\psi}^\dagger(x) \partial_x \bar{\psi}(x) \right]. \quad (2.15)$$

A representation very similar to this will be the starting point of chapter 5.

The reason why these operators are called left- and right-moving is clearest when one calculates their time evolution with the Schrödinger equation in the Heisenberg picture  $\dot{O} = i[H, O]$ , where  $O$  is an arbitrary operator. For the time-dependent operators one finds

$$\begin{aligned} \psi(x, t) &= \frac{1}{\sqrt{L}} \sum_k e^{ik(x-v_F t)} c(k + k_F), \\ \bar{\psi}(x, t) &= \frac{1}{\sqrt{L}} \sum_k e^{ik(x+v_F t)} c(k - k_F). \end{aligned} \quad (2.16)$$

The important point to notice is that the right-moving field  $\psi$  only depends on  $x$  and  $t$  through the linear combination  $x - v_F t$  and the left-moving field only depends on the linear combination  $x + v_F t$ . This justifies calling  $\psi$  and  $\bar{\psi}$  left and right moving, but it also suggests that it might be beneficial to introduce new coordinates, such that the fields only depend on a single coordinate each.

## 2 Background

---

It turns out to be very useful to introduce certain complex coordinates. The idea comes from conformal field theory and is commonly used for two-dimensional field theories [17, 46]. In particular we define the complex coordinates

$$\begin{aligned} z &= -i(x - v_F t) = v_F \tau - ix, \\ \bar{z} &= i(x + v_F t) = v_F \tau + ix, \end{aligned} \tag{2.17}$$

where we once gave the definition for real times  $t$  and for imaginary times  $\tau = it$ . The corresponding transformations of the derivatives are

$$\begin{aligned} \partial_z &= -\frac{i}{2} \left( \frac{1}{v_F} \partial_t - \partial_x \right) = \frac{1}{2} \left( \frac{1}{v_F} \partial_\tau + i \partial_x \right), \\ \partial_{\bar{z}} &= -\frac{i}{2} \left( \frac{1}{v_F} \partial_t + \partial_x \right) = \frac{1}{2} \left( \frac{1}{v_F} \partial_\tau - i \partial_x \right). \end{aligned} \tag{2.18}$$

In order to simplify the notation we will often set  $v_F$  to 1. This makes the equations more symmetric between  $x$  and  $t$ . Units can be restored by substituting  $t \rightarrow v_F t$ . Generally an operator that depended on  $x$  and  $t$  will now depend on  $z$  and  $\bar{z}$  in complex coordinates. But as we pointed out earlier, there is a separation into left- and right-moving fields, such that there are operators that will only depend on either  $z$  or  $\bar{z}$ . For example the operators  $\psi$  and  $\bar{\psi}$  now take the form

$$\begin{aligned} \psi(z) &= \frac{1}{\sqrt{L}} \sum_k e^{-kz} c(k + k_F), \\ \bar{\psi}(\bar{z}) &= \frac{1}{\sqrt{L}} \sum_k e^{k\bar{z}} c(k - k_F). \end{aligned}$$

Note that we replaced the two real coordinates  $x$  and  $t$  with two complex coordinates  $z$ ,  $\bar{z}$ . Therefore we increased the number of real parameters by two. The physical part of the description is obtained when one sets  $\bar{z} = z^*$ , where the star denotes complex conjugation. The real usefulness of the complex coordinates is only apparent within conformal field theory where one can exploit the relationship between complex analysis and conformal symmetry. This will not be important for us, so the complex coordinates may simply be regarded as convenient coordinates. In particular because we will use results from the literature which are formulated in terms of complex coordinates.

Before we continue and bosonize the fermionic fields we will calculate their propagator,

which assumes time ordering, in imaginary time. One finds

$$\begin{aligned}
 \langle \psi(z)\psi^\dagger(w) \rangle &= \frac{1}{L} \sum_{k,k'} \langle 0|c(k+k_F)c^\dagger(k'+k_F)|0 \rangle e^{-kz+k'w} \\
 &= \frac{1}{L} \sum_{k>0} e^{-k(z-w)} \\
 &= \frac{1}{2\pi} \int_{k>0} dk e^{-k(z-w)} \\
 &= \frac{1}{2\pi} \frac{1}{z-w}.
 \end{aligned} \tag{2.19}$$

Here we used that the “vacuum”  $|0\rangle$  is defined with respect to the Fermi energy, such that the vacuum expectation value is only finite for  $k > 0$ . Furthermore we used that because of the time ordering  $\text{Re } z > \text{Re } w$  and therefore the integral always converges. Similarly one finds

$$\langle \psi^\dagger(z)\psi(w) \rangle = \frac{1}{2\pi} \frac{1}{z-w}. \tag{2.20}$$

### 2.4.1 Translation into Bosons

We will state the identities that relate the one-dimensional fermionic system to the one-dimensional bosonic one. We will skip some important parts of the derivation in particular most aspects of the mode expansion. The interested reader is referred to [21, 46] for the omitted details. We will however demonstrate some consistency requirements, in particular to demonstrate some computational techniques that will be useful later on.

As a starting point we consider the Lagrangian of a massless bosonic field  $\varphi$ . It takes the form

$$L[\varphi] = \frac{C}{2} \int dx [(\partial_t \varphi)^2 - (\partial_x \varphi)^2] \tag{2.21}$$

where we chose units with  $v_F = 1$ . The constant  $C$  will be important for the convention by which we will translate between fermions and bosons. We will fix it later in order to arrive at the desired convention, which is the one used by [21]. For that  $C$  takes a value of  $\frac{1}{\pi}$ . We do not fix the constant right away to make it easier to compare different references. The action corresponding to the Lagrangian (2.21) is

$$S[\varphi] = \frac{C}{2} \iint dt dx [(\partial_t \varphi)^2 - (\partial_x \varphi)^2] \tag{2.22}$$

The conjugate momentum of  $\varphi$  is given by

$$\Pi = \frac{\delta L}{\delta(\partial_t \varphi)} \tag{2.23}$$

$$= C \partial_t \varphi, \tag{2.24}$$

such that

$$[\varphi(x), \Pi(x')] = i\delta(x - x'). \quad (2.25)$$

It can be shown, that the field  $\varphi$  can be decomposed into left and right moving fields  $\phi$  and  $\bar{\phi}$  according to

$$\begin{aligned} \varphi(x, t) &= \phi(x - t) + \bar{\phi}(x + t), \\ \varphi(z, \bar{z}) &= \phi(z) + \bar{\phi}(\bar{z}). \end{aligned} \quad (2.26)$$

Deriving this decomposition relies on a mode expansion for  $\varphi$  and we will not present the details here.

One often introduces an additional bosonic field  $\theta$  as  $C\partial_x\theta = \Pi^1$ . It is related to  $\phi$  and  $\bar{\phi}$  as

$$\begin{aligned} C\partial_x\theta &= \Pi \\ &= C\partial_t\varphi \\ &= iC(\partial_z + \partial_{\bar{z}})(\phi + \bar{\phi}) \\ &= iC(\partial_z - \partial_{\bar{z}})(\phi - \bar{\phi}) \\ &= -C\partial_x(\phi - \bar{\phi}). \end{aligned} \quad (2.27)$$

Therefore we have

$$\theta = \bar{\phi} - \phi, \quad (2.28)$$

up to an additive constant, which we set to zero. This way the chiral fields take the form

$$\begin{aligned} \phi &= \frac{1}{2}(\varphi - \theta), \\ \bar{\phi} &= \frac{1}{2}(\varphi + \theta). \end{aligned} \quad (2.29)$$

We now want to associate the field  $\varphi$  with a electron quantity that behaves like a boson. Such a quantity is the density  $n$ . We postulate the relationship

$$\varphi = \lambda \int_x^\infty dy n(y), \quad (2.30)$$

where we will determine  $\lambda$  later according to our choice for  $C$ . This means that creating an electron at position  $x'$  increases  $\varphi(x)$  by  $\lambda$  for  $x < x'$ . This is the same effect the operator

$$\exp \left[ -i\lambda \int_{-\infty}^{x'} dy \Pi(y) \right] \quad (2.31)$$

---

<sup>1</sup>Note that this convention differs by a sign compared to [46] in order to be consistent with [21]

has, because  $\Pi$  is the canonical momentum of  $\varphi$ . Using our definition  $\Pi = C\partial_x\theta$ , we can rewrite (2.31) as

$$\exp\left[-i\lambda\int_{-\infty}^{x'} dy \Pi(y)\right] = \exp[-Ci\lambda\theta(x)] \quad (2.32)$$

This operator would be a good candidate for our electronic creation operators for left or right movers, if it only depended on  $z$  or  $\bar{z}$ . This is currently not the case because  $\theta$  depends on both. On the other hand if we replace  $\theta \rightarrow \theta \mp \varphi$  we still have the same shift properties, because  $\varphi$  commutes with itself. Additionally everything now depends on the chiral fields according to (2.29). We can therefore make a consistent ansatz for our electronic operators. It has the form

$$\psi^\dagger(x) = Ae^{2iC\lambda\phi(x)}, \quad \bar{\psi}^\dagger(x) = Ae^{-2iC\lambda\bar{\phi}(x)}. \quad (2.33)$$

We will determine the constants after we explain how to calculate correlation functions in the bosonic representation. The constants will then be determined such that the fermionic correlation functions are reproduced.

In order to calculate the correlation functions we first have to note some subtle points about the exponential operators of the form  $e^{i\alpha\phi}$ , called vertex operators. As before we will only point out some issues and state their solutions without going into detail. Details can be found in the references [17, 46]. Because the operator  $\phi$  is a fluctuating field, care has to be taken when defining its exponential. In particular the exponential is defined according to normal ordering. Normal ordering means that in terms of a mode expansion of the operator, all the creation operators are to the left of all the annihilation operators. Generally we will denote normal ordering with colons, such that the normal-ordered version of an operator  $O$  is  $:O:$ . The vertex operators which we discussed above are always implicitly assumed to be normal ordered. The difficulty that now arises is that some of the normal properties of the exponential function do not hold for normal-ordered exponentials. In particular we have  $:e^{i\alpha\phi(z)}: :e^{i\beta\phi(w)}: \neq :e^{i(\alpha\phi(z)+\beta\phi(w))}:.$

In our case we have instead the very important identity [17]

$$:e^{i\alpha\phi(z)}: :e^{i\beta\phi(w)}: = e^{-\alpha\beta\langle\phi(z)\phi(w)\rangle} :e^{i(\alpha\phi(z)+\beta\phi(w))}: \quad (2.34)$$

Together with the property

$$\langle :e^{i(\alpha\phi(z)+\beta\phi(w))}: \rangle = \delta_{\alpha+\beta,0} \quad (2.35)$$

this enables us to calculate the correlation functions of the bosonized fermions. The only missing ingredient is the correlation function  $\langle\phi(z)\phi(w)\rangle$ . In order to calculate it we can start from the correlation function for  $\varphi$  in imaginary time, which we call

$$G(x, \tau) = \langle\varphi(x, \tau)\varphi(0, 0)\rangle. \quad (2.36)$$

Rewriting the action (2.22) in the form

$$S[\varphi] = \frac{C}{2} \iint dx d\tau [\varphi(-\partial_x^2 - \partial_\tau^2)\varphi] \quad (2.37)$$

we know that  $G$  has to satisfy

$$-\nabla^2 G = \frac{1}{C} \delta(x) \delta(\tau). \quad (2.38)$$

The solution is the well known fundamental solution of the Laplace equation in two dimensions. It is given by

$$G(x, \tau) = -\frac{1}{4\pi C} \ln(x^2 + \tau^2) + \text{const.} \quad (2.39)$$

Here the choice of the constant is quite interesting. It does not affect the asymptotic behavior of the Green function for large or small values, but it can be used to affect the units inside the logarithm. In particular the only other length scale that exists in our system is the one associated with the cutoff. We call this length scale  $a$ . One can then set the constant to  $\frac{1}{4\pi C} \ln(a^2)$ , such that the Green function becomes

$$G(x, \tau) = -\frac{1}{4\pi C} \ln\left(\frac{x^2 + \tau^2}{a^2}\right).$$

This way  $G$  does not have any units, but has an implicit dependence on the cutoff scale  $a$ . We will sometimes choose to have an explicit cutoff dependence instead. In that case the constant in (2.39) is simply put to zero and  $G$  has logarithmic units. We will generally not include  $a$ , but it can easily be restored by replacing  $z \rightarrow z/a$  and  $\bar{z} \rightarrow \bar{z}/a$ .

We can also write the Green function as

$$\begin{aligned} G(x, \tau) &= -\frac{1}{4\pi C} \ln(z\bar{z}) \\ &= -\frac{1}{4\pi C} \ln(z) - \frac{1}{4\pi C} \ln(\bar{z}). \end{aligned} \quad (2.40)$$

Together with the identity

$$\langle \varphi(x, \tau) \varphi(0, 0) \rangle = \langle \phi(z) \phi(0) \rangle + \langle \bar{\phi}(\bar{z}) \bar{\phi}(0) \rangle \quad (2.41)$$

this implies

$$\begin{aligned} \langle \phi(z) \phi(0) \rangle &= -\frac{1}{4\pi C} \ln(z), \\ \langle \bar{\phi}(\bar{z}) \bar{\phi}(0) \rangle &= -\frac{1}{4\pi C} \ln(\bar{z}). \end{aligned} \quad (2.42)$$

We are now in a position to calculate the correlation functions of the bosonized fermions (2.33) and fix the constants by comparing with the fermionic correlation function (2.19). We find

$$\begin{aligned}\langle\psi(z)\psi^\dagger(w)\rangle &= A^2\langle e^{-2iC\lambda(\phi(z)-\phi(w))}\rangle(z-w)^{-\frac{C\lambda^2}{\pi}} \\ &= A^2(z-w)^{-\frac{C\lambda^2}{\pi}}.\end{aligned}\tag{2.43}$$

From this we find that

$$C\lambda^2 = \pi.\tag{2.44}$$

For  $A$  we find

$$A^{-1} = \sqrt{2\pi}\tag{2.45}$$

if we do not include  $a$  in the Green function. With  $a$  included in the Green function we have to replace  $(z-w) \rightarrow (z-w)/a$  in equation (2.43) and therefore in that case we have

$$A^{-1} = \sqrt{2\pi a}.\tag{2.46}$$

This difference can be understood as follows. We know that the fermionic operators  $\psi$  and  $\bar{\psi}$  have dimensions  $(\text{length})^{-\frac{1}{2}}$ . If the Green function contains  $a$ , it is unitless and therefore  $\phi$  and its exponentials are unitless. The prefactor  $A$  therefore has to contain the units in the form of the cutoff  $a$ . If the Green function does not contain  $a$  then  $\phi$  has units and its exponential in (2.33) actually already has the units  $(\text{length})^{-\frac{1}{2}}$ . Therefore the prefactor  $A$  is unitless. To summarize let us state the complete formulas for translating from fermions to bosons in the case when we use the convention  $C = \frac{1}{\pi}$ . They are

$$\psi^\dagger(x) = \frac{1}{\sqrt{2\pi}}e^{2i\phi(x)}, \quad \bar{\psi}^\dagger(x) = \frac{1}{\sqrt{2\pi}}e^{-2i\bar{\phi}(x)}.\tag{2.47}$$

One of the main advantages of bosonization can now be seen in the context of interactions. It can be shown that for spinless fermions the only effect of interactions is to change the constants  $C$  and  $v_F$  in the action (2.22). This is then typically written as

$$S[\varphi] = \frac{1}{2\pi K} \iint dt dx [(\partial_t\varphi)^2 - (\partial_x\varphi)^2],\tag{2.48}$$

such that the system is non-interacting for  $K = 1$ . The changed  $v_F$  we will call  $u$  and it appears when restoring units by the replacement  $t \rightarrow ut$ . The remarkable advantage of bosonization is that the bosonized Hamiltonian is still quadratic in the presence of interactions. Furthermore it is still possible to decompose the bosonic system into chiral modes that do not interact with each other, by repeating the procedure outlined above for a different value of  $C$ , namely  $C = \frac{1}{\pi K}$ . These chiral modes, however, do not correspond to left- and right-moving fermions anymore (because we bosonized with the non-interacting  $C$  value), but to a mixture of both.

When different species of fermions are present, for example spin up and spin down, interactions lead to additional non-quadratic terms as described in the next subsection.

### 2.4.2 Klein Factors and Spin and Charge Sectors

One aspect of bosonization, which we have not addressed yet, is how to bosonize multiple types of electrons or fermions at the same time. This could for instance be electrons with opposite spin directions. We will denote the different kinds of fermions by an index  $\mu$ . The simplest ansatz would then be to describe the fermions of kind  $\mu$  by independent chiral fields of type  $\mu$ . This results in the problem that different bosonized fermions no longer anti-commute. This problem is resolved by defining the bosonized fermions as

$$\psi_\mu^\dagger(x) = \frac{\eta_\mu}{\sqrt{2\pi}} e^{2i\phi_\mu(x)} \quad \bar{\psi}_\mu^\dagger(x) = \frac{\eta_\mu}{\sqrt{2\pi}} e^{-2i\bar{\phi}_\mu(x)} \quad (2.49)$$

Where the  $\eta_\mu$  are Majorana fermion, which are called Klein factors. Klein factors have nothing to do with the Majorana fermions which are the primary interest of this thesis, namely the Majorana bound states. The only purpose of Klein factors is to make the bosonized versions of different kinds of fermions anti-commute.

When studying a spinful system with electron-electron interactions it turns out to be convenient to transform variables from  $\phi_{\uparrow/\downarrow}$  to

$$\begin{aligned} \phi_c &= \frac{1}{\sqrt{2}}(\phi_\uparrow + \phi_\downarrow), \\ \phi_s &= \frac{1}{\sqrt{2}}(\phi_\uparrow - \phi_\downarrow). \end{aligned} \quad (2.50)$$

The new variables describe charge and spin degrees of freedom respectively. The advantage of spin and charge sectors is that they decouple for a lot of systems even in the presence of interactions.

The transformation to the spin and charge representation is unitary therefore the quadratic actions for the fields take the same form as for the spin-up and spin-down field. Similar to equation (2.22) we have

$$S_\mu[\varphi_\mu] = \frac{1}{2\pi} \iint dt dx [(\partial_t \varphi_\mu)^2 - (\partial_x \varphi_\mu)^2], \quad (2.51)$$

where  $\mu$  is now c or s, and we have chosen the convention  $C = \frac{1}{\pi}$ . Alternatively the systems are described by the action for the dual fields  $\theta_\mu$ . These take the same form

$$S_\mu[\theta_\mu] = \frac{1}{2\pi} \iint dt dx [(\partial_t \theta_\mu)^2 - (\partial_x \theta_\mu)^2]. \quad (2.52)$$

In case when the  $\varphi_\mu$  and  $\theta_\mu$  are coupled, one needs to describe the system by a phase-space action which contains both fields.

The effect of interactions is now twofold. Firstly it renormalizes the Fermi velocity and changes the prefactor of the Lagrangian as for a single species of fermions. The change in Fermi velocity again only appears when restoring units and one has to replace

$t \rightarrow ut$  where  $u$  is the Fermi velocity of the interacting system. Secondly interactions add a non-quadratic term to the spin sector. This term describes the backscattering of electrons. The quadratic actions with interactions take the form

$$S_\mu[\varphi_\mu] = \frac{1}{2\pi K_\mu} \iint dt dx [(\partial_t \varphi_\mu)^2 - (\partial_x \varphi_\mu)^2], \quad (2.53)$$

or

$$S_\mu[\varphi_\mu] = \frac{K_\mu}{2\pi} \iint dt dx [(\partial_t \theta_\mu)^2 - (\partial_x \theta_\mu)^2]. \quad (2.54)$$

The additional non-quadratic term in the spin sector is

$$S_{\text{bs}}[\varphi_s] = \frac{\lambda_{\text{bs}}}{2\pi^2} \iint dt dx \cos(\sqrt{8}\varphi_s), \quad (2.55)$$

In the preceding equations the  $K_\mu$  are due to interactions. In particular  $K_s = K_c = 1$  corresponds to the non-interacting case. For repulsive interaction  $K_c < 1$  and  $K_s > 1$ .

## 2.5 Renormalization Group Theory

We saw in the previous section that bosonization can simplify one-dimensional problems, in particular because part of the interactions is included in the quadratic terms in the action. Nonetheless there remain non-quadratic interaction terms that one needs to study. One possible way to study these is by means of renormalization group theory and we will describe some of its basic ideas in this section. This short introduction mostly follows [10].

### 2.5.1 The Renormalization Group Idea, Phase Transitions and Fixed Points

The basic idea behind renormalization group theory is to study the long-range/low-energy behavior of systems in the following way. One starts with the partition function which is for example given by a functional integral of the form

$$Z = \int \mathcal{D}\phi e^{-S[\phi]}. \quad (2.56)$$

One then divides the degrees of freedom into small-distance/high-energy degrees of freedom  $\phi_>$  and long-distance/low-energy degrees of freedom  $\phi_<$  such that

$$\begin{aligned} \phi &= \phi_< + \phi_>, \\ \int \mathcal{D}\phi &= \int \mathcal{D}\phi_< \int \mathcal{D}\phi_>. \end{aligned} \quad (2.57)$$

One can now calculate the effective action for  $S'[\phi_<]$  as

$$e^{-S'[\phi_<]} = \int \mathcal{D}\phi_> e^{-S[\phi]}, \quad (2.58)$$

such that

$$\int \mathcal{D}\phi e^{-S[\phi]} = \int \mathcal{D}\phi_{<} e^{-S'[\phi_{<}]}. \quad (2.59)$$

One now assumes that the two actions  $S$  and  $S'$  have the same structure and as such are simply described by different sets of dimensionless parameters  $K_i$  and  $K'_i$ . The whole process can therefore be viewed as generating a transformation  $K_i \rightarrow K'_i$ . The main idea behind renormalization-group theory is studying these kind of parameter transformations. They are called renormalization-group transformations and their iterated (potentially continuous version) is called flow of the parameters. Note that the assumption that the two actions  $S$  and  $S'$  have the same structure is always trivially true when one does not restrict the number of terms that the actions are allowed to have. That is because one could always include terms, that are only present in  $S'$  after integrating  $\phi_{>}$  out, in  $S$  with a trivial prefactor of zero. Fortunately it turns out that even with a limited number of terms one can often obtain good approximative renormalization-group results.

There is one special parameter dependence of the action  $S'[\phi_{<}]$ , which is the dependence on an additive constant independent of the fields  $\varphi_{<}$ . This constant corresponds to the free energy of the degrees of freedom that were integrated out. One usually ignores it for two reasons. Firstly because it does not contribute to the low energy dynamics of the system, and secondly because this contribution is usually well behaved close to a critical point, whereas other contributions to the free energy are singular close to a critical point [10]. It is therefore sensible to only consider the singular components.

One of the main motivations for using renormalization-group techniques is the study of phase transitions. During a phase transition some bulk properties of a system change and therefore this has to happen on all length scales. But if the length scale is not important for the physics of the system right at the transition point, then our renormalization procedure described above should yield the identity transformation  $K_i \rightarrow K_i$ . This means that fixed points in the renormalization group transformation are related to phase transitions, which motivates studying the renormalization group transformation at and close to these fixed points. In particular one often studies the linearized transformation close to a fixed point.

### 2.5.2 Scaling Operators and Scaling Dimension

The eigenvalues and eigenvectors of the linearized renormalization group transformation close to a fixed point have special significance in renormalization group theory. Before we continue let us assume that during a renormalization step the length scales are scaled by a factor  $b > 1$ . This means that a small distance cutoff  $a$ , for example lattice spacing transforms as  $ba$  or alternatively it means that a high energy cutoff  $\Lambda$  scales as  $b^{-1}\Lambda$ . We denote the eigenvalues and eigenvectors of the linearized renormalization group transformation with  $\eta_i$  and  $g_i$  respectively. It is common to write the eigenvalue as  $\eta_i = b^{y_i}$ . Under repeated application of the renormalization group transformation the sign of  $y_i$  plays an important role. If it is positive the coupling will increase. In

that case the coupling is called relevant. If  $y_i$  is negative the coupling will decrease and is called irrelevant. In the case where  $y_i$  vanishes, the coupling stays the same and is called marginal. However, marginal couplings usually change if the renormalization group transformation is calculated to higher accuracy.

If we denote the fields to which the  $g_i$  couple with  $\phi_i$  then the deviations from the fixed point have the form

$$\sum_i g_i \int \frac{d^d x}{a^d} \phi_i. \quad (2.60)$$

Under a renormalization group transformation  $a \rightarrow ba$  and  $g_i \rightarrow b^{y_i} g_i$ . In order for the partition function to remain unchanged, as required by (2.59) we have to require the transformation property  $\phi_i(x) \rightarrow b^{x_i} \phi(x)$ , where

$$x_i = d - y_i. \quad (2.61)$$

The quantity  $x_i$  is called scaling dimension of the operator  $\phi_i$ . The required transformation behavior of  $\phi_i$  is also consistent with another of its properties which can be shown (chapter 3.8 in [10]), namely that for long distances  $\langle \phi_i(r_1) \phi_i(r_2) \rangle \propto \frac{1}{|r_1 - r_2|^{2x_i}}$ . This suggest that  $\phi_i$  has units (length) $^{-x_i}$  which implies the same transformation behavior under rescaling.

Note the important implication that given a fixed point together with set of corresponding scaling operators and their scaling dimensions, one can actually do renormalization group studies without explicitly integrating out any degrees of freedom. This is because the information about the result of such a calculation is already contained in the scaling operators and their scaling dimensions.

### 2.5.3 Continuous Renormalization and Flow Equations

When we study renormalization group transformations we will always consider infinitesimally small ones. This is commonly done by setting  $b = (1 + d\ell)$ . This way one can obtain differential equations for the change of the coupling constants. In particular the first-order transformation  $g_i \rightarrow b^{y_i} g_i$  implies

$$\frac{dg_i}{d\ell} = y_i g_i. \quad (2.62)$$

Such equations are called flow equations. Chapter 4 will focus on deriving and analyzing such equations in a Majorana bound state context.



### 3 Braiding in Class DIII

Majorana bound states, which can exist in class D systems, exhibit non-abelian statistics under exchange [1, 29]. This is one of the reasons why Majorana bound states have received a lot of attention in the literature because it would be interesting to realize non-abelian statistics in the lab. Furthermore, non-abelian statistics can be used for fault tolerant quantum gates, which is commonly referred to as topological quantum computation [42].

In this chapter we will study the exchange properties of a close cousin of the Majorana bound state, namely Kramers pairs of Majorana bound states. Kramers pairs of Majorana bound states can appear in systems of class DIII.

We will begin by briefly discussing how Majorana fermion operators transform under time-reversal symmetry. This is important for two reasons. Firstly we want to construct time-reversal invariant DIII Hamiltonians and secondly given a Majorana bound state we want to obtain its Kramers partner by application of time-reversal symmetry.

Subsequently we will review relevant aspects of adiabatic physics, in particular the notion of Berry phases (abelian as well as non-abelian). We will then demonstrate how these Berry phases can be calculated in different formulations of the problem. In particular we will start with Berry phases of the many-body Fock space states and show how they can be calculated in terms of second-quantized operators or equivalently in terms of first-quantized Bogoliubov-de Gennes (BdG) states.

We will then discuss an effect that we call local mixing of a Kramers pair of Majorana bound states. This effect alone shows that generically the result of exchanging two Kramers pairs of Majorana bound states is path dependent and therefore cannot fulfill any particular set of statistics. As such Kramers pairs of Majorana bound states cannot be used for fault tolerant quantum operations. We will also discuss sufficient conditions under which local mixing is absent.

Finally we will discuss the most general transformation that can occur when exchanging Kramers pairs of Majorana bound states. We will argue generally that it takes a simple form in the absence of local mixing.

#### 3.1 Time-Reversal Symmetry and Majorana Fermion Operators

We consider a Kramers pair of ordinary fermions and denote their second-quantized operators with  $c_\uparrow$  and  $c_\downarrow$  respectively. Even though we use a spin index for concreteness, the following discussion applies to Kramers pairs in general.

It is well known that such fermions transform under time-reversal symmetry,  $\mathcal{T}$ ,

according to

$$\begin{aligned}\mathcal{T}c_{\uparrow}\mathcal{T}^{-1} &= c_{\downarrow}, \\ \mathcal{T}c_{\downarrow}\mathcal{T}^{-1} &= -c_{\uparrow}.\end{aligned}\tag{3.1}$$

We decompose these fermions into Majorana fermions as

$$\begin{aligned}c_{\uparrow} &= \frac{1}{2}(\chi_{a\uparrow} + i\chi_{b\uparrow}), \\ c_{\downarrow} &= \frac{1}{2}(\chi_{a\downarrow} + i\chi_{b\downarrow}).\end{aligned}\tag{3.2}$$

Comparing equation (3.1) and (3.2) we notice that the type  $a$  and type  $b$  Majorana fermions transform oppositely under time reversal. This is due to the  $i$  in the decomposition (3.2) and due to the anti-unitarity of  $\mathcal{T}$ . In particular the Majorana fermions transform as

$$\begin{aligned}\mathcal{T}\chi_{a\uparrow}\mathcal{T}^{-1} &= \chi_{a\downarrow}, \\ \mathcal{T}\chi_{a\downarrow}\mathcal{T}^{-1} &= -\chi_{a\uparrow}, \\ \mathcal{T}\chi_{b\uparrow}\mathcal{T}^{-1} &= -\chi_{b\downarrow}, \\ \mathcal{T}\chi_{b\downarrow}\mathcal{T}^{-1} &= \chi_{b\uparrow}.\end{aligned}\tag{3.3}$$

Note the sign difference between the type  $a$  and type  $b$  transformations.

It is possible to use a different convention where all the Majorana fermions transform the same way under time-reversal symmetry. This is done by changing the decomposition of the ordinary fermion into Majorana fermions. In particular one would change the definition of  $c_{\downarrow}$  to

$$c_{\downarrow} = \frac{1}{2}(\chi_{a\downarrow} - i\chi_{b\downarrow}).$$

We will not use this convention and continue with the one described above, where the decomposition of ordinary fermions is always the same, but therefore type  $a$  and type  $b$  Majorana fermions transform differently.

Before we conclude this section we briefly discuss the transformation properties of complex fermions that are constructed from a single Majorana Kramers pair. We start from the Majorana Kramers pair  $\chi_{\uparrow}, \chi_{\downarrow}$  such that  $\mathcal{T}\chi_{\uparrow}\mathcal{T}^{-1} = \chi_{\downarrow}$  and  $\mathcal{T}\chi_{\downarrow}\mathcal{T}^{-1} = -\chi_{\uparrow}$  and construct the fermion

$$d = \frac{1}{2}(\chi_{\uparrow} + i\chi_{\downarrow}).\tag{3.4}$$

The time-reversal form of this is

$$\begin{aligned}\mathcal{T}d\mathcal{T}^{-1} &= \mathcal{T}\frac{1}{2}(\chi_{\uparrow} + i\chi_{\downarrow})\mathcal{T}^{-1} \\ &= \frac{1}{2}(\chi_{\downarrow} + i\chi_{\uparrow}) \\ &= +id^{\dagger}.\end{aligned}\tag{3.5}$$

Related to this the parity of  $d$ ,  $i\chi_\uparrow\chi_\downarrow$ , flips sign under time-reversal symmetry. This is no reason for concern, because if we started out with a Kramers pair of fermions, we can actually form two fermions (type  $a$  and type  $b$ ) of the form (3.4), which behave atypical under time reversal. Therefore the overall parity is always conserved. The interesting thing is, however, that in class DIII systems the fermions of the form (3.4) are spatially separated, so that local parity is not conserved under time reversal. This is referred to as the parity anomaly. To guarantee that time reversal never changes the overall parity, there always has to be an even number of zero-energy Kramers pairs of Majorana bound states (which are equivalent to fermions of the kind of equation (3.4)). This transformation behavior is also the reason why it is often more intuitive to construct time-reversal invariant Hamiltonians in terms of Majorana fermions, even when one wants to describe fermions of the form (3.4).

### 3.2 The Adiabatic Theorem and Berry Phases

The adiabatic theorem of quantum mechanics [9, 31] deals with the adiabatic time evolution of systems. Adiabatic time evolution means that the system depends on parameters that change slowly as a function of time (quantified below) and there is no additional time dependence. The systems are assumed to have a Hamiltonian of the form

$$H(\boldsymbol{\lambda}(t)), \tag{3.6}$$

such that  $\boldsymbol{\lambda}$  is the collection of time-dependent parameters. The precise meaning of the parameters  $\boldsymbol{\lambda}$  changing slowly is as follows. For fixed values of the parameters  $\boldsymbol{\lambda}$  we can diagonalize the Hamiltonian. Out of the eigenstates of the Hamiltonian we will focus on a particular degenerate subspace such that

$$H(\boldsymbol{\lambda})|a_i(\boldsymbol{\lambda})\rangle = \epsilon(\boldsymbol{\lambda})|a_i(\boldsymbol{\lambda})\rangle, \tag{3.7}$$

where  $i$  runs over the states spanning the degenerate subspace. In order to lighten the notation we will often use capitalized letters to denote an implicit parameter dependence. This way equation (3.7) reads  $H|A_i\rangle = E|A_i\rangle$ . It is now further assumed that for each parameter value  $\boldsymbol{\lambda}$  the states  $|A_i\rangle$  are separated by an energy gap from all the other states of the system. The requirement that the parameters  $\boldsymbol{\lambda}$  change slowly means that they change slowly compared to the energy gap separating the degenerate states  $|A_i\rangle$  from all other states. Furthermore it is assumed that the degeneracy of our subspace is not lifted for any parameter value  $\boldsymbol{\lambda}$ . This way we have associated the states  $|a_i(\boldsymbol{\lambda})\rangle$  at different values of  $\boldsymbol{\lambda}$  with each other, because we can simply follow the eigenstates with energy eigenvalues  $\epsilon(\boldsymbol{\lambda})$ .

In case of Majorana bound states the degenerate subspace that we are investigating is formed by the ground states of the system. The parameters that we will change are the positions of the Majorana bound states, but we will also consider other parameters for illustrative purposes.

Under the conditions of adiabatic time evolution described above, the adiabatic theorem states that states that are initially in a superposition of basis states  $|a_i(\boldsymbol{\lambda}_{\text{initial}})\rangle$  will evolve into states that are a superposition of basis states  $|a_i(\boldsymbol{\lambda}_{\text{final}})\rangle$ .

The question that remains is how these states evolve exactly. We will first consider the case of non-degenerate subspaces. We define the adiabatic time-evolution operator,  $U_{\text{adiabatic}}$ , as the limit of the normal time-evolution operator with varying parameters. The limit is that of these parameters varying slowly in time in the sense described above. One then finds for the time evolution of a state  $|A_{\text{initial}}\rangle$

$$U_{\text{adiabatic}}|A_{\text{initial}}\rangle = e^{-i\varphi_{\text{dynamic}} - i\varphi_{\text{geometric}}}|A_{\text{final}}\rangle, \quad (3.8)$$

where the dynamical phase is given by the energy dependence of the state

$$\varphi_{\text{dynamic}} = \int_0^t dt' \epsilon(\boldsymbol{\lambda}(t')) \quad (3.9)$$

and the geometric phase is given by

$$\varphi_{\text{geometric}} = \int_{\mathcal{C}} \langle A | \nabla_{\boldsymbol{\lambda}} | A \rangle \cdot d\boldsymbol{\lambda}, \quad (3.10)$$

where the integral is taken over the path  $\mathcal{C}$  that the system took in parameter space, starting at  $\boldsymbol{\lambda}_{\text{initial}}$  and ending at  $\boldsymbol{\lambda}_{\text{final}}$ .

The dynamical phase will not appear in any further discussion, as it is not relevant for the systems which we have in mind. We will consider the adiabatic evolution of ground states of systems. Therefore we will always have  $\epsilon(\boldsymbol{\lambda}) = 0$  and hence  $\varphi_{\text{dynamical}} = 0$ .

The central object of our studies will be the geometric phase. It is important to note that the geometric phase in equation (3.10) is not uniquely defined, because instead of the parameter-dependent state  $|A\rangle$  we could just as well have chosen the parameter-dependent state  $e^{if(\boldsymbol{\lambda})}|A\rangle$ , where  $f$  is a real-valued function. We refer to the different choices of  $\boldsymbol{\lambda}$ -dependence of the state as gauge choices. It is now easy to see that the geometric phase (3.10) is in fact gauge dependent. In particular one has

$$|A\rangle \rightarrow e^{if(\boldsymbol{\lambda})}|A\rangle \quad \implies \quad \varphi_{\text{geometric}} \rightarrow \varphi_{\text{geometric}} - (f(\boldsymbol{\lambda}_{\text{final}}) - f(\boldsymbol{\lambda}_{\text{initial}})). \quad (3.11)$$

From the gauge property (3.11) one could get the impression that the geometric phase is meaningless, as one can always choose a gauge in which it vanishes identically. Michael Berry realized that this gauge dependence of the geometric phase actually vanishes if one considers closed loops [8]. This can easily be seen in equation (3.11) in the case when  $\boldsymbol{\lambda}_{\text{initial}} = \boldsymbol{\lambda}_{\text{final}}$ . Since we are now dealing with a gauge-independent quantity one can readily expect to find physical implications. An example of a physical manifestations of geometric phases is the well known Aharonov-Bohm effect. In honor of Berry's insight, the geometric phase is often referred to as Berry phase.

Before we move on to the more general case of degenerate subspaces, we state some common and useful quantities in relation to the Berry phase. For completeness let us state the definition of the gauge independent geometric phase as

$$\varphi_{\text{geometric}} = \oint_{\mathcal{C}} \langle A | \nabla_{\lambda} | A \rangle \cdot d\lambda. \quad (3.12)$$

The integrand times  $i$  is often referred to as the Berry potential  $\mathcal{A}$ ,

$$\mathcal{A} = i \langle A | \nabla_{\lambda} | A \rangle. \quad (3.13)$$

The Berry potential is a gauge dependent quantity with the transformation property

$$|A\rangle \rightarrow e^{if(\lambda)} |A\rangle \implies \mathcal{A} \rightarrow \mathcal{A} - \nabla_{\lambda} f. \quad (3.14)$$

Another useful concept is the Berry curvature. It is defined by applying Stokes' theorem to equation (3.12). In particular one has

$$\varphi_{\text{geometric}} = \iint_{\mathcal{S}} \Omega_{ij} d\lambda_i d\lambda_j, \quad (3.15)$$

where the integration is over a surface such that its boundary is the closed loop from equation (3.12),  $\partial\mathcal{S} = \mathcal{C}$ . Also note that equation (3.15) uses a summation convention over repeated indices. The advantage of the Berry curvature is that it is a gauge invariant quantity. Its components can be expressed in terms of the components of the Berry potential as

$$\Omega_{ij} = \partial_i \mathcal{A}_j - \partial_j \mathcal{A}_i, \quad (3.16)$$

where the partial derivatives refer to components of  $\lambda$  such that  $\partial_i = \partial_{\lambda_i}$ . Henceforth we will drop the subscript “geometric” for  $\varphi$ , since we will only study geometric phases.

We now discuss the more general situation in which we consider the adiabatic evolution of a degenerate subspace. This case was first discussed in [50]. In order to understand this case it is helpful to think about the evolution as being generated by the Berry potential and generalize from there on. The major difference is now that the components of the Berry potential are no longer scalars but matrices. In particular the components are defined as

$$\mathcal{A}_i^{jk} = i \langle A_j | \partial_i | A_k \rangle. \quad (3.17)$$

In order to calculate the adiabatic evolution we have to perform an integration over a path in parameter space again. At the same time we have to take into account that the different Berry-potential matrices along the path might not commute with each other. The correct generalization of the Berry phase  $e^{i\varphi}$  is therefore the transformation

$$U_{\text{adiabatic}} = \mathcal{P} \exp \left( \oint_{\mathcal{C}} \mathcal{A}_i d\lambda_i \right), \quad (3.18)$$

where  $\mathcal{P}$  denotes path ordering of the non-commuting matrices.

The class of gauge transformations in the general case is the class of all parameter-dependent basis transformations  $W(\boldsymbol{\lambda})$  and the Berry potential transforms as

$$|A_i\rangle \rightarrow W(\boldsymbol{\lambda})|A_i\rangle \implies \mathcal{A}_i \rightarrow W\mathcal{A}_iW^\dagger - W\partial_iW^\dagger. \quad (3.19)$$

The unitary transformation (3.18) transforms under a gauge transformation as

$$|A_i\rangle \rightarrow W(\boldsymbol{\lambda})|A_i\rangle \implies U \rightarrow W(\boldsymbol{\lambda}_{\text{initial}})UW^\dagger(\boldsymbol{\lambda}_{\text{initial}}). \quad (3.20)$$

As such it is not fully gauge invariant, but the remaining gauge freedom simply corresponds to a choice of basis for the transformation as a whole.

### 3.3 Relation between Fock Space States and Operators

We will now apply the concept of Berry phases to the degenerate ground states of topological superconductors that host Kramers pairs of Majorana bound states. We consider a systems with two such Kramers pairs, which we denote with  $X_\eta, \tilde{X}_\eta$  where  $\eta = 1, 2$ . The tilde denotes the Kramers partner of an operator. There is a gauge freedom in the choice of Kramers pairs because any pair of linear combination of the form

$$\cos \alpha_\eta X_\eta \pm \sin \alpha_\eta \tilde{X}_\eta \quad (3.21)$$

is an equally valid choice of Kramers pairs.

It will often be convenient to write Kramers pairs of Majorana fermions as an operator spinor of the form  $\mathbf{X}_\eta = (X_\eta, \tilde{X}_\eta)^T$ . This way a different gauge choice of Kramers pairs will take the form

$$e^{i\alpha_\eta \sigma_y} \mathbf{X}_\eta, \quad (3.22)$$

where  $\sigma_y$  is a Pauli matrix that operates on the spinor space.

Now in order to calculate Berry potentials we have to specify a  $\boldsymbol{\lambda}$ -dependent basis of our ground states. We obtain such a basis by forming fermionic operators out of the Majorana bound states of the form

$$D_\eta = \frac{1}{2} (X_\eta + i\tilde{X}_\eta). \quad (3.23)$$

We can now label the ground states by the occupation numbers of the  $D_\eta$  fermions. In particular we use the basis

$$\begin{aligned} &|00\rangle, \\ &|01\rangle = D_2^\dagger|00\rangle, \\ &|10\rangle = D_1^\dagger|00\rangle, \\ &|11\rangle = D_1^\dagger D_2^\dagger|00\rangle, \end{aligned} \quad (3.24)$$

where one has to keep in mind that the  $D_{\eta}$ s as well as the  $|00\rangle$  state are parameter dependent.

Before we begin the calculation of Berry potentials we will briefly discuss the role of symmetries. Because we have a parameter-dependent problem we expect that the physics is only influenced by symmetries that are present independently of the parameter values. In the case of superconductors one such symmetry is the fermion parity. Given such a symmetry and a basis that is also an eigenbasis of the symmetry operator, there are no Berry-potential terms relating states with different eigenvalues under this symmetry. This can be seen directly from (3.17). Let us assume we have a symmetry  $S$  such that  $S|A_i\rangle = \mu_i|A_i\rangle$ . Since  $S$  is assumed to be parameter independent we also have that derivatives of  $|A_i\rangle$  with respect to  $\lambda$  are eigenstates of  $S$ , because  $S\nabla_{\lambda}|A_i\rangle = \nabla_{\lambda}S|A_i\rangle = \mu_i\nabla_{\lambda}|A_i\rangle$ . As such, the derivatives of  $|A_i\rangle$  are not going to have any overlap with states that have a different eigenvalue under this symmetry and therefore corresponding Berry potentials vanish.

Following the preceding discussion we consider parity as a parameter-independent symmetry for our system. Parity conservation then implies that there are no Berry potentials between states of even parity spanned by  $|00\rangle$  and  $|11\rangle$  and states of odd parity spanned by  $|01\rangle$  and  $|10\rangle$ .

The question remains whether states with different local parity couple adiabatically. More specifically, whether there are Berry potentials between  $|01\rangle, |10\rangle$  and  $|00\rangle, |11\rangle$  respectively. An explicit calculation for the odd-parity sector gives

$$\begin{aligned} i\langle 10|\partial_i|01\rangle &= i\langle 00|D_1\partial_i D_2^\dagger|00\rangle \\ &= i\langle 00|D_1(\partial_i D_2^\dagger)|00\rangle \\ &= i\langle 00|\{D_1, \partial_i D_2^\dagger\}|00\rangle \\ &= i\{D_1, \partial_i D_2^\dagger\}. \end{aligned} \tag{3.25}$$

In the last line we assumed that the system is non-interacting. This implies that the  $D_{\eta}$ s are superpositions of fermionic single-particle operators. Therefore the same is true for their derivatives and consequently the anti-commutator is simply a c-number and the expectation value can be computed trivially. Similarly one finds for the even-parity sector

$$i\langle 00|\partial_i|11\rangle = i\{D_1^\dagger, \partial_i D_2^\dagger\}. \tag{3.26}$$

Recall that by assumption the different Kramers pairs of Majorana bound states (and therefore the  $D_{\eta}$ s) are sufficiently separated in space such that they do not overlap. This will still be true after taking derivatives, such that the operators  $D_1$  and  $\partial_i D_2^\dagger$  are spatially separated and do not have any overlap. This implies that their anti-commutators vanish and there is no mixing between different local parity states. We will show this more explicitly later on, when we discuss the BdG formulation.

We have shown that not only global parity but also local parity is conserved. Therefore there are no Berry potentials between different states and each state acquires an abelian

Berry phase independently. Hence the total transformation acting on the ground state subspace is abelian as well. This seems to contradict the non-abelian statistics, which are known for Majorana bound states in class D systems, and is especially worrisome because arguments similar to the ones we just gave seem to apply in those kind of systems. We will explain how all that fits into our formalism once we discuss braiding explicitly. For now we will only focus on adiabatic processes that do not braid the Kramers pairs of Majorana bound states in order to develop some more formalism.

An adiabatic process now simply multiplies all the basis states from equation (3.24) by different geometric phases. Because we cannot measure an overall phase, but only phase differences, we have to choose a reference phase. We choose the Berry phase which is picked up by the state  $|00\rangle$  throughout the process. It is then convenient to redefine the Berry potentials such that their integrals directly yield the phase difference to our reference phase. The redefined Berry potentials have the form

$$\mathcal{A}_i^{jj} = i\langle A_j | \partial_i | A_j \rangle - i\langle 00 | \partial_i | 00 \rangle. \quad (3.27)$$

Note that this redefinition includes the fact that only the diagonal  $jj$  components of  $\mathcal{A}$  do not vanish.

Direct calculation of the Berry potentials yields

$$\mathcal{A}_i^{10,10} = i(\langle 10 | \partial_i | 10 \rangle - \langle 00 | \partial_i | 00 \rangle) = i \left\{ D_1, \partial_i D_1^\dagger \right\}, \quad (3.28a)$$

$$\mathcal{A}_i^{01,01} = i(\langle 01 | \partial_i | 01 \rangle - \langle 00 | \partial_i | 00 \rangle) = i \left\{ D_2, \partial_i D_2^\dagger \right\}, \quad (3.28b)$$

$$\mathcal{A}_i^{11,11} = i(\langle 11 | \partial_i | 11 \rangle - \langle 00 | \partial_i | 00 \rangle) = i \left\{ D_1, \partial_i D_1^\dagger \right\} + i \left\{ D_2, \partial_i D_2^\dagger \right\}. \quad (3.28c)$$

We again assumed that the system is non-interacting in order to compute the expectation values. Interestingly all the information about phase differences is contained in the parameter dependence of the second quantized operators. This is important because it implies that those quantities can be calculated in a BdG formulation. Another important thing to note about equations (3.28) is that both fermions,  $D_\eta$ , contribute independently to the Berry potentials and therefore to the Berry phases. Hence it is meaningful to study them individually in this local basis choice.

Because we want to compare the results to the results for Majorana bound states in class D systems, we write the quantities of interest in terms of Kramers pairs of Majorana bound states. We find that the anti-commutators of the  $D_\eta$  fermions take the form

$$i \left\{ D_\eta, \partial_j D_\eta^\dagger \right\} = \frac{1}{2} \left\{ X_\eta, \partial_j \tilde{X}_\eta \right\}. \quad (3.29)$$

Therefore one of the most important Berry-potential formulas that we will use is

$$\mathcal{A}_i^\eta = \frac{1}{2} \left\{ X_\eta, \partial_i \tilde{X}_\eta \right\}. \quad (3.30)$$

This gives us Berry-phase differences

$$\varphi_\eta = \oint_C \mathcal{A}^\eta \cdot d\boldsymbol{\lambda}, \quad (3.31)$$

which are the phase differences between states with  $D_\eta^\dagger(\lambda_{\text{initial}})D_\eta(\lambda_{\text{initial}}) = 0, 1$ . The unitary transformations that correspond to those phase differences are simply given by

$$U_\eta = \exp\left(\frac{\varphi_\eta}{2} X_\eta(\lambda_{\text{initial}}) \tilde{X}_\eta(\lambda_{\text{initial}})\right). \quad (3.32)$$

Of course the unitary transformations are only defined up to an overall phase, which we do not care about. The unitary transformations for  $\eta = 1, 2$  commute and can simply be multiplied to get the total unitary transformation. This is in accordance with the previous argument, that one can study the separated Kramers pairs of Majorana fermions independently of each other. Equations (3.30), (3.31) and (3.32) set the framework for our calculations, because they relate the parameter-dependent single-particle operators of the system to the adiabatic transformation that acts on the many-body states.

Before we go ahead and calculate those quantities for actual systems we will connect them to the BdG formalism, which is very useful in practice because it is a single-particle first-quantized formalism. This means that the Hilbert space in this formalism is much smaller than in the second-quantized many body formalism. We will state the important connection between the BdG formalism and the formalism for adiabatic phases. This connection is an expression for the Berry potential in terms of BdG states.

### 3.3.1 Connection to BdG States

When dealing with non-interacting superconducting systems, that is systems where superconductivity is taken into account on the mean-field level, it is often convenient to use the BdG formalism. The starting point is a quadratic many-body Hamiltonian  $H$ , which may contain superconducting-pairing terms. We assume that  $H$  has been written in terms of local fermionic field operators  $\psi_i(x)$ , where the index  $i$  may correspond to spin and/or orbital degrees of freedom. In short we will write all local field operators together as a vector  $\boldsymbol{\psi}(x) = (\psi_1(x), \dots, \psi_n(x))^T$ . With a slight abuse of notation we also define the short notation  $\boldsymbol{\psi}^\dagger(x) = (\psi_1^\dagger(x), \dots, \psi_n^\dagger(x))^T$ , where the abuse of notation is that even though we take the adjoint on the left hand side we still define the whole expression as column vector.

The idea behind the BdG formulation is now to introduce operator spinors of the form

$$\boldsymbol{\Psi}(x) = \begin{pmatrix} \boldsymbol{\psi}(x) \\ U\boldsymbol{\psi}^\dagger(x) \end{pmatrix}, \quad (3.33)$$

where  $U$  is a unitary matrix. From this definition  $\boldsymbol{\Psi}(x)$  satisfies  $\Psi_i^\dagger(x) = P_{ij}\Psi_j(x)$  (with summation convention) where the matrix  $P$  is given by

$$P = \begin{pmatrix} 0 & U^\dagger \\ U & 0 \end{pmatrix}. \quad (3.34)$$

This matrix is closely related to the particle-hole symmetry operator  $\mathcal{P}$  which appears in the BdG formalism and which is given by

$$\mathcal{P} = P\mathcal{K}, \quad (3.35)$$

where  $\mathcal{K}$  denotes complex conjugation.

Common examples are the case where  $U$  is simply taken to be the identity in which case  $\mathcal{P} = \tau_x\mathcal{K}$ , where  $\tau_x$  denotes a Pauli matrix in particle-hole space. Another common choice is to choose  $U$  such that it maps fermions to their time-reversed partners. For spin- $\frac{1}{2}$  particles that means  $U = i\sigma_y$ , where  $\sigma_y$  denotes a Pauli matrix in spin space. In this case one has  $\mathcal{P} = \sigma_y\tau_y\mathcal{K}$ .

With the help of the spinors  $\Psi(x)$  one can rewrite any electronic Hamiltonian as

$$H = \frac{1}{2} \int dx \Psi^\dagger(x) \mathcal{H}(x) \Psi(x) + \text{const.}, \quad (3.36)$$

where  $\mathcal{H}$  is particle hole symmetric

$$\{\mathcal{H}, \mathcal{P}\} = 0 \quad (3.37)$$

and we assumed for simplicity that  $H$  is local, i.e.  $\mathcal{H}$  only depends on one position coordinate. We can now think of  $\mathcal{H}$  as a first-quantized Hamiltonian acting on  $2N$ -dimensional spinors. If we have such a spinor  $\mathbf{c}(x)$  we can associate with it a second-quantized single-particle operator,  $c$ , by defining

$$c = \int dx \mathbf{c}^\dagger(x) \Psi(x). \quad (3.38)$$

This association is useful because one can show that

$$\mathcal{H}(x)\mathbf{c}(x) = \epsilon\mathbf{c}(x) \implies [c, H] = \epsilon c, \quad (3.39)$$

which means that diagonalizing the first-quantized Hamiltonian  $\mathcal{H}$  diagonalizes the second quantized Hamiltonian  $H$  by means of (3.38).

To more directly take advantage of the first-quantized nature of the Hamiltonian  $\mathcal{H}$ , we will often discuss it and its eigenstates independently of the position basis and use Dirac notation. In particular we define  $c_i(x) = \langle i, x | c \rangle$ , where  $c_i(x)$  are the components of  $\mathbf{c}(x)$ . We will write the equivalence between operators and states given by (3.38) as  $c \equiv |c\rangle$ . For us the most important relationship between second quantization and the BdG formulation is the relationship between inner products of BdG states and anti-commutators of the corresponding fermionic operators. Given two BdG states  $|c_1\rangle, |c_2\rangle$  and the corresponding operators  $c_1, c_2$ , the relationship reads

$$\langle c_1 | c_2 \rangle = \left\{ c_1^\dagger, c_2 \right\}. \quad (3.40)$$

Equations (3.40) and (3.28) enable us to calculate Berry potentials directly from the BdG formulation, which is very useful especially for numerical calculations. With the help of (3.40) we can also more directly support the statement we made earlier about the anti-commutator  $\{D_1, \partial_i D_2^\dagger\}$ . The wave functions of the associated BdG states  $|D_1\rangle, |D_2\rangle$  are localized at different points in space and therefore have no overlap. The same is true if we take derivatives of them and consequently the anti-commutator vanishes.

Let us state the explicit form of the Berry potentials in the BdG formulation. We get

$$\mathcal{A}_\eta = \langle X | \nabla_\lambda | \tilde{X} \rangle. \quad (3.41)$$

Note the difference of a factor of two between (3.41) and (3.30). This originates from us choosing the convention  $\langle X | X \rangle = \langle \tilde{X} | \tilde{X} \rangle = 1$  instead of 2, which it should be by direct application of (3.40), because Majoranas operators anti-commute with themselves to 2. The reason for choosing this convention is that we use the BdG formulation for numerical calculations and LAPACK's<sup>1</sup> diagonalization returns vectors that are normalized to 1. Therefore Majorana fermions do not have the usual association  $c \equiv |c\rangle$ , but instead  $X \equiv \sqrt{2}|X\rangle$ .

## 3.4 Local Mixing

In this section we will focus on adiabatic manipulations that only affect one Kramers pair of Majorana bound states. The situation we have in mind is a loop in parameter space that does not exchange nor braid the Kramers pairs and after which all the Kramers pairs of Majorana bound states are back at their original positions. In this case the adiabatic transformation is described by the abelian Berry potential (3.30) but we will drop the index  $\eta$  because we are only considering one Kramers pair. We will refer to such transformations as local mixing.

The presence or absence of local mixing is very important in the context of topological quantum computation. The reason is that local mixing, by its definition, is a local adiabatic manipulation which is therefore not compatible with topological protection.

In this section we will compute non-vanishing Berry curvatures for two toy models, analytically for one model and numerically for the other. Later we will discuss in detail some sufficient symmetry conditions that guarantee the absence of local mixing. This is important because we will show later that the presence or absence of local mixing is equivalent to whether the braiding transformation of the exchange of the Kramers pairs of Majorana bound states takes a particularly simple path-independent form or not.

### 3.4.1 Analytical Toy Model

We construct our analytical toy model starting from the model of two Kitaev chains, which transform into each other under time-reversal symmetry. We consider these two

<sup>1</sup>LAPACK is a standard linear-algebra library, which is used by most higher level programming languages to perform linear-algebra calculations

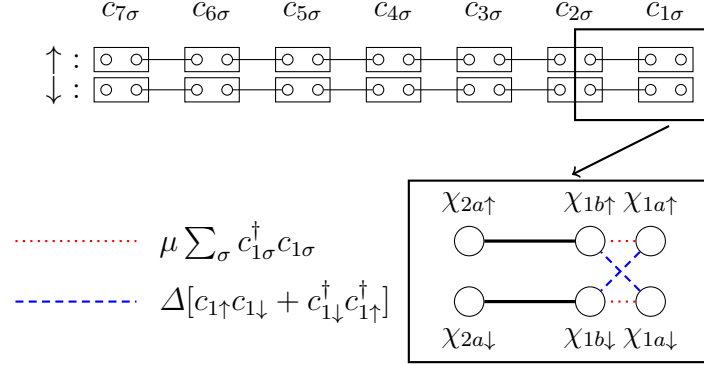


Fig. 3.1: The figure shows our DIII model, which is built out of two Kitaev chains at the topological-dimerization point in parameter space. The rectangles correspond to the original electronic states, and the circles to their decomposition into Majorana operators. Lines indicate couplings. Our model consists out of the indicated end of the wire with one Kramers pair of Majorana bound states and a Kramers pair of bulk states. Furthermore it is illustrated how a local chemical potential and s-wave pairing couple the Majorana operators in our model. Blue dashed lines represent s-wave pairing and red dotted lines the chemical potential. Importantly the s-wave pairing couples the two initial Kitaev chains.

chains at the topological-dimerization point in parameter space where they have an unpaired Majorana bound state at each end. With those parameter values there are Kramers pairs of Majorana bound states perfectly localized at both ends of the chains. For our analytical toy model we consider one of these Kramers pairs of Majorana bound states as well as the Kramers pair of bulk states right next to it. In order to observe interesting adiabatic physics we introduce additional coupling parameters: a chemical potential term and an s-wave pairing term on the last fermionic site of the two Kitaev chains. The situation is depicted in figure 3.1. The Hamiltonian has the form

$$H = H_{\text{bulk}} + H_{\mu} + H_{\Delta}. \quad (3.42)$$

The bulk Hamiltonian is given by

$$H_{\text{bulk}} = \frac{E_g}{2} \sum_{\sigma} i\chi_{2a\sigma}\chi_{1b\sigma}. \quad (3.43)$$

The chemical potential term on the last site has the form

$$\begin{aligned} H_{\mu} &= \mu \sum_{\sigma} c_{1\sigma}^{\dagger} c_{1\sigma} \\ &= \frac{\mu}{2} \sum_{\sigma} i\chi_{1a\sigma}\chi_{1b\sigma} + \text{const.} \end{aligned} \quad (3.44)$$

The additional s-wave pairing Hamiltonian has the form

$$\begin{aligned} H_{\Delta} &= \Delta \left( c_{1\uparrow} c_{1\downarrow} + c_{1\downarrow}^{\dagger} c_{1\uparrow}^{\dagger} \right) \\ &= \frac{\Delta}{2} (i\chi_{1a\uparrow}\chi_{1b\downarrow} + i\chi_{b\uparrow}\chi_{1a\downarrow}). \end{aligned} \quad (3.45)$$

If we only consider  $H_{\text{bulk}}$  then by construction the Majorana bound states are  $\chi_{1a\sigma}$ . If we also introduce the other couplings we have to solve for the new parameter-dependent zero-energy Majorana bound states, which we denote with  $X$  and  $\tilde{X}$  in accordance with our convention that parameter-dependent quantities are denoted by capitalized letters.

We find  $X$  by solving for

$$[H, X] = 0. \quad (3.46)$$

$\tilde{X}$  is simply found by means of  $\mathcal{T}$ , namely

$$\tilde{X} = \mathcal{T}X\mathcal{T}^{-1}. \quad (3.47)$$

This way we find  $X$  and  $\tilde{X}$  to be

$$\begin{aligned} X &= \cos\theta\chi_{1a\uparrow} - \sin\theta(\cos\alpha\chi_{2a\uparrow} + \sin\alpha\chi_{2a\downarrow}), \\ \tilde{X} &= \cos\theta\chi_{1a\uparrow} - \sin\theta(\cos\alpha\chi_{2a\uparrow} - \sin\alpha\chi_{2a\downarrow}), \end{aligned} \quad (3.48)$$

where we parametrized the Majorana bound states using the two angles  $\theta$  and  $\alpha$ . We define  $\alpha$  by

$$\begin{aligned} \mu &= \sqrt{\mu^2 + \Delta^2} \cos\alpha, \\ \Delta &= \sqrt{\mu^2 + \Delta^2} \sin\alpha \end{aligned} \quad (3.49)$$

and  $\theta$  by

$$\tan\theta = \frac{\sqrt{\mu^2 + \Delta^2}}{E_g}. \quad (3.50)$$

The parameters  $\alpha$  and  $\theta$  can be interpreted as follows. How much our initial Kramers pair  $\chi_{1a\uparrow}, \chi_{1a\downarrow}$  is mixed with the bulk is controlled by  $\theta$ . Here  $\theta = 0$  corresponds to the initial Kramers pair and  $\theta = \frac{\pi}{2}$  corresponds to a Kramers pair of Majorana fermions that has no overlap with the initial Kramers pair. One can interpret  $\alpha$  as follows. It controls how much the individual Kramers partners get mixed within their own spin direction as opposed to the opposite one.

We now calculate the Berry potential according to equation (3.30). We find

$$\begin{aligned} \mathcal{A}_{\theta} &= 0, \\ \mathcal{A}_{\alpha} &= -\frac{1}{2} \sin^2\theta. \end{aligned} \quad (3.51)$$

It can easily be seen that this can lead to non-zero Berry phases. In particular we can make a loop in parameter space by taking  $\alpha = 0 \rightarrow 2\pi$ . Because the Berry potential is

$\alpha$ -independent, we get a Berry phase of  $\varphi = -\pi \sin^2 \theta$ , which is clearly finite. Therefore our simple toy model demonstrates local mixing. We also calculate the Berry curvature with respect to  $\alpha$  and  $\theta$  and find

$$\Omega_{\alpha\theta} = \sin \theta \cos \theta. \quad (3.52)$$

Before we proceed to our numerical demonstration of local mixing, we discuss some important aspects of the toy-model result. In particular we saw that varying  $\alpha$  alone gives us a Berry phase. The same is not true for  $\theta$ . As discussed earlier  $\alpha$  controls how the initial Kramers pair of Majorana fermions gets mixed within the two different wires as opposed to between them. Note, however, that even for a generic value of  $\alpha$  (corresponding to a finite  $\Delta$ ), a change in  $\theta$  does not contribute to the Berry phase. This is because for fixed  $\alpha$  one could choose a different spin directions in which one has two decoupled wires (or wire ends for that matter). Therefore it is important that  $\alpha$  changes making it impossible to decompose the system into independent wires throughout the entire process.

### 3.4.2 Numerical Demonstration of Local Mixing

We will now numerically demonstrate local mixing. This way we can study a slightly more complicated model, that does not rely on perfectly localized Kramers pairs of Majorana bound states. We will study a single-particle BdG Hamiltonian of a wire with two Kramers pairs of Majorana bound states. As we discussed earlier the Berry potential is now given by (3.41), such that we can calculate Berry phases according to (3.31) or the Berry curvature equivalent. For numerical studies it is usually more convenient to work with the Berry curvature, because it is gauge independent, and numerical eigenstates usually have a random gauge. So unless one does explicit gauge fixing, which we will do later when we study braiding, the Berry curvature is more convenient to work with. The explicit expression of the Berry Curvature for Majorana bound states is given by

$$\Omega_{\lambda_i \lambda_j} = \sum_N \frac{1}{E_N^2} [\langle X | (\partial_{\lambda_i} \mathcal{H}) | N \rangle \langle N | (\partial_{\lambda_j} \mathcal{H}) | \tilde{X} \rangle - \langle X | (\partial_{\lambda_j} \mathcal{H}) | N \rangle \langle N | (\partial_{\lambda_i} \mathcal{H}) | \tilde{X} \rangle], \quad (3.53)$$

where the sum is over all (parameter-dependent) bulk states  $N$  with eigenenergies  $E_N$ .

For our BdG Hamiltonian we choose the spinor convention

$$\Psi(x) = (\psi_{\uparrow}(x), \psi_{\downarrow}(x), \psi_{\downarrow}^{\dagger}(x), -\psi_{\uparrow}^{\dagger}(x))^{\text{T}}.$$

This way the particle-hole operator takes the form  $\mathcal{P} = \sigma_y \tau_y \mathcal{K}$  and the time-reversal operator takes the form  $\mathcal{T} = i \sigma_y \mathcal{K}$ , as mentioned earlier. Here the  $\tau$ s denote Pauli matrices in particle-hole space and  $\sigma$ s denote Pauli matrices in spin space.

With the given conventions the BdG Hamiltonian that we study reads

$$\mathcal{H} = \left( \frac{p^2}{2m} - \mu(x) \right) \tau_z + p(\boldsymbol{\alpha} \cdot \boldsymbol{\sigma}) \tau_z + p(\mathbf{v}_{\Delta} \cdot \boldsymbol{\sigma}) \tau_x + \Delta \tau_x. \quad (3.54)$$

This Hamiltonian describes a one-dimensional system with p-wave pairing  $\mathbf{v}_\Delta$ , s-wave pairing  $\Delta$ , and spin-orbit interaction  $\boldsymbol{\alpha}$ . For  $\boldsymbol{\alpha} = 0$ ,  $\Delta = 0$  and  $\mathbf{v}_\Delta = (v_x, 0, 0)^T$  this model is the continuum version of two Kitaev wires with opposite spin and p-wave pairing.

For certain parameters the Hamiltonian (3.54) is in its topological phase. This can be controlled by the chemical-potential term, such that the Hamiltonian is in the topological phase for  $\mu > \mu_c$  and in the trivial phase for  $\mu < \mu_c$ , where  $\mu_c$  is some critical value. The precise value of  $\mu_c$  is determined by the other parameters of the Hamiltonian, but we will not provide an explicit expression. The important thing to remember is that there will be a Kramers pair of Majorana bound states at the phase boundary between the topological phase and the trivial phase. Therefore the chemical potential term in the Hamiltonian (3.54) is position dependent, such that we can create a phase boundary. In particular we choose the position dependence

$$\mu(x) = \mu_0 + \mu \tanh\left(\frac{x - x_0}{w}\right), \quad (3.55)$$

where  $\mu_0$  and  $\mu$  will be chosen such that  $\mu(x)$  crosses  $\mu_c$  close to  $x_0$ . Therefore there will be a Kramers pair of Majorana bound states close to  $x_0$ . We will study local mixing of this Kramers pair as we change the parameters  $\mu_0$  and  $w$ . Note that these parameters do not couple to spin as they only appear in the chemical potential, but as we will see they can still cause local mixing.

In order to see that there is finite local mixing we calculate the Berry curvature, which is shown in the inset of figure 3.2. Although the values of the Berry curvature are small they are finite. We also want to study how they depend on the other parameters of the system. In order to do that we calculate the Berry curvature for a specific point in the  $\mu_0 w$ -plane and look at its dependence as a function of the other parameters. This is depicted in figure 3.2. This is of course insufficient to calculate any Berry phases because they involve an integral of the Berry curvature over an area in  $\mu_0 w$ -plane, but because the Berry curvature seems fairly smooth in the color plot, even studying a single point will give us some good indication of the Berry curvature's parameter dependence.

We study the parameter dependence as follows. We start with the Hamiltonian with  $\boldsymbol{\alpha} = \Delta = 0$  and  $\mathbf{v}_\Delta = (v_x, 0, 0)^T$ , where it corresponds to two decoupled Kitaev wires. Here we expect a vanishing Berry curvature, because we calculate it with respect to parameters that do not couple these two Kitaev wires. Afterwards we increase one of the spin-orbit-coupling parameters or  $\Delta$  and look for changes in the Berry curvature. Figure 3.2 clearly shows that for one direction of spin-orbit coupling as well as for s-wave pairing, we get a finite Berry curvature. In the next subsection we will discuss in detail how one can understand that there is local mixing for some parameter values but not for others. We will do that in the context of studying sufficient conditions that guarantee the absence of local mixing. Before we get there we will discuss some technical but important aspects of the numerical calculations.

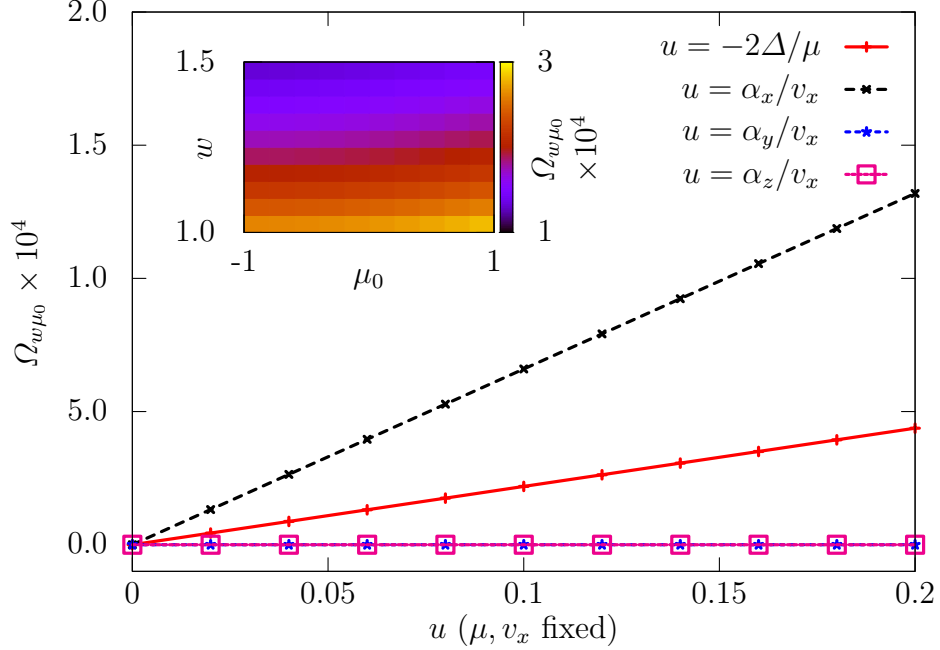


Fig. 3.2: The plot shows the Berry curvature for the Hamiltonian (3.54) with  $m = 1$ ,  $\mu = 10$ ,  $\mu_0 = 0$ ,  $\mathbf{v}_\Delta = (5, 0, 0)^T$  and  $\Delta = \boldsymbol{\alpha} = 0$ . It is plotted as a function of different dimensionless parameters on the  $x$ -axis. The key shows the meaning of the dimensionless parameters for each individual plot. The inset shows a larger area of the Berry curvature for the case  $\alpha_x/v_x = 0.2$ . The unit of length for all plots is 1. The total wire has a length of 40.

### Identifying Majorana Bound States in Numerical Diagonalization

The technical issue we want to discuss is related to the study of single Kramers pairs of Majorana bound states, that are not split by the finite length of the wire. Because we can always obtain the Kramers partner by applying  $\mathcal{T}$  we will only discuss the issue of how to obtain single Majorana bound states that are not split by finite size.

First of all, let us be more specific about what we mean when we say “not split by finite size”. We mean that the splitting is below the accuracy of our numerical calculation.

We start by discussing how to obtain Majorana bound states in the situation when they are actually slightly split and then discuss the problems that arise once that assumption is no longer true. When they are slightly split we are going to have two fermionic states  $|d\rangle$  and  $|\bar{d}\rangle$  such that

$$\begin{aligned} \mathcal{H}|d\rangle &= \varepsilon|d\rangle, \\ \mathcal{H}|\bar{d}\rangle &= -\varepsilon|\bar{d}\rangle, \\ \mathcal{P}|d\rangle &\propto |\bar{d}\rangle. \end{aligned} \tag{3.56}$$

For our purpose the most important consequence of this is that  $\langle d|\mathcal{P}|d\rangle = 0$ , because the states are eigenvectors with different eigenvalues. This will no longer be true when we consider degenerate states ( $\varepsilon = 0$ ).

We can now define the two operators

$$\begin{aligned} M_1 &= \frac{1}{\sqrt{2}}(\mathbb{1} + \mathcal{P}), \\ M_2 &= \frac{i}{\sqrt{2}}(\mathbb{1} - \mathcal{P}), \end{aligned} \tag{3.57}$$

which respectively particle-hole symmetrize or anti-symmetrize a state. We can now define two Majorana states as  $|\chi_1\rangle = M_1|d\rangle$  and  $|\chi_2\rangle = M_2|d\rangle$ . The orthogonality of  $|d\rangle$  and  $\mathcal{P}|d\rangle$  guarantees that  $|\chi_1\rangle$  and  $|\chi_2\rangle$  are normalized and in particular cannot be zero. Even though we now found two Majorana states, we actually want to find the localized Majorana states  $|\chi_L\rangle$  and  $|\chi_R\rangle$  and generally the two states we found are superpositions of the two localized states. We expect to have

$$\begin{aligned} |\chi_1\rangle &= \cos\beta_0|\chi_L\rangle + \sin\beta_0|\chi_R\rangle, \\ |\chi_2\rangle &= -\sin\beta_0|\chi_L\rangle + \cos\beta_0|\chi_R\rangle, \end{aligned} \tag{3.58}$$

for some arbitrary angle  $\beta_0$ . The most systematic way to obtain the localized Majorana states is to define new angle-dependent symmetrized and anti-symmetrized states as

$$\begin{aligned} |\chi_1^\beta\rangle &= M_1 e^{i\beta}|d\rangle, \\ |\chi_2^\beta\rangle &= M_2 e^{i\beta}|d\rangle. \end{aligned} \tag{3.59}$$

We can now express those states again in terms of the localized basis and obtain

$$\begin{aligned} |\chi_1^\beta\rangle &= \cos(\beta_0 + \beta)|\chi_L\rangle + \sin(\beta_0 + \beta)|\chi_R\rangle, \\ |\chi_2^\beta\rangle &= -\sin(\beta_0 + \beta)|\chi_L\rangle + \cos(\beta_0 + \beta)|\chi_R\rangle. \end{aligned} \tag{3.60}$$

The goal is to find  $\beta = -\beta_0$  such that the Majorana states we constructed are the localized ones.

The problem of finding the right value of  $\beta$  can be phrased as a simple optimization problem. All we need is a quantity that measures how localized on a particular side a state is. This quantity could for instance be the norm of a state that has been projected onto the left half of the system. The advantage of this procedure, for slightly split Majorana bound states, is that it makes sure that the Majorana states are guaranteed to be a superposition of the states  $|d\rangle$  and  $|\bar{d}\rangle$ .

We now consider the case where the Majorana bound states do not have any overlap. In this case the particle-hole conjugate of a state, which we obtain numerically, is not necessarily orthogonal to that state. In particular that means that given a zero-energy eigenstate, it does not necessarily correspond to a fermionic state. We will therefore

denote it with  $|\varphi_0\rangle$  instead of  $|d\rangle$ . Generally a zero-energy state will have the form  $|\varphi_0\rangle = a|\chi_L\rangle + b|\chi_R\rangle$ , where  $a$  and  $b$  are arbitrary complex numbers. We can again form states  $|\chi_1\rangle$  and  $|\chi_2\rangle$  by means of the operators (3.57), but this time this will not result in properly normalized Majorana states. Consider for example the case where both  $a$  and  $b$  are real. We then have  $|\chi_1\rangle = \sqrt{2}(a|\chi_L\rangle + b|\chi_R\rangle)$  and  $|\chi_2\rangle = 0$ . Inserting an additional phase  $\beta$  into the calculation, as we did above, will mix the states  $|\chi_1\rangle$  and  $|\chi_2\rangle$ , but we will never obtain a localized Majorana bound state in this way.

Since the phase procedure discussed above does not work we do a projection in real space of e.g.  $|\chi_1\rangle$ . If we project onto the left part of the wire, the projected state will not contain  $|\chi_R\rangle$ . We then possibly retain a non-normalized Majorana state on the left. If we can reliably normalize it, we achieve our goal and obtained a localized Majorana bound state. The problem is that this may lead to considerable numerical errors if the amplitude of our non-normalized Majorana is too small or zero. To prevent this the normalization procedure should only be performed if the initial weight is high enough. If it is not, one repeats the procedure with  $|\chi_2\rangle$ . If the weight is still not large enough, one starts anew with a different zero-energy state  $|\varphi'_0\rangle$ . Because the zero energy states that one obtains numerically are still orthogonal, one of them is guaranteed to have sufficient weight on the left.

The projection in real space does not commute with our Hamiltonian. Therefore we have to ensure that the resulting state is still a zero-energy eigenstate. We do this by calculating the norm of  $\mathcal{H}|\chi_{\text{projected}}\rangle$  and comparing it to the gap of the system. If this is smaller than a certain chosen precision, we have a localized Majorana bound state. This can be thought of as a variational method for finding the localized Majorana bound states, but essentially it is just a systematized way to ensure that the wave function is localized on one end. As an equation the final condition reads

$$\frac{\langle\chi_{\text{projected}}|\mathcal{H}^2|\chi_{\text{projected}}\rangle}{E_{\text{gap}}^2} < \epsilon, \quad (3.61)$$

where  $\epsilon$  is the required precision. In most numerical experiments we chose  $\epsilon = 10^{-5}$ .

### 3.4.3 Sufficient Conditions for the Absence of Local Mixing

We will now discuss sufficient conditions for the absence of local mixing in detail. We discuss it in detail, because we will argue later that the braiding transformation of Kramers pairs of Majorana bound states simplifies and becomes path-independent in the absence of local mixing.

The basic idea comes from the model of two copies of the Kitaev chain. It is obvious that there will be no local mixing as long as the two chains are not coupled. Of course, even if we introduce some coupling it could be the case that we can decompose the model in a different way into two uncoupled chains. In fact time-reversal symmetry actually guarantees that we can decompose the model at each point in parameter space into two chains which are each others Kramers partners. The question arises why this did not

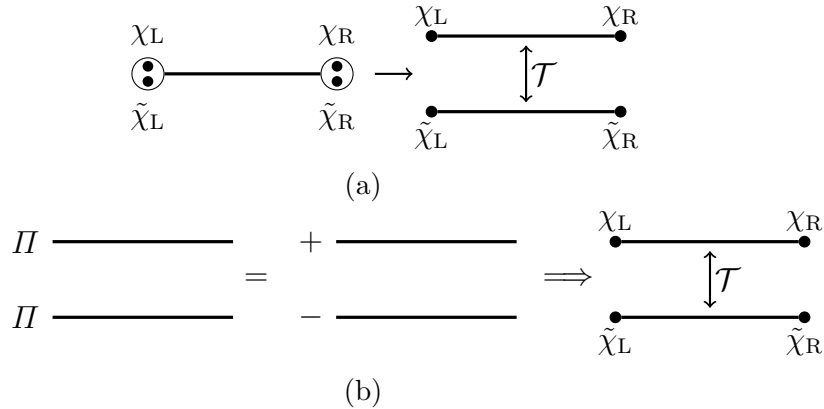


Fig. 3.3: Figure (a) is a sketch of how time-reversal symmetry can always decompose a system into two subsystems that are related by time-reversal symmetry. Figure (b) is an illustration of a symmetry  $\Pi$  that allows for the same decomposition.

prevent local mixing. The reason is that, even though time-reversal symmetry guarantees such a decomposition, this decomposition may change as a function of the parameters and as such does not constrain the adiabatic evolution. We therefore look for symmetries that decompose the system analogously to time-reversal symmetry, but do not depend on parameters. This situation is illustrated in figure 3.3.

We will only consider BdG Hamiltonians and study symmetries of these. We call the symmetry operator, which we are looking for,  $\Pi$  and assume that its eigenvalues will have magnitude one.  $\Pi$  is supposed to decompose the system into two parts which are related by time reversal symmetry. This condition can easily be satisfied by requiring

$$\{\Pi, \mathcal{T}\} = 0.$$

This way the part of the system with eigenvalue  $+1$  is the Kramers partner of the part of the system with eigenvalue  $-1$ . This condition is for example satisfied by  $U(1)$  spin-rotation symmetries such as  $\sigma_x$ ,  $\sigma_y$  and  $\sigma_z$ . Interestingly our numerical results show that spin-rotation symmetry does not prevent local mixing. In particular figure 3.2 shows finite local mixing for the case of the Hamiltonian (3.54) with  $\boldsymbol{\alpha} = 0$ ,  $\mathbf{v}_\Delta = (v_x, 0, 0)^T$  and  $\Delta$  finite. In this case the Hamiltonian is clearly  $\sigma_x$ -symmetric. Consequently we have to constrain  $\Pi$  more to exclude spin-rotation symmetries.

Spin rotation-symmetries have to be excluded because Majorana bound states are actually never eigenstates of spin. If we consider a single “spin-up” Kitaev wire at the topological-dimerization point in parameter space, then the Majorana state at the end of the wire has the form  $\chi_{a\uparrow} = c_\uparrow^\dagger + c_\uparrow$ . This means it is a superposition of an electron with spin up and a missing electron with spin up, which is a spin-down hole. Actually a single Kitaev wire does not consist of a single spin direction, but out of spin-up electrons and spin-down holes. We only used the terminologies spin-up/spin-down wires for convenience and we will continue to do so when no confusion is possible. With respect to figure 3.3b

it means that  $\Pi$  only implies the  $\mathcal{T}$  relationship, but not the Majorana bound states at the end of the individual wires.

The Majorana bound states not being spin eigenstates means that if we decompose the wire into two wires using a spin symmetry, then the Majorana bound states necessarily have some weight in both wires. As such the symmetry does not help us to make statements about them. We solve this problem by considering what distinguishes Majorana bound states from other choices of zero-energy states. Majorana bound states are eigenstates of the particle-hole operator  $\mathcal{P}$ , because this is the BdG equivalent of self-adjoint single-particle operators in second quantization. So if we want to ensure that the eigenstates of our symmetry operator  $\Pi$  are also eigenstates of  $\mathcal{P}$ , we have to require

$$[\Pi, \mathcal{P}] = 0.$$

Since the requirements we discussed so far turn out to be sufficient, we summarize them before proving the absence of local mixing in that case. For a parameter-dependent BdG Hamiltonian  $\mathcal{H}(\boldsymbol{\lambda})$  we require a parameter-independent symmetry operator  $\Pi$  such that

$$[\mathcal{H}(\boldsymbol{\lambda}), \Pi] = 0, \tag{3.62a}$$

$$\{\mathcal{T}, \Pi\} = 0, \tag{3.62b}$$

$$[\mathcal{P}, \Pi] = 0. \tag{3.62c}$$

We now demonstrate how such a symmetry  $\Pi$  can be used to choose a gauge in which the Berry potential vanishes identically. The gauge choice is such that the parameter-dependent Majorana states are also eigenstates of  $\Pi$ . In particular we require

$$\begin{aligned} \Pi|X(\boldsymbol{\lambda})\rangle &= +|X(\boldsymbol{\lambda})\rangle, \\ \Pi|\tilde{X}(\boldsymbol{\lambda})\rangle &= -|\tilde{X}(\boldsymbol{\lambda})\rangle, \end{aligned} \tag{3.63}$$

where we made the  $\boldsymbol{\lambda}$ -dependence explicit. We now briefly discuss how our assumptions (3.62) went into (3.63). We choose simultaneous eigenstates of  $\mathcal{H}$ ,  $\Pi$  and  $\mathcal{P}$ , which is only possible if all these operators commute pairwise. By our assumptions (3.62a) and (3.62c) this is the case. The only thing one might be worried about is that  $\mathcal{H}$  and  $\mathcal{P}$  are actually anti-commuting instead of commuting. This is related to the question whether it is always possible to choose a Majorana basis for the zero energy states, which is a more fundamental question than the one we address here. For completeness we give the argument for the statement that  $\mathcal{H}$  and  $\mathcal{P}$  commute on the zero-energy subspace of the Hilbert space. Given that  $\mathcal{H}$  and  $\mathcal{P}$  anti-commute we have  $[\mathcal{H}, \mathcal{P}] = -2\mathcal{P}\mathcal{H}$ , which is clearly zero on the zero-energy subspace of  $\mathcal{H}$ . The last assumption that went into (3.63) is (3.62b) and it results in  $X$  and  $\tilde{X}$  having opposite eigenvalues with respect to  $\Pi$ .

Given the basis choice (3.63) it is easy to see that  $\partial_i|\tilde{X}(\boldsymbol{\lambda})\rangle$  is also an eigenstate of  $\Pi$  with eigenvalue  $-1$  because

$$\begin{aligned} \Pi\partial_i|\tilde{X}(\boldsymbol{\lambda})\rangle &= \partial_i\Pi|\tilde{X}(\boldsymbol{\lambda})\rangle \\ &= -\partial_i|\tilde{X}(\boldsymbol{\lambda})\rangle, \end{aligned} \tag{3.64}$$

where we used that  $\Pi$  is  $\lambda$  independent. It now follows that all the Berry potentials are zero, because when we calculate them according to (3.41) we calculate the inner product between two eigenvectors of  $\Pi$  with different eigenvalues. This has to be zero for any hermitian operator  $\Pi$ .

We will now discuss how to systematically find symmetries  $\Pi$  and apply it to our numerical model.

### Systematically Finding $\Pi$

We now describe a practical strategy for finding  $\Pi$ . The idea is to construct a basis for hermitian operators that fulfill (3.62b) and (3.62c). Subsequently we attempt to construct an operator out of this basis that commutes with the Hamiltonian, that is an operator that fulfills (3.62a).

We start with a basis for all hermitian matrices which we decompose as follows into a tensor product out of the following constituents. There are particle-hole Pauli matrices  $\tau_i$ , spin Pauli matrices  $\sigma_i$  and matrices describing any remaining orbital structure  $\lambda_i$ . We assume that we have a particularly chosen basis for the  $\lambda_i$ , such that its members are either fully real or imaginary. We denote these by  $\lambda_i^R$  and  $\lambda_i^I$  respectively. This choice of basis for the  $\lambda_i$  is helpful with respect to time-reversal symmetry.

It turns out to be most convenient to work with the chiral symmetry operator  $\mathcal{C}$  instead of either  $\mathcal{T}$  or  $\mathcal{P}$ .  $\mathcal{C}$  is defined as

$$\mathcal{C} = \mathcal{T}\mathcal{P}. \quad (3.65)$$

The advantage of working with  $\mathcal{C}$  is that it is linear as opposed to anti-linear. We choose to work with  $\mathcal{C}$  and  $\mathcal{T}$ . The conditions that the elements in our  $\Pi$ -operator basis have to fulfill are then  $\{\mathcal{C}, \Pi\} = [\mathcal{T}, \Pi] = 0$ , which means that (3.62c) is replaced by

$$\{\mathcal{C}, \Pi\} = 0. \quad (3.66)$$

If (3.62b) and (3.66) are satisfied, (3.62c) will be as well.

We will now construct a basis for the  $\Pi$  operators for the choices of  $\mathcal{T}$  and  $\mathcal{P}$ , which we used earlier. Those where  $\mathcal{T} = i\sigma_y\mathcal{K}$  and  $\mathcal{P} = \sigma_y\tau_y\mathcal{K}$ . In that case  $\mathcal{C} = i\tau_y$ . The requirement (3.66) implies that the basis operators have to be proportional to  $\tau_x$  or  $\tau_z$ . The next constraint is (3.62b). This means that the operators have to be either proportional to a spin Pauli matrix  $\sigma_i$  or they have to be fully imaginary, which means proportional to  $\lambda_i^I$ . Putting everything together we obtain the basis

$$\{\lambda_i^R\sigma_j\tau_x, \lambda_i^R\sigma_j\tau_z, \lambda_i^I\tau_x, \lambda_i^I\tau_z\}. \quad (3.67)$$

We assume that the real  $\lambda$  matrices contain the identity matrix in  $\lambda$  space, so we also have basis elements that effectively do not operate in  $\lambda$  space. Contrary to this the Pauli matrices here do not contain an identity element  $\sigma_0$ , because it transforms differently under time reversal.

We will now apply this to our numerical study. In that case we do not have any orbital degrees of freedom, so we only have  $\lambda^R = 1$  and no imaginary  $\lambda$ s. Because of the chemical potential in the Hamiltonian, basis elements proportional to  $\tau_z$  cannot appear in  $\Pi$ . Similarly the s-wave pairing term eliminates terms proportional to  $\tau_z$ , so if we have both a chemical-potential term and an s-wave term we cannot find a  $\Pi$  operator. We will therefore assume that  $\Delta = 0$ . In that case there are three basis operators remaining and we can construct a  $\Pi$  operator of the form  $\Pi_{\hat{l}} = \hat{l} \cdot \boldsymbol{\sigma} \tau_z$ , where  $\hat{l}$  is a unit vector. The condition that it commutes with the other terms in the Hamiltonian becomes

$$\begin{aligned} 0 &= [\mathcal{H}_{\boldsymbol{\alpha}}, \Pi_{\hat{l}}] = 2i(\boldsymbol{\alpha} \times \hat{l}) \cdot \boldsymbol{\sigma}, \\ 0 &= [\mathcal{H}_{\mathbf{v}_{\Delta}}, \Pi_{\hat{l}}] = -ip(\mathbf{v}_{\Delta} \cdot \hat{l})\tau_y, \end{aligned} \tag{3.68}$$

The first condition requires  $\hat{l} \parallel \boldsymbol{\alpha}$  whereas the second one requires  $\hat{l} \perp \mathbf{v}_{\Delta}$ . Hence we can find a symmetry that prevents local mixing if  $\boldsymbol{\alpha} \perp \mathbf{v}_{\Delta}$  as well as  $\Delta = 0$ . This is in complete agreement with the numerical results, which we presented earlier.

There is an obvious generalization of our symmetry condition. It comes from the fact that we used global symmetries to make statements about localized states. All the above arguments would still hold if the symmetry conditions are only satisfied locally around the Kramers pairs of Majorana bound states. This might be helpful because one might be able to induce local symmetries at least approximately by means of tuning.

### 3.5 Braiding of Kramers pairs of Majorana Bound States

In this section we study braiding of Kramers pairs of Majorana bound states. In contrast to the previous section we therefore have to consider two Kramers pairs at the same time. We use the local basis (3.24) and will study braiding in the case of a simple toy model.

There is an issue with the local basis choice (3.24). After we have exchanged the two Kramers pairs of Majorana fermions this basis will not go back to itself because by definition of the exchange  $D_1(\boldsymbol{\lambda}_{\text{final}}) \propto D_2(\boldsymbol{\lambda}_{\text{initial}})$  and  $D_2(\boldsymbol{\lambda}_{\text{final}}) \propto D_1(\boldsymbol{\lambda}_{\text{initial}})$ . This is a problem because having the same basis after a loop in parameter space was precisely what got rid of some ambiguities of the Berry phases and made them well-defined quantities. We can correct for this basis mismatch by transforming the basis after the exchange from the final to the initial basis. This way the transformation of the exchange decomposes into

$$U = BU_{\text{local}}, \tag{3.69}$$

where  $U_{\text{local}}$  is similar to the local transformations from the previous section with the difference that the path in the integral corresponding to (3.31) is not closed but goes from  $\boldsymbol{\lambda}_{\text{initial}}$  to  $\boldsymbol{\lambda}_{\text{final}}$ .  $B$  is determined as the transformation that takes the final  $D$ s back to the initial ones. Equivalently in terms of the Kramers pairs of Majorana bound states, it is defined by the requirement that

$$B\mathbf{X}_{\eta}^{\text{final}}B^{\dagger} = \mathbf{X}_{\eta}^{\text{initial}}. \tag{3.70}$$

One might be worried about the transformation properties of equation (3.69) under gauge transformations. First of all it is clear that the decomposition can only hold as long as we restrict ourselves to local gauge transformations. Under a gauge transformation  $W(\boldsymbol{\lambda})$  the operator  $U$  should transform according to equation (3.20). We explicitly show that this relation holds for our decomposition (3.69) under local gauge transformations, which have the form

$$W_{\text{local}} = e^{f_1(\boldsymbol{\lambda})X_1\tilde{X}_1}e^{f_2(\boldsymbol{\lambda})X_2\tilde{X}_2}. \quad (3.71)$$

This is important, because we will show below that  $B$  and  $U_{\text{local}}$  do not satisfy the same transformation property individually.

We denote  $W_{\text{local}}(\boldsymbol{\lambda}_{\text{initial/final}})$  by  $W_{i/f}$  respectively. It follows directly from  $B\mathbf{X}_\eta^{\text{final}}B^\dagger = \mathbf{X}_\eta^{\text{initial}}$  that

$$W_i B W_f^\dagger W_f \mathbf{X}_\eta^{\text{final}} W_f^\dagger W_f B^\dagger W_i^\dagger = W_i \mathbf{X}_\eta^{\text{initial}} W_i^\dagger.$$

Hence  $B$  transforms as

$$B \rightarrow W_i B W_f^\dagger.$$

If one replaces  $X_\eta, \tilde{X}_\eta$  by  $W_{\text{local}}X_\eta W_{\text{local}}^\dagger, W_{\text{local}}^\dagger\tilde{X}_\eta W_{\text{local}}$  in (3.30) and calculates (3.31) one easily finds that the local phases transform as  $\varphi_\eta \rightarrow \varphi_\eta + (2f_\eta(\boldsymbol{\lambda}_{\text{final}}) - 2f_\eta(\boldsymbol{\lambda}_{\text{initial}}))$ , from which it follows that  $U_{\text{local}}$  transforms as

$$U_{\text{local}} \rightarrow W_f U_{\text{local}} W_i^\dagger.$$

Hence neither  $B$  nor  $U_{\text{local}}$  transform according to (3.20), in particular because they depend on the gauge choice at  $\boldsymbol{\lambda}_{\text{final}}$ . This dependence however drops out of their product, such that  $U$  indeed fulfills (3.20) proving that our decomposition (3.69) is valid for any local gauge choice.

A pictorial representation of the decomposition (3.69) is given in figure 3.4, where the circles represent Kramers pairs and the gauge freedom in the choice of Kramers partners is represented by the choice of angle at which the circles are split into two halves.

## Application to Class D

Before we study our toy model for class DIII systems, we demonstrate how the same ideas apply (even though quite trivially) to class D systems. In class D systems we only have two well-separated Majorana bound states  $X_1$  and  $X_2$ . We can form a fermion out of these states of the form  $D = \frac{1}{2}(X_1 + iX_2)$ . With this fermion we can specify a basis for the ground states as

$$|0\rangle, D^\dagger|0\rangle.$$

Similar to before, the continuous Berry phase difference between these states is generated by the Berry potential  $\mathcal{A} = \frac{1}{2}\{X_1, \nabla_\lambda X_2\}$ . Because the two Majorana bound states are spatially separated, the Berry potential vanishes identically. This corresponds to

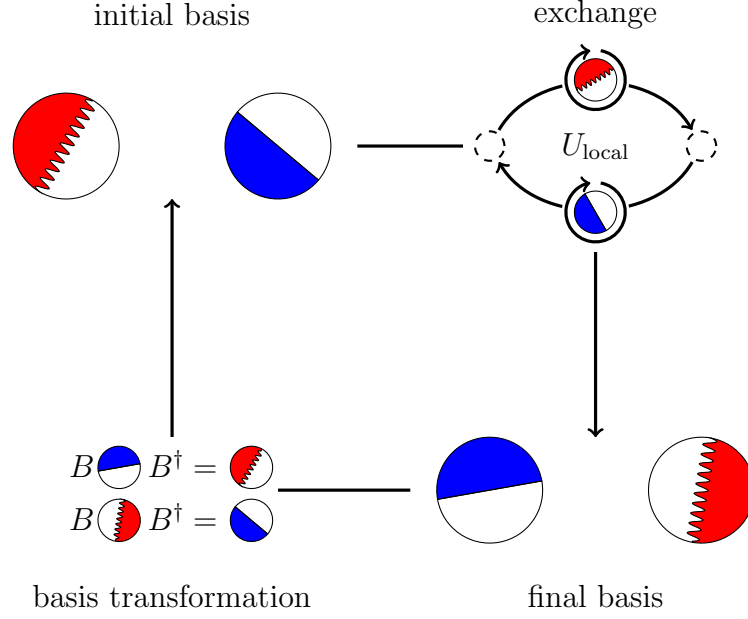


Fig. 3.4: This figure shows a pictorial representation of the decomposition (3.69). A loop in parameter space is achieved by a continuous exchange followed by a basis transformation. The circles represent Kramers pairs of Majorana fermions. The ambiguity of dividing a circle into two halves represents the gauge freedom in choosing Kramers partners. Two different lines and colors are used to divide the circles to distinguish the two Kramers pairs.

$U_{\text{local}} = \mathbb{1}$  in equation (3.69). Therefore all the braiding statistics in class D are generated by  $B$ . The conditions for  $B$  in this case are

$$\begin{aligned} BX_1^{\text{final}} B^\dagger &= X_1^{\text{initial}}, \\ BX_2^{\text{final}} B^\dagger &= X_2^{\text{initial}}. \end{aligned} \quad (3.72)$$

By definition of the exchange we have that  $X_{1/2}^{\text{final}} \propto X_{2/1}^{\text{initial}}$ . Since Majorana fermions are self-adjoint, the proportionality constants can only be  $\pm 1$ . This way the equations (3.72) become

$$\begin{aligned} Bs_1 X_2^{\text{initial}} B^\dagger &= X_1^{\text{initial}}, \\ Bs_2 X_1^{\text{initial}} B^\dagger &= X_2^{\text{initial}}, \end{aligned} \quad (3.73)$$

where  $s_1$  and  $s_2$  are signs. The rest of the argument is the same as the usual argument why Majorana fermions obey their particular braiding statistics. The idea is that fermion parity is conserved throughout the exchange and it is given by  $P = \text{si}X_1X_2$ , where  $s$  is

again a sign factor. Therefore we have

$$\begin{aligned} P &= \text{si}X_1^{\text{initial}}X_2^{\text{initial}} \\ &= \text{si}X_1^{\text{final}}X_2^{\text{final}} \\ &= s_1s_2\text{si}X_2^{\text{initial}}X_1^{\text{initial}}. \end{aligned}$$

It follows that  $s_1s_2 = -1$  due to parity conservation. If one inserts this into equation (3.73) one obtains the well-known equation

$$B = U = \exp\left(\pm\frac{\pi}{4}X_1^{\text{initial}}X_2^{\text{initial}}\right).$$

The remaining sign cannot be determined from general arguments and depends on the details of the system and exchange, in particular whether one exchanges in a clockwise or counterclockwise direction.

Even though the usual argument for the class D statistics is only the last part of the argument presented here, we presented it in a larger context, which will be important for class DIII.

### 3.5.1 Toy Model

The toy model that we study is the time-reversal symmetric analog of braiding by tuning couplings [43]. It consists out of four Kramers pairs of Majorana fermions  $\chi_i, \tilde{\chi}_i = \mathcal{T}\chi_i\mathcal{T}^{-1}$ , which we again write as spinors  $\boldsymbol{\chi}_i = (\chi_i, \tilde{\chi}_i)^T$ . The Hamiltonian will be build out of coupling terms between Kramers pairs of Majorana fermions. The coupling between Kramers pair  $i$  and  $j$  takes the form

$$H_{ij} = it\boldsymbol{\chi}_i^T\sigma_z e^{i\beta_{ij}\sigma_y}\boldsymbol{\chi}_j. \quad (3.74)$$

This is the most general form of a time-reversal invariant coupling between two Kramers pairs.

In the toy model there will be exactly three coupling terms,  $H_{41}$ ,  $H_{42}$  and  $H_{43}$ . So we have  $H = aH_{41} + bH_{42} + cH_{43}$ , where  $a, b, c$  are parameter dependent. In order to have the appropriate ground-state degeneracy at every point in parameter space, there is at least one non-zero coupling and at most two at each point in parameter space. This way there always exist exactly two zero-energy Kramers pairs of Majorana bound states at every point in parameter space. Furthermore, only the relative coupling strength between Kramers pairs of Majorana fermions is important, therefore we parametrize the Hamiltonian generally as

$$H = \cos\theta H_{ij} + \sin\theta H_{ik}, \quad (3.75)$$

where  $\theta$  controls the relative strength of the two couplings. We will refer to this Hamiltonian as a switching Hamiltonian, because changing  $\theta$  from 0 to  $\frac{\pi}{2}$  moves a zero energy Kramers pair from site  $k$  to site  $j$ . This situation is depicted in figure 3.5. Strictly

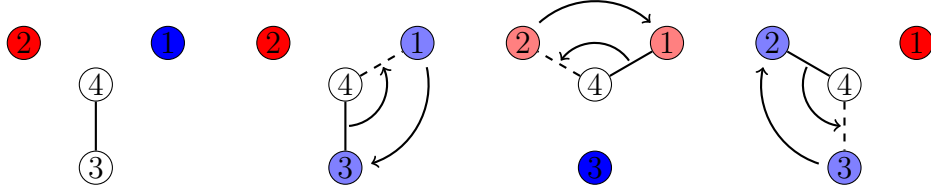


Fig. 3.5: Each circle denotes a site with a Kramers pair of Majorana fermions. The two different colors denote the two Kramers pairs of Majorana bound states. Lines between the sites denote couplings. As a single coupling is switched from one position to the next, the corresponding Kramers pair of Majorana bound states moves in the opposite direction. Note that the sites label the static basis and therefore the numbers do not change.

speaking we have different parameters  $\theta$  for the different switching processes, but because it will be possible to understand everything from a single switching process, we will not add additional indices to  $\theta$ .

We already know how to calculate  $U_{\text{local}}$  from our discussions of local mixing. In order to calculate  $B$  it is therefore important to find  $\mathbf{X}_\eta^{\text{final}}$ . We do that by finding the initial and final states of each switching process individually and then piecing them together.

During each individual switching process one of the Kramers pairs of Majorana bound states does not change (for a given local gauge choice). We study what happens to the other one by solving  $[H, \mathbf{X}_\eta] = 0$  for the Hamiltonian (3.75). We find

$$\mathbf{X}_\eta = e^{i\alpha\sigma_y} \left( \cos \theta e^{i\beta_{ij}\sigma_y} \boldsymbol{\chi}_j - \sin \theta e^{i\beta_{ik}\sigma_y} \boldsymbol{\chi}_k \right), \quad (3.76)$$

where  $\alpha$  is an arbitrary gauge choice that may depend on the  $\beta$ s and  $\theta$ .

We want to patch three switching processes together such that  $\mathbf{X}_\eta$  is continuous. In order to do that conveniently, we pick a particular parameter dependence for  $\alpha$ , such that  $\mathbf{X}_\eta(\theta = 0) = \pm \boldsymbol{\chi}_j$  and  $\mathbf{X}_\eta(\theta = \frac{\pi}{2}) = \mp \boldsymbol{\chi}_k$ . The sign change is motivated by analogy to switching processes for single Majorana bound states in class D systems. A particular gauge choice of  $\alpha$ , which gives the desired  $\mathbf{X}_\eta$  at  $\theta = 0, \frac{\pi}{2}$ , is

$$\alpha_\pm = -\beta_{ij} \cos \theta - \beta_{ik} \sin \theta + (1 \mp 1) \frac{\pi}{2}.$$

Table 3.1 shows  $\mathbf{X}_\eta$  initially and after each switching process. It has exactly the same structure as for single class D Majorana bound states. During the process the initial Kramers pairs transform into the final ones according to

$$\begin{aligned} \mathbf{X}_1^{\text{initial}} = \boldsymbol{\chi}_1 &\rightarrow \mathbf{X}_1^{\text{final}} = \boldsymbol{\chi}_2, \\ \mathbf{X}_2^{\text{initial}} = \boldsymbol{\chi}_2 &\rightarrow \mathbf{X}_2^{\text{final}} = -\boldsymbol{\chi}_1. \end{aligned} \quad (3.77)$$

Therefore the basis transformation that generates this transformation is simply

$$B = \exp \left( \frac{\pi}{4} (\boldsymbol{\chi}_1 \boldsymbol{\chi}_2 + \tilde{\boldsymbol{\chi}}_1 \tilde{\boldsymbol{\chi}}_2) \right), \quad (3.78)$$

	$H_{43}$	$H_{41}$	$H_{42}$	$H_{43}$
$\mathbf{X}_1$	$\chi_1$	$-\chi_3$	$-\chi_3$	$\chi_2$
$\mathbf{X}_2$	$\chi_2$	$\chi_2$	$-\chi_1$	$-\chi_1$

Tab. 3.1: The table shows the instantaneous  $\mathbf{X}_\eta$  between switching processes. The instantaneous  $\mathbf{X}_\eta$  are required to be continuous. Therefore the initial and final conditions of the individual switching processes have to match. The braiding process is of the form depicted in figure 3.5.

which is structurally the same as two independent braiding transformations of pairs of Majorana bound state. According to (3.69) the total braiding transformation is

$$U = \exp\left(\frac{\pi}{4}(\chi_1\chi_2 + \tilde{\chi}_1\tilde{\chi}_2)\right) \exp\left(\frac{\varphi_1}{2}\chi_1\tilde{\chi}_1 + \frac{\varphi_2}{2}\chi_2\tilde{\chi}_2\right). \quad (3.79)$$

The question arises how general the transformation (3.79) is. After all it was derived in the context of our simple toy model. From the construction it is clear that we can always choose a local gauge such that (3.77) holds and therefore (3.78) remain true, even in a more complicated system. Therefore the question about the generality of equation (3.79) reduces to the question of how general our  $U_{\text{local}}$  is. We argued earlier that we have local parity conservation which means the quantities  $D_\eta^\dagger D_\eta = \frac{i}{2}X_\eta\tilde{X}_\eta + \frac{1}{2}$  are conserved. This means that the  $D_\eta$  fermions can only pick up phases, which is equivalent to the mixing of the Kramers pairs described by equation (3.32). Therefore  $U_{\text{local}}$  is fully general, which implies that (3.79) is fully general.

The general transformation (3.79) that we found contains path-dependent phases, which means that the transformation cannot be used for topological quantum computation. The natural question to ask is whether there are additional conditions under which these phases become path independent. It turns out that the question of whether there is any path dependence in (3.79) is equivalent to the question whether there is local mixing. The absence of local mixing is equivalent to path independence and the presence of local mixing is equivalent to path dependence.

As we mentioned already in the context of local mixing, if the phases in (3.79) are path independent, then there cannot be any local mixing. Otherwise we could append a local mixing path to a braiding path and we would obtain a transformation with different phases. We will now argue that the converse is also true and that in the absence of local mixing the transformation can always be brought into a particular form.

To show that in the absence of local mixing there is no path dependence in the phases  $\varphi_\eta$ , we assume that we have two braiding paths 1 and 2 such that the mixing angles along those paths are  $\varphi_\eta$  and  $\bar{\varphi}_\eta$ . The corresponding braiding transformations are given by  $U$  and  $\bar{U}$ . We can now form a local mixing operation  $\bar{U}^\dagger U$  with mixing angles  $\varphi_\eta - \bar{\varphi}_\eta$ ,

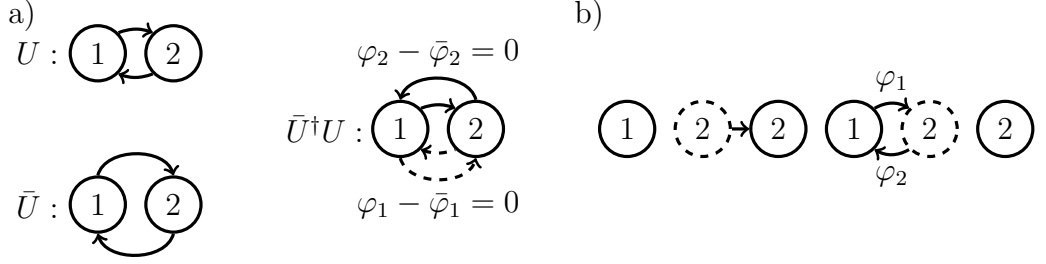


Fig. 3.6: (a) Two exchanges along different paths can be combined into two local operations (solid and dashed line). Consequently the mixing angles are path independent if local mixing angles are zero. (b) One Kramers pair gets moved out of the way for the other to make a loop. During the first half pair 1 rotates by  $\varphi_1$  and during the second half it rotates by  $\varphi_2$ . If there is no local mixing this implies  $\varphi_1 + \varphi_2 = 0$ .

but since there is no local mixing by assumption, we have  $\varphi_\eta - \bar{\varphi}_\eta = 0$ . Therefore the  $\varphi_\eta$  are path independent. The argument is illustrated in figure 3.6a).

We now argue that for path-independent phases we necessarily have  $\varphi_1 = -\varphi_2$ . For our simple toy model this can be verified by means of a straightforward calculation of  $U_{\text{local}}$ , but we give a more general argument instead.  $U_{\text{local}}$  always decomposes into two independent local rotations. Therefore the phase picked up by one Kramers pair of Majorana bound states does not depend on the other Kramers pair. We can therefore imagine moving the second Kramers pair a little out of the way such that the first Kramers pair can make a loop which does not encircle the second one, but passes through the initial position of the second one. During the first half of this loop the Kramers pair, e.g.  $\mathbf{X}_1$ , will acquire a mixing angle  $\varphi_1$ , the same it would acquire during an exchange. During the second half of this loop  $\mathbf{X}_1$  will acquire a mixing angle  $\varphi_2$ , the same which  $\mathbf{X}_2$  would have acquired during an exchange. The absence of local mixing now implies that  $\varphi_1 + \varphi_2 = 0$ , which we wanted to show. The situation is illustrated in figure 3.6b).

Now that we showed that in the absence of local mixing we have  $\varphi_1 = -\varphi_2$ , we can bring equation (3.79) to a particularly simple form. We can do this by means of the gauge transformation  $W = e^{\frac{\varphi_1}{4}\chi_1\tilde{\chi}_1} e^{-\frac{\varphi_1}{4}\chi_2\tilde{\chi}_2}$ , such that

$$WUW^\dagger = \exp\left(\frac{\pi}{4}(\chi_1\chi_2 + \tilde{\chi}_1\tilde{\chi}_2)\right). \quad (3.80)$$

The transformation is, of course, only meaningful because the  $\varphi_\eta$  do not depend on the specific braiding path, otherwise we would need a different transformation for each path. In this simplified form of the transformation, (3.80) corresponds to two independent exchanges of Majorana bound states  $\chi_1, \chi_2$  and  $\tilde{\chi}_1, \tilde{\chi}_2$  respectively.

The question arises how to physically interpret the particular gauge choice that simplifies the transformation. This question can only be answered in the context of criteria that guarantee the absence of local mixing to begin with. In particular the

sufficient symmetry condition which we discussed earlier allowed us to choose a gauge that decomposes the system into two independent parts that are each others time-reversed partners and that do not get mixed throughout the process. In that case this gauge choice will be precisely the one leading to the simplified transformation (3.80).

### 3.5.2 Numerical Simulation

As the last part of this chapter we discuss numerical simulations of braiding of Kramers pairs of Majorana bound states. In particular we will discuss how we can dynamically exploit the gauge freedom to obtain the braiding transformation very efficiently. We will then demonstrate braiding in the absence and presence of local mixing.

Let us consider the decomposition (3.69) again. We discussed earlier how  $U$  and  $B$  transform under gauge transformations. In particular we can choose bases for which  $U_{\text{local}}$ 's local phases  $\varphi_\eta$  take any value. We exploit this to choose a gauge where  $U_{\text{local}} = \mathbb{1}$ . This way we simply have  $U = B$ , which means that the Berry potential disappeared from the calculation. This is ideal for numerical calculations because in order to calculate the Berry potential, one has to numerically take derivatives. Therefore for this particular gauge choice the braiding path in parameter space does not need to be discretized in such a fine grid as to allow for the approximation of derivatives.

All that is left to discuss is how to actually make the preferable gauge choice in practice. In order to do that let us assume that we have  $N$  numerical solutions for a Kramers pair of Majorana bound states for a discretized approximation to the braiding path. We will denote those states with  $|X_n\rangle$  and  $|\tilde{X}_n\rangle$ , where  $n = 1 \dots N$ , denotes position along the braiding path. This means that we already obtained Majorana bound states from the numerical solutions by the method described earlier, but they are not necessarily in the  $U_{\text{local}} = \mathbb{1}$  gauge. We will now obtain this gauge by successively rotating the Kramers pairs. We will denote the rotated pairs with  $|X_n^R\rangle$  and  $|\tilde{X}_n^R\rangle$ . Because we only rotate the Kramers pairs relative to each other the starting point is arbitrary and we simply set  $|X_1^R\rangle = |X_1\rangle$  and  $|\tilde{X}_1^R\rangle = |\tilde{X}_1\rangle$ . We will now describe how to obtain  $|X_{n+1}^R\rangle, |\tilde{X}_{n+1}^R\rangle$  from  $|X_n^R\rangle, |\tilde{X}_n^R\rangle$  and  $|X_{n+1}\rangle, |\tilde{X}_{n+1}\rangle$ .

In order to calculate the rotation we assume that the Kramers pair at  $n$  still has some overlap with the Kramers pair at  $n + 1$ , but this overlap does not need to be large. We can therefore write the Kramers pair at  $n + 1$  in terms of the eigenbasis at  $n$ . It will be a superposition of the  $n$ th Kramers pair (because we assumed overlap) and some particle-hole symmetric combination of bulk states. Additionally it is very important that the  $n$ th Kramers pair may appear rotated in this decomposition. Therefore we have

$$\begin{aligned} |X_{n+1}\rangle &= \cos \theta R(\varphi) |X_n^R\rangle + \sin \theta |\chi_{\text{bulk},n}\rangle \\ |\tilde{X}_{n+1}\rangle &= \cos \theta R(\varphi) |\tilde{X}_n^R\rangle + \sin \theta \mathcal{T} |\chi_{\text{bulk},n}\rangle, \end{aligned} \tag{3.81}$$

where  $R(\varphi)$  is the rotation we referred to and  $|\chi_{\text{bulk},n}\rangle$  is a particle-hole symmetric linear

combination of bulk states. The rotation matrix is given by

$$\begin{aligned} R(\varphi)|X_n\rangle &= \cos\varphi|X_n\rangle + \sin\varphi|\tilde{X}_n\rangle \\ R(\varphi)|\tilde{X}_n\rangle &= -\sin\varphi|X_n\rangle + \cos\varphi|\tilde{X}_n\rangle, \end{aligned} \quad (3.82)$$

and is fully determined by the parameter  $\varphi$ . Up to a factor of  $\cos\theta$ ,  $R(\varphi)$  is given by the matrix elements  $\langle X_n^R|X_{n+1}\rangle$ ,  $\langle \tilde{X}_n^R|X_{n+1}\rangle$ ,  $\langle X_n^R|\tilde{X}_{n+1}\rangle$  and  $\langle \tilde{X}_n^R|\tilde{X}_{n+1}\rangle$ . The factor of  $\cos\theta$  can be obtained by solving  $\langle X_n^R|X_{n+1}\rangle^2 + \langle \tilde{X}_n^R|X_{n+1}\rangle^2 = \cos^2\theta$ . Therefore  $R(\varphi)$  is easily calculated. We then define

$$\begin{aligned} |X_{n+1}^R\rangle &= R(\varphi)^\dagger|X_{n+1}\rangle = \cos\varphi|X_{n+1}\rangle - \sin\varphi|\tilde{X}_{n+1}\rangle, \\ |\tilde{X}_{n+1}^R\rangle &= R(\varphi)^\dagger|\tilde{X}_{n+1}\rangle = \sin\varphi|X_{n+1}\rangle + \cos\varphi|\tilde{X}_{n+1}\rangle. \end{aligned} \quad (3.83)$$

It can now easily be verified that the discrete analog of the Berry potential vanishes:

$$\begin{aligned} \langle X_n^R| \left( |\tilde{X}_{n+1}^R\rangle - |\tilde{X}_n^R\rangle \right) &= \langle X_n^R| \left( (\cos\theta - 1)|\tilde{X}_n^R\rangle + \sin\theta \mathcal{T}R|X_{\text{bulk},n}\rangle \right) \\ &= 0. \end{aligned} \quad (3.84)$$

Therefore our new gauge given by the bases  $|X_n^R\rangle$  and  $|\tilde{X}_n^R\rangle$  satisfies  $U_{\text{local}} = \mathbf{1}$ . In order to obtain this gauge choice we had to calculate  $R(\varphi)$ , for which we had to divide by  $\cos\theta$ , which described the overlap of consecutive Kramers pairs. Therefore for this procedure the discretization has to be fine enough such that  $\cos\theta$  is not too small. This is far less restrictive than requiring a discretization which is fine enough to approximate derivatives well.

After fixing the gauge for both sequences of Kramers pairs of Majorana bound states we still need to calculate  $B$ . For this we only need the states  $|\tilde{X}_{1,1}^R\rangle$ ,  $|\tilde{X}_{2,1}^R\rangle$ ,  $|\tilde{X}_{1,N}^R\rangle$ ,  $|\tilde{X}_{2,N}^R\rangle$  and their Kramers partners. Here the first index denotes the two Kramers pairs respectively and the second index denotes the position along the discretized braiding path. Note that all the work from the gauge fixing procedure described above enters in the properly gauged final states at position  $N$ , which are only obtained after consecutively rotating the whole sequence of bases. We now calculate the rotation matrices  $R(\varphi_\eta)$  which relate  $|\tilde{X}_{1,1}^R\rangle$ ,  $|\tilde{X}_{2,N}^R\rangle$  and their Kramers partners and  $|\tilde{X}_{2,1}^R\rangle$ ,  $-|\tilde{X}_{1,N}^R\rangle$  and their Kramers partners. Note the minus sign, which is in accordance with our earlier conventions. With the  $\varphi_\eta$ s from these rotation matrices the braiding transformation is given by (3.79).

We will now describe our actual numerical simulation. We consider a Y-junction, which we describe by a block Hamiltonian with 4 blocks on the diagonal. Three blocks describe the one-dimensional arms of the Y. The fourth block is a single site for the only purpose of coupling the other three blocks. The only additional finite entries in the Hamiltonian couple the last site of every wire block to our additional 1-site coupling block. To supplement our theory on braiding of Kramers pairs of Majorana fermions, we plot the sum  $\varphi_1 + \varphi_2$  for different braiding situations with and without local mixing. Without local mixing the sum should vanish and otherwise we expect it to be finite. The

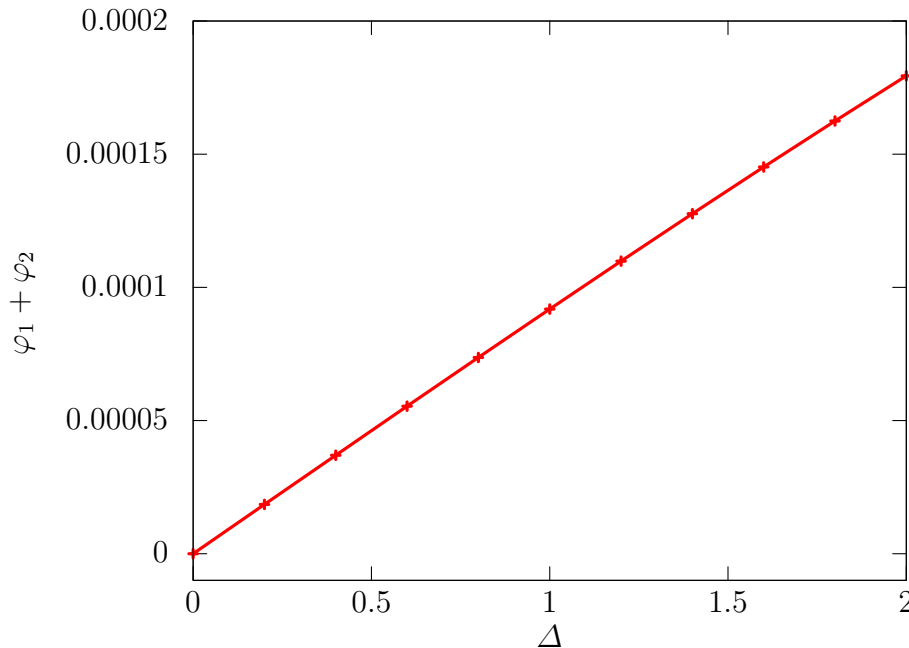


Fig. 3.7: The plot shows the sum of the phases, which the two Kramers pairs pick up after one exchange, as a function of s-wave pairing. Without s-wave pairing the sum vanishes and therefore the process can be mapped to the independent exchange of two pairs of Majorana bound states. For finite s-wave pairing the sum of the phases is finite and therefore such a mapping is no longer possible.

parameters that are changing are the positions of the phase boundaries to which the Kramers pairs of Majorana bound states are pinned. Figure 3.7 shows the sum  $\varphi_1 + \varphi_2$  as a function of s-wave pairing. The sum is clearly finite for finite s-wave pairing. This is consistent with our earlier results, which showed that s-wave pairing induces local mixing.

### 3.6 Summary

In this chapter we studied braiding of Kramers pairs of Majorana bound states as they appear in class DIII topological superconductors in one and two dimensions. We constructed a detailed framework relating the Berry phases of the many-body Fock-space states to the second quantized single-particle operators and to BdG states. We used this to show that local adiabatic manipulations of Kramers pairs of Majorana bound states are possible. This implies that Kramers pairs of Majorana bound states cannot be used for topological quantum computation. We termed this local manipulation local mixing and also discussed sufficient symmetry conditions of the BdG Hamiltonian that guarantee the absence of local mixing. Finally we classified the possible transformations

that can be achieved as a result of braiding Kramers pairs of Majorana bound states. We did this in the context of a simple toy model but argued that the result is as general as symmetries allow. Generally braiding leads to path-dependent transformations as we already expected from the local mixing results. Interestingly the absence of local mixing is enough to guarantee the path independence of the braiding transformation. Furthermore in the absence of local mixing the braiding transformation takes a particularly simple form for a certain basis choice. In that form it corresponds to two independent braiding transformations of two Majorana bound states and their Kramers partners respectively. We also used our theoretical framework for braiding to perform numerical braiding simulations for a Y-junction using a BdG calculation. In particular we exploited that a certain gauge choice allows one to calculate the braiding outcome without the need of taking derivatives numerically, which allows for a more coarse discretization and therefore decreases the numerical effort.

## 4 Topologically Non-Trivial DIII Phase Through Interactions

In this chapter we study how interactions can help to achieve a topologically non-trivial phase in one-dimensional class DIII systems. For non-interacting systems it is well understood for which parameter values one-dimensional DIII systems will be in a topological phase. In particular it is understood which relative magnitudes the superconducting-pairing terms need to have [22, 24]. The problem with those parameter values is that they cannot be attained without electron-electron interaction [20, 51]. It is therefore important to study DIII phases in the presence of interactions. This has been studied by several authors in the context of mean-field theory both analytically [11] and numerically [24]. It was also studied in the case of attractive interactions in the spin sector [32]. We will consider the case of repulsive interactions and perform a renormalization group (RG) analysis to investigate the effect of interactions. This is a natural generalization of the existing work.

In the first part of this chapter we will introduce the general framework in which we will work and then comment on the connection between the non-trivial topological phase and interactions in general. This is an important point, because the general classification of topological phases is only valid for non-interacting systems. We will therefore discuss when an interacting one-dimensional class DIII phase is topologically non-trivial, and how that relates to the non-interacting case. This discussion will partially follow [32]. Afterwards we begin with the (RG) analysis. In particular we will use a result that relates second-order perturbative flow equations to coefficients of operator product expansions (OPE) [10]. The focus will be on the application of this particular result instead of its derivation. We explicitly present the calculations for a simple case that can be treated analytically to a large extent and later state the generalized flow equations which can only be solved numerically.

### 4.1 Fixed-Point System and Perturbations

In this section we will first specify the non-interacting Hamiltonian of the system that we want to study. We will then bosonize the individual terms, add interactions and define the perturbations for which we will perform an RG analysis.

The starting point is a spinful linearized low-energy Hamiltonian for free electrons, where each spin direction has the form of equation (2.15). The Hamiltonian has the form

$$H_0 = iv_F \sum_{\sigma} \int dx \left[ -\psi_{\sigma}^{\dagger}(x) \partial_x \psi_{\sigma}(x) + \bar{\psi}_{\sigma}^{\dagger}(x) \partial_x \bar{\psi}_{\sigma}(x) \right]. \quad (4.1)$$

Note that we assume the same Fermi velocity  $v_F$  for all the electrons, which means that the Hamiltonian is  $SU(2)$  symmetric additionally to being time-reversal symmetric.

Additionally to the free Hamiltonian we consider induced superconducting pairing. We consider singlet and triplet pairing. The Hamiltonian for the singlet pairing is

$$H = \Delta_s \int dx (\psi_\uparrow(x)\bar{\psi}_\downarrow(x) - \psi_\downarrow(x)\bar{\psi}_\uparrow(x) + \text{h.c.}). \quad (4.2)$$

The triplet pairing is assumed to be the result of a combination of induced singlet pairing and some inversion symmetry breaking. Therefore we only consider  $m = 0$  triplet pairing. The Hamiltonian is

$$H = -\Delta_t \int dx (\psi_\uparrow(x)\bar{\psi}_\downarrow(x) + \psi_\downarrow(x)\bar{\psi}_\uparrow(x) + \text{h.c.}). \quad (4.3)$$

We will now translate the Hamiltonians to their bosonized forms. The free electron part  $H_0$  translates in the usual way to

$$H = \frac{1}{2\pi} \sum_\sigma \int dx [(\partial_x \varphi_\sigma)^2 + (\partial_x \theta_\sigma)^2]. \quad (4.4)$$

Since want to include interactions we will use the charge and spin sector defined in (2.50), instead of spin-up and spin-down sectors. For convenience let us restate the translation rules for the bosons (2.49) but in terms of charge- and spin-sector fields. We have

$$\begin{aligned} \psi_\sigma^\dagger(x) &= \frac{\eta_\sigma}{\sqrt{2\pi}} e^{2i\phi_\sigma(x)} & \bar{\psi}_\sigma^\dagger(x) &= \frac{\eta_\sigma}{\sqrt{2\pi}} e^{-2i\bar{\phi}_\sigma(x)} \\ &= \frac{\eta_\sigma}{\sqrt{2\pi}} e^{\frac{i}{\sqrt{2}}(\varphi_c + \sigma\varphi_s - \theta_c - \sigma\theta_s)} & &= \frac{\eta_\sigma}{\sqrt{2\pi}} e^{\frac{i}{\sqrt{2}}(-\varphi_c - \sigma\varphi_s - \theta_c - \sigma\theta_s)}, \end{aligned} \quad (4.5)$$

where  $\sigma$  as a prefactor is 1 for  $\uparrow$  and  $-1$  for  $\downarrow$ .

The superconducting terms take the following forms. For the singlet pairing we get

$$\begin{aligned} H_s &= \frac{\Delta_s}{2\pi} \int dx \left( \eta_\uparrow \eta_\downarrow e^{-2i(\phi_\uparrow - \bar{\phi}_\downarrow)} - \eta_\downarrow \eta_\uparrow e^{-2i(\phi_\downarrow - \bar{\phi}_\uparrow)} + \text{h.c.} \right) \\ &= i\eta_\uparrow \eta_\downarrow \frac{\Delta_s}{\pi} \int dx \left( \sin(-2(\phi_\uparrow - \bar{\phi}_\downarrow)) + \sin(-2(\phi_\downarrow - \bar{\phi}_\uparrow)) \right) \\ &= i\eta_\uparrow \eta_\downarrow \frac{\Delta_s}{\pi} \int dx \left( \sin(\sqrt{2}(\theta_c - \varphi_s)) + \sin(\sqrt{2}(\theta_c + \varphi_s)) \right) \\ &= i\eta_\uparrow \eta_\downarrow \frac{2\Delta_s}{\pi} \int dx \sin(\sqrt{2}\theta_c) \cos(\sqrt{2}\varphi_s). \end{aligned} \quad (4.6)$$

Similarly one finds for the triplet pairing

$$H_t = i\eta_\uparrow \eta_\downarrow \frac{2\Delta_t}{\pi} \int dx \cos(\sqrt{2}\theta_c) \sin(\sqrt{2}\varphi_s). \quad (4.7)$$

Because the Klein factors will not appear anywhere else, we replace the combination  $i\eta_\uparrow\eta_\downarrow$  with its eigenvalues  $\pm 1$ . For the most part the signs of the singlet and triplet pairing will not play a role and therefore we will simply replace  $i\eta_\uparrow\eta_\downarrow$  with 1.

It is very useful to realize that the superconducting-pairing terms only depend on  $\theta_c$  and  $\varphi_s$ . When we include interactions we will get an additional non-quadratic backscattering term, which will also only depend on  $\varphi_s$ . It is therefore possible to formulate the whole interacting problem in terms of an action  $S[\theta_c, \varphi_s]$ . The fixed point part is  $S_0[\theta_c, \varphi_s] = S_0[\theta_c] + S_0[\varphi_s]$ , where

$$S_0[\theta_c] = \frac{K_c}{2\pi} \iint d\tau dx [(\partial_\tau \theta_c)^2 + (\partial_x \theta_c)^2], \quad (4.8)$$

and

$$S_0[\varphi_s] = \frac{1}{2\pi K_s} \iint d\tau dx [(\partial_\tau \varphi_s)^2 + (\partial_x \varphi_s)^2]. \quad (4.9)$$

It is important to note that these actions actually describe fixed points for all values of  $K_s$  and  $K_c$ . Additional to the fixed point action we have perturbations away from the fixed points. They are

$$S_s[\theta_c, \varphi_s] = \frac{2\Delta_s}{\pi} \iint d\tau dx \sin(\sqrt{2}\theta_c) \cos(\sqrt{2}\varphi_s), \quad (4.10)$$

$$S_t[\theta_c, \varphi_s] = \frac{2\Delta_t}{\pi} \iint d\tau dx \cos(\sqrt{2}\theta_c) \sin(\sqrt{2}\varphi_s), \quad (4.11)$$

$$S_{bs}[\varphi_s] = \frac{\lambda_{bs}}{2\pi^2} \iint d\tau dx \cos(\sqrt{8}\varphi_s). \quad (4.12)$$

For the renormalization group method that we are going to use we have to write our perturbations in the form

$$S_{\text{pert}} = \sum_i g_i a^{x_i-2} \iint d\tau dx O_i(x, \tau), \quad (4.13)$$

where the  $g_i$  are the coupling constants for which we will calculate the flow,  $a$  is the small scale cutoff and  $x_i$  the scaling dimension of the operator  $O_i$ . The purpose of this particular form of the perturbations is to make the coupling constants  $g_i$  dimensionless such that they can be compared with each other. In order for the  $g_i$  to be dimensionless it is important that the cutoff is not part of the  $O_i$  and their correlation functions in the sense discussed in chapter 2. The simplest way to account for the cutoff is to work in units of the cutoff and restore units when necessary such that the  $g_i$  are unitless.

There is an ambiguity in the choice of the of the initial  $g_i^0$  and the normalization of the operators  $O_i$ . The ambiguity can readily be seen by the trivial scaling  $g_i \rightarrow cg_i$  and  $O_i \rightarrow c^{-1}O_i$ . It is therefore important to specify all the perturbation operators explicitly, together with their initial conditions for the coupling constants. During the renormalization-group transformations additional perturbations will be generated, but

for these the normalization can be determined later because the initial condition for the coupling constants are going to be zero.

For the perturbation operators and the initial coupling constants we choose

$$g_s^0 = \frac{\Delta_s}{\pi} \quad O_s = 2 \sin(\sqrt{2}\theta_c) \cos(\sqrt{2}\varphi_s), \quad (4.14)$$

$$g_t^0 = \frac{\Delta_t}{\pi} \quad O_t = 2 \cos(\sqrt{2}\theta_c) \sin(\sqrt{2}\varphi_s), \quad (4.15)$$

$$g_{bs}^0 = \frac{\lambda_{bs}}{\sqrt{8}\pi^2} \quad O_{bs} = \sqrt{2} \cos(\sqrt{8}\varphi_s). \quad (4.16)$$

In order to have a more systematic notation we will change the subscripts to numbers. We replace  $s \rightarrow 1$ ,  $t \rightarrow 2$  and  $bs \rightarrow 3$ . Additionally to these perturbations the renormalization group flow will generate other perturbations to the fixed point action. The corresponding operators  $O_i$  are

$$\begin{aligned} O_4 &= ((\partial_x \varphi_s)^2 + (\partial_\tau \varphi_s)^2) \\ &= 4\partial_z \varphi_s \partial_{\bar{z}} \varphi_s, \end{aligned} \quad (4.17)$$

$$\begin{aligned} O_5 &= ((\partial_x \theta_c)^2 + \partial_\tau \theta_c)^2) \\ &= 4\partial_z \theta_c \partial_{\bar{z}} \theta_c, \end{aligned} \quad (4.18)$$

$$\begin{aligned} O_6 &= \sqrt{2} (\partial_\tau \theta_c \partial_\tau \varphi_s + \partial_x \theta_c \partial_x \varphi_s) \\ &= \sqrt{8} (\partial_z \theta_c \partial_{\bar{z}} \varphi_s + \partial_{\bar{z}} \theta_c \partial_z \varphi_s), \end{aligned} \quad (4.19)$$

$$O_7 = \sqrt{2} \cos(\sqrt{8}\theta_c). \quad (4.20)$$

Since  $O_4$ ,  $O_5$  and  $O_6$  represent correction to quadratic parts of the Hamiltonian, they can in principle be included exactly. This is not by default part of the RG formalism which we will use, but we will explain later how to include them exactly. While  $O_4$  and  $O_5$  have the same form as the existing parts of the quadratic actions,  $O_6$  is not present in our initial action.  $O_6$  corresponds to interactions that are odd under inversion symmetry. As such it can be thought of as a result of inversion symmetry breaking.  $O_7$  is another non-quadratic perturbation and represents Cooper-pair interactions.

For the renormalization group analysis two other properties of the operators  $O_i$  are needed. Both of them are contained in the correlation functions  $\langle O_i(w, \bar{w}) O_i(z, \bar{z}) \rangle$  at the fixed points. Those correlation functions generally have the form

$$\langle O_i(z, \bar{z}) O_i(w, \bar{w}) \rangle = \frac{c_i}{(z-w)^{2h_i} (\bar{z}-\bar{w})^{2\bar{h}_i}}, \quad (4.21)$$

where  $c_i$  is a constant, which determines the normalization of  $O_i$ . The constants  $h$  and  $\bar{h}$  are called holomorphic and anti-holomorphic conformal dimensions respectively. They are related to the scaling dimension of the operator through

$$x_i = h_i + \bar{h}_i, \quad (4.22)$$

additionally they are related to the conformal spin

$$s_i = h_i - \bar{h}_i. \quad (4.23)$$

We will not investigate perturbations with finite conformal spin, because they are not generated during the RG flow. We will comment on this in the appendix of this chapter. As we will be mostly dealing with operators and correlation functions that do not have conformal spin, it is instructive to simplify those expression in terms of  $x$  and  $\tau$  coordinates. For example equation (4.21) takes the the form

$$\langle O_i(x, \tau) O_i(x', \tau') \rangle = \frac{c_i}{((x - x')^2 + (\tau - \tau')^2)^{x_i}}. \quad (4.24)$$

Note that it only depends on the magnitude of the distance.

We will now demonstrate the calculation of the correlation function for one of the trigonometric perturbations,  $O_3$ , and for one of the quadratic perturbations  $O_4$ . The values for all the constants of all the  $O_i$  are given in table 4.1. The correlation function of  $O_3$  can be calculated by an application of (2.34) and (2.35). One finds

$$\begin{aligned} \langle O_3(z, \bar{z}) O_3(w, \bar{w}) \rangle &= \frac{1}{2} \left\langle e^{i\sqrt{8}\varphi(z, \bar{z})} e^{-i\sqrt{8}\varphi(w, \bar{w})} + e^{-i\sqrt{8}\varphi(z, \bar{z})} e^{i\sqrt{8}\varphi(w, \bar{w})} \right\rangle \\ &\quad + \frac{1}{2} \left\langle e^{i\sqrt{8}\varphi(z, \bar{z})} e^{i\sqrt{8}\varphi(w, \bar{w})} + e^{-i\sqrt{8}\varphi(z, \bar{z})} e^{-i\sqrt{8}\varphi(w, \bar{w})} \right\rangle \\ &= \frac{1}{2} \frac{1}{(z - w)^{2K_s} (\bar{z} - \bar{w})^{2K_s}} \left\langle e^{i\sqrt{8}\varphi(z, \bar{z}) - i\sqrt{8}\varphi(w, \bar{w})} + e^{-i\sqrt{8}\varphi(z, \bar{z}) + i\sqrt{8}\varphi(w, \bar{w})} \right\rangle \\ &\quad + \frac{1}{2} (z - w)^{2K_s} (\bar{z} - \bar{w})^{2K_s} \left\langle e^{i\sqrt{8}\varphi(z, \bar{z}) + i\sqrt{8}\varphi(w, \bar{w})} + e^{-i\sqrt{8}\varphi(z, \bar{z}) - i\sqrt{8}\varphi(w, \bar{w})} \right\rangle \\ &= \frac{1}{(z - w)^{2K_s} (\bar{z} - \bar{w})^{2K_s}}. \end{aligned} \quad (4.25)$$

This implies that  $c_3 = 1$ ,  $x_3 = 2K_s$  and  $s_3 = 0$ . For the quadratic terms one can calculate the correlation functions using Wick's theorem. We will use lines to indicate the possible contractions. We find

$$\begin{aligned} \langle O_4(z, \bar{z}) O_4(w, \bar{w}) \rangle &= 16 \overbrace{\partial_z \varphi_s(z) \partial_{\bar{z}} \varphi_s(\bar{z}) \partial_z \varphi_s(w) \partial_{\bar{z}} \varphi_s(\bar{w})} \\ &= \frac{K_s^2}{(z - w)^2 (\bar{z} - \bar{w})^2}. \end{aligned} \quad (4.26)$$

From this expression we see that  $c_4 = K_s^2$ ,  $x_4 = 2$  and  $s_4 = 0$ .

We are now able to go ahead with the operator product expansion based renormalization group calculation and will explain how to apply this method below, but first we discuss how different topological phases can be distinguished in the Luttinger-liquid picture.

	$c_i$	$x_i$
$O_1$	1	$\frac{1}{2}(K_s + K_c^{-1})$
$O_2$	1	$\frac{1}{2}(K_s + K_c^{-1})$
$O_3$	1	$2K_s$
$O_4$	$K_s^2$	2
$O_5$	$K_c^{-2}$	2
$O_6$	$K_s K_c^{-1}$	2
$O_7$	1	$2K_c^{-1}$

Tab. 4.1: This table lists the important perturbations away from the Luttinger-liquid fixed points, together with their normalization and their scaling dimensions.

## 4.2 Superconducting Pairing and Interactions

In this section we present arguments, why interactions favors triplet pairing over singlet pairing. In particular we discuss how the backscattering term, which is due to interactions, relates to the different superconducting pairings. All those terms are trigonometric functions of the fields. They therefore have several minima and have the smallest energy if the fields assume a constant value throughout the system corresponding to a minimum of the trigonometric term. This will generally not happen, because there are other terms in the action which favor non-constant fields. Nevertheless it is instructive to consider which constant values reduce the energy associated with the trigonometric terms the most. We will refer to this as pinning of the fields to a certain value. For the discussion we will assume that the sign of the backscattering coupling constant is positive, which corresponds to repulsive interaction. We will make no such assumption for the superconducting terms, because they are the product of two trigonometric functions and the overall sign can therefore be changed by pinning one field to a maximum rather than a minimum.

We start of by observing that the backscattering term (4.12) ideally pins the field  $\varphi_s$  to

$$\sqrt{8}\varphi_s^{\text{bs}} = \pi + 2\pi n_{\text{bs}}. \quad (4.27)$$

where  $n_{\text{bs}}$  is an integer. For the superconducting pairings the  $\varphi_s$  field ideally gets pinned to a maximum or a minimum of the trigonometric function in which it appears. Whether it is pinned to a minimum or a maximum depends on the sign of the superconducting order parameter and on the pinning value of the other field  $\theta_c$ . For the singlet pairing (4.10) the extrema are obtained for  $\varphi_s$  values of

$$\sqrt{2}\varphi_s^{\text{s}} = 2\pi n_{\text{s}}, \quad (4.28)$$

where  $n_{\text{s}}$  is an integer. For the triplet pairing (4.11) the extrema are obtained for values of

$$\sqrt{2}\varphi_s^{\text{t}} = \frac{\pi}{2} + 2\pi n_{\text{t}}, \quad (4.29)$$

where  $n_t$  is an integer. It can now be seen that there are no compatible pinning values for the singlet pairing term and the backscattering term. On the other hand there are compatible values for the triplet pairing and the backscattering term when  $n_{bs} = 2n_t$ .

It is furthermore instructive to look at the spin field close to a system boundary. At the boundary we have the boundary condition

$$\begin{aligned}\psi_\uparrow &= e^{i\alpha_\uparrow} \bar{\psi}_\uparrow, \\ \psi_\downarrow &= e^{i\alpha_\downarrow} \bar{\psi}_\downarrow,\end{aligned}\tag{4.30}$$

describing complete normal reflection. Due to time-reversal symmetry we actually have  $\alpha_\uparrow = \alpha_\downarrow$ . For the spin field in the bosonized formulation this implies

$$\sqrt{8}\varphi_s = 0 \text{ mod } 2\pi.\tag{4.31}$$

This boundary condition is compatible with the pinning values of the singlet pairing, but it is not compatible with any pinning values of the triplet pairing. Therefore if the system is dominated by triplet superconductivity in the bulk, the pinning value of  $\varphi_s$  has to change from its bulk value to an allowed boundary value close to the boundary. The lowest energy configuration is achieved by the smallest change in  $\varphi_s$ , because of the  $(\partial_x \varphi_s)^2$  term in the action. The change close to the boundary will therefore be towards the allowed boundary value, which is closest to the bulk value, but it turns out that there are actually two values that are equally close. One of which is smaller than the bulk value and one of which is larger. Therefore there are two degenerate ground states associated with the boundary. This is illustrated in figure 4.1. Depending on which value of  $\varphi_s$  is chosen at the boundary,  $\partial_x \varphi_s$  will be positive or negative close to the boundary. This corresponds to finite spin densities with opposite sign. A magnetic field, which breaks time-reversal symmetry, will therefore lift this ground state degeneracy. We have therefore seen that for the triplet-pairing dominated phase we have a ground-state degeneracy associated with a system boundary, which is lifted by a magnetic field. This is therefore similar to the usual Kramers pair of Majorana fermions, which is known to appear in non-interacting one-dimensional DIII systems at a system boundary. Furthermore one can directly associate a spin with the boundary by means of

$$\begin{aligned}\int dx n_s &= -\frac{1}{\sqrt{2\pi}} \int dx \partial_x \varphi_s \\ &= -\frac{1}{\sqrt{2\pi}} (\varphi_s(\text{bulk}) - \varphi_s(\text{boundary})) \\ &= \pm \frac{1}{4}.\end{aligned}\tag{4.32}$$

This is also consistent with the fractional spin, which is associated with Kramers pairs of Majorana bound states [33].

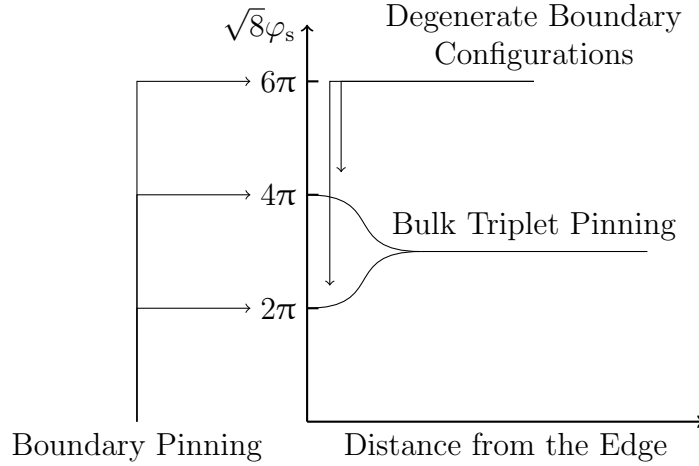


Fig. 4.1: This figure illustrates at which values of  $\varphi_s$  the bulk-triplet-pairing term would like to pin the field. It also indicates at which values the boundary condition would like to pin the field. As a result there has to be a kink close to the boundary, and there are two degenerate possibilities whose derivatives have exactly opposite sign at each point.

#### 4.2.1 Systems with Initial Triplet Pairing

So far we have discussed how interactions may favor triplet pairing over singlet pairing and in the following section we will study how this is reflected in the RG flow. In order to have a strong effect to low orders in the RG flow, we will consider systems that initially already have some triplet pairing. We assume this to be weaker than the existing singlet pairing, but still finite. This is a realistic situation, because one usually proximitizes systems with s-wave superconductors. Without initial triplet pairing, it will be very difficult to reach a topological phase, because triplet pairing then has to be generated by the RG flow to second order. Since singlet pairing is a relevant perturbation, it will dominate the RG flow if the initial triplet pairing is too small or absent. If the initial singlet- and triplet-pairing are comparable, higher order correction will determine which term dominates the flow, because to first order they have the same scaling dimension.

In order to understand why one may expect initial triplet pairing it is helpful to define

$$H_+ = \Delta_+ \int dx \psi_\uparrow(x) \bar{\psi}_\downarrow(x), \quad (4.33)$$

$$H_- = \Delta_- \int dx \bar{\psi}_\uparrow(x) \psi_\downarrow(x). \quad (4.34)$$

This way the singlet-pairing term (4.2) is given by  $H_+ + H_-$  and the triplet-pairing term (4.3) is given by  $H_+ - H_-$ . In order to have triplet pairing it therefore suffices to have different values of  $\Delta_+$  and  $\Delta_-$ .

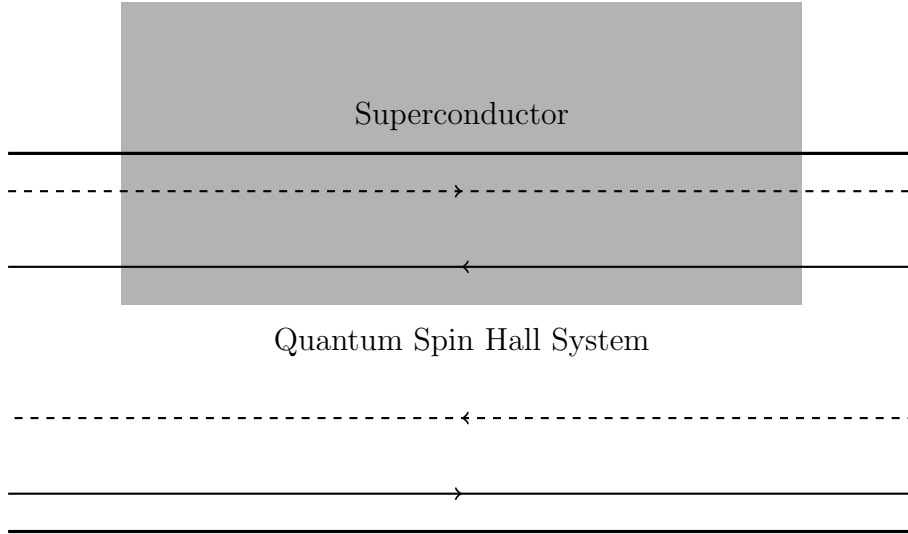


Fig. 4.2: The figure shows narrow quantum-spin-Hall system. The edge states are indicated by lines, where the solid lines have spin up and the dashed lines have spin down. The edges are assumed to be tunnel coupled and one edge of the system is proximitized by a superconductor. This yields a finite  $\Delta_+$  and almost vanishing  $\Delta_-$ .

In order to realize a situation in which  $\Delta_+$  and  $\Delta_-$  are different it is useful to note that  $H_+$  and  $H_-$  are related by inversion symmetry. Inversion symmetry relates right and left movers as

$$\begin{aligned}\psi_\sigma &\rightarrow \bar{\psi}_\sigma, \\ \bar{\psi}_\sigma &\rightarrow \psi_\sigma.\end{aligned}\tag{4.35}$$

In order to have different values of  $\Delta_+$  and  $\Delta_-$  it is therefore necessary to break inversion symmetry in accordance with the non-interacting results [20]. If inversion symmetry is broken,  $\Delta_+$  and  $\Delta_-$  will generally be different. This property can very easily be illustrated in a conceptually simple system, due to our collaborator Arbel Haim. The system consists of a narrow quantum-spin-Hall system, such that the opposite edges are tunnel coupled. The total of the four edge states constitutes the one dimensional system that we are looking at. In this system the inversion symmetry relates the channels of the two edges. Consequently we can break the inversion symmetry by proximitizing only one of the edges with a superconductor. This way  $\Delta_+$  will be finite and  $\Delta_-$  will be close to 0. The situation is depicted in figure 4.2.

### 4.3 Operator Product Expansion and Flow Equations

Our goal is to calculate flow equations to second order in the coupling constants according to the formula [10]

$$\frac{dg_k}{d\ell} = (2 - x_k)g_k - \pi \sum_{ij} c_{ijk} g_i g_j, \quad (4.36)$$

where  $c_{ijk}$  are the coefficients of an OPE. An OPE is an expansion of the form

$$O_i(z, \bar{z})O_j(w, \bar{w}) \sim \sum_k \frac{c_{ijk}}{(z-w)^{2h_i+2h_j-2h_k}(\bar{z}-\bar{w})^{2\bar{h}_i+2\bar{h}_j-2\bar{h}_k}} O_k(w, \bar{w}). \quad (4.37)$$

The idea behind an OPE is that we can express the product of two local operators with arguments that are very close in terms of a sum of local operators. Those local operators only depend on one of the coordinates, and have a divergent prefactor that depends on the coordinate difference. The divergent prefactor captures the fluctuations as the arguments come closer to one another. For dimensional reasons the exponents of the divergent terms are given by the conformal dimensions of the operators which are involved. The constants  $c_{ijk}$  are the OPE coefficients, and are precisely the numbers which we want to calculate for equation (4.36). In an OPE only the divergent terms are kept. It is therefore not an exact expansion and should only be applied inside an expectation value and only if the arguments are close. Furthermore we will only use the terms in the OPE which do not have any conformal spin. Terms with conformal spin will not be used in equation (4.36) and will not be included. The reason for that is explained in the appendix 4.A.

In order to calculate OPEs we will generally use the following strategies. If we have vertex-operator terms, the first step is to use equation (2.34) which we restate here for convenience:

$$:e^{i\alpha\phi(z)}: :e^{i\beta\phi(w)}: = e^{-\alpha\beta\langle\phi(z)\phi(w)\rangle} :e^{i(\alpha\phi(z)+\beta\phi(w))}: .$$

Because the correlation function is a negative logarithm, the first exponential on the right-hand side is divergent if  $\alpha\beta < 0$ . The second exponential on the right-hand side is normal ordered and does therefore not contain any divergence. As an OPE only consists out of divergent terms, this means that we do not need to consider terms where  $\alpha\beta > 0$ . The second step is now to Taylor expand the normal-ordered exponential in a Taylor series in  $z-w$  and/or  $\bar{z}-\bar{w}$ . This way high enough orders in the Taylor expansion are not going to yield divergent terms and we can omit them. On top of that we end up with operators that only depend on one coordinate, as we are supposed to in an OPE.

We will demonstrate this for the OPE for  $O_3$  with itself. We find

$$\begin{aligned}
 O_3 O_3 &= \frac{1}{2} \left( e^{i\sqrt{8}\varphi(z,\bar{z})} e^{-i\sqrt{8}\varphi(w,\bar{w})} + e^{-i\sqrt{8}\varphi(z,\bar{z})} e^{i\sqrt{8}\varphi(w,\bar{w})} \right) \\
 &\quad + \frac{1}{2} \left( e^{i\sqrt{8}\varphi(z,\bar{z})} e^{i\sqrt{8}\varphi(w,\bar{w})} + e^{-i\sqrt{8}\varphi(z,\bar{z})} e^{-i\sqrt{8}\varphi(w,\bar{w})} \right) \\
 &\sim \frac{1}{2} \frac{1}{(z-w)^{2K_s} (\bar{z}-\bar{w})^{2K_s}} \left( e^{i\sqrt{8}\varphi(z,\bar{z})-i\sqrt{8}\varphi(w,\bar{w})} + e^{-i\sqrt{8}\varphi(z,\bar{z})+i\sqrt{8}\varphi(w,\bar{w})} \right) \\
 &\sim \frac{1}{2} \frac{1}{(z-w)^{2K_s} (\bar{z}-\bar{w})^{2K_s}} \left( e^{i\sqrt{8}(\partial_z\varphi(z-w)+\partial_{\bar{z}}\varphi(\bar{z}-\bar{w}))} + e^{-i\sqrt{8}(\partial_z\varphi(z-w)+\partial_{\bar{z}}\varphi(\bar{z}-\bar{w}))} \right) \\
 &\sim \frac{1}{2} \frac{1}{(z-w)^{2K_s} (\bar{z}-\bar{w})^{2K_s}} \left( 2 - 8(z-w)^2 (\partial_z\varphi)^2 - 8(\bar{z}-\bar{w})^2 (\partial_{\bar{z}}\varphi)^2 \right. \\
 &\quad \left. - 16(z-w)(\bar{z}-\bar{w}) \partial_z\varphi \partial_{\bar{z}}\varphi \right) \\
 &\sim \text{const.} + \text{conf. spin} - \frac{2}{(z-w)^{2K_s-1} (\bar{z}-\bar{w})^{2K_s-1}} O_4. \tag{4.38}
 \end{aligned}$$

Here we assumed for the moment that  $K_s < 1$ . This way all higher order terms will no longer be singular and therefore do not contribute to the OPE. We also assumed that  $K_s > \frac{1}{2}$ , such that there are some singular terms at all. In the last line we did not explicitly write the term which couples to the identity operator and the two terms which have integer conformal spin. The reason is that they do not contribute to the flow equations. We have thus derived one OPE coefficient  $c_{334} = -2$  under the assumption  $K_s > \frac{1}{2}$ . We also noted that we would get additional terms if  $K_s > 1$ .

For quadratic terms the strategy is to use Wick's theorem. We demonstrate this with  $O_4$ . For clarity we write the normal ordering within Wick's theorem explicitly. One finds

$$\begin{aligned}
 O_4(z,\bar{z})O_4(w,\bar{w}) &= 16 \left( \overbrace{:\partial_z\varphi_s(z)\partial_{\bar{z}}\varphi_s(\bar{z})\partial_z\varphi_s(w)\partial_{\bar{z}}\varphi_s(\bar{w}):} \right. \\
 &\quad + \overbrace{:\partial_z\varphi_s(z)\partial_{\bar{z}}\varphi_s(\bar{z})\partial_z\varphi_s(w)\partial_{\bar{z}}\varphi_s(\bar{w}):} \\
 &\quad + \overbrace{:\partial_z\varphi_s(z)\partial_{\bar{z}}\varphi_s(\bar{z})\partial_z\varphi_s(w)\partial_{\bar{z}}\varphi_s(\bar{w}):} \\
 &\quad \left. + \overbrace{:\partial_z\varphi_s(z)\partial_{\bar{z}}\varphi_s(\bar{z})\partial_z\varphi_s(w)\partial_{\bar{z}}\varphi_s(\bar{w}):} \right) \\
 &\sim \frac{K_s^2}{(z-w)^2(\bar{z}-\bar{w})^2} - \frac{4K_s}{(z-w)^2} : \partial_{\bar{z}}\varphi(\bar{z})\partial_z\varphi(w) : \\
 &\quad - \frac{4K_s}{(\bar{z}-\bar{w})^2} : \partial_z\varphi(z)\partial_{\bar{z}}\varphi(\bar{w}) : \\
 &\sim \text{const.} + \text{conf. spin.} \tag{4.39}
 \end{aligned}$$

The OPE of  $O_4$  with itself does therefore not contribute to the flow equations. Note that the conformal spin terms in principle have to be expanded in the difference between  $z-w$  or  $\bar{z}-\bar{w}$ . Within this expansion each term separately will have conformal spin and can therefore be dropped.

Finally the strategy for OPEs between quadratic and trigonometric terms is the following. When individually looking at the OPE of exponentials with quadratic terms, we can expand the exponentials and apply Wick's theorem to the expansion. Up to a correlation function this results in a derivative of the exponential. We will use the shorthand notation

$$:\underbrace{\partial_z \varphi(z)}: e^{i\alpha\varphi(w, \bar{w})} = \frac{-i\alpha K_s}{4} \frac{1}{z-w} e^{i\alpha\varphi(w, \bar{w})}, \quad (4.40)$$

to denote all the possible contractions of a term with the series expansion of the exponential. The result can again be written as an exponential yielding (4.40). A similar identity holds for contractions with  $\bar{z}$  derivatives. As an example we calculate the OPE between  $O_4$  and  $O_3$ . We find

$$\begin{aligned} O_4 O_3 &= \sqrt{8} \sum_{\delta=\pm 1} : \partial_z \varphi(z) \partial_{\bar{z}} \varphi(\bar{z}) : e^{i\delta\sqrt{8}\varphi(w, \bar{w})} \\ &= \sqrt{8} \sum_{\delta=\pm 1} \left[ : \partial_z \varphi(z) \partial_{\bar{z}} \varphi(\bar{z}) : e^{i\delta\sqrt{8}\varphi(w, \bar{w})} \right. \\ &\quad + : \partial_z \varphi(z) \partial_{\bar{z}} \varphi(\bar{z}) : e^{i\delta\sqrt{8}\varphi(w, \bar{w})} \\ &\quad + : \partial_z \varphi(z) \partial_{\bar{z}} \varphi(\bar{z}) : e^{i\delta\sqrt{8}\varphi(w, \bar{w})} \\ &\quad \left. + : \partial_z \varphi(z) \partial_{\bar{z}} \varphi(\bar{z}) e^{i\delta\sqrt{8}\varphi(w, \bar{w})} : \right] \\ &\sim \sqrt{8} \sum_{\delta=\pm 1} \left[ \frac{-K_s^2}{2} \frac{1}{(z-w)(\bar{z}-\bar{w})} e^{i\delta\sqrt{8}\varphi(w, \bar{w})} \right. \\ &\quad - \frac{i\delta K_s}{\sqrt{2}} \frac{1}{z-w} : \partial_{\bar{z}} \varphi(\bar{z}) e^{i\delta\sqrt{8}\varphi(w, \bar{w})} : \\ &\quad \left. - \frac{i\delta K_s}{\sqrt{2}} \frac{1}{\bar{z}-\bar{w}} : \partial_z \varphi(z) e^{i\delta\sqrt{8}\varphi(w, \bar{w})} : \right] \\ &\sim \frac{-2K_s^2}{(z-w)(\bar{z}-\bar{w})} O_3 + \text{conf. spin.} \end{aligned} \quad (4.41)$$

This means that we have found  $c_{433} = -2K_s^2$ .

All other OPEs can straightforwardly be calculated in the same way. Before we present the results and discuss the flow equations, we will discuss two technical points. The first one is about a symmetry of the OPE coefficients and the second one is about the multitude of fixed points for different parameter values of  $K_s$  and  $K_c$ .

### 4.3.1 Symmetry of the OPE Coefficients

In this subsection we are going to explain how to use some standard results from conformal field theory in order to relate certain OPE coefficients to each other. The results which we will use can be found in any related textbook, for example [17]. They will help us to reduce the amount of coefficients that one has to calculate or alternatively allows for consistency checks as discussed in [10], for example. The first simple relation is related to terms without conformal spin, which are the ones that we are interested in. As already mentioned before, when the exponents of  $z$  and  $\bar{z}$  are the same their product only depends on the magnitude of  $z$ . With respect to the OPE coefficients this implies that they are symmetric in their first two indices when we consider only operator without conformal spin.

Another important result from conformal field theory that we need is that the general 2-point function of scaling operators has the form (4.21). Additionally the general 3-point function has the form

$$\langle O_i(1)O_j(2)O_k(3) \rangle = \frac{C_{ijk}}{z_{12}^{h_1+h_2-h_3} z_{23}^{h_2+h_3-h_1} z_{31}^{h_3+h_1-h_2} \bar{z}_{12}^{\bar{h}_1+\bar{h}_2-\bar{h}_3} \bar{z}_{23}^{\bar{h}_2+\bar{h}_3-\bar{h}_1} \bar{z}_{31}^{\bar{h}_3+\bar{h}_1-\bar{h}_2}}. \quad (4.42)$$

Here we introduced two shorthand notations. Firstly a number  $n$  as an argument is short for  $z_n, \bar{z}_n$  and secondly  $z_{ij}$  is short for  $z_i - z_j$ . As an OPE is valid inside an expectation value when the arguments of the two operators approach each other, it is possible to calculate the 3-point function in the limit of two approaching arguments by first applying an OPE and then using equation (4.21). This can be done for any pair of operators in the three-point function. One therefore has a relationship between the normalization constants  $c_i$ , the three-point function constants  $C_{ijk}$  and the OPE coefficients  $c_{ijk}$ . It takes the form

$$\begin{aligned} C_{ijk} &= c_{ijk}c_k \\ &= c_{ikj}c_j \\ &= c_{jki}c_i. \end{aligned} \quad (4.43)$$

This means that we can always relate OPE coefficients when the set of their indices is the same. As an example let us look at the OPE coefficients which we calculated above, namely  $c_{334} = -2$  and  $c_{433} = -2K_s^2$ . Together with  $c_3 = 1$  and  $c_4 = K_s^2$  from table 4.1 we actually see that they fulfill equation (4.43).

There is a subtle point about (4.43), because OPE coefficients only exist for singular terms. In particular we noted earlier that  $c_{334}$  only appears when  $K_s > \frac{1}{2}$ . On the other hand there is no such restriction for  $c_{433}$ . Therefore even though there is a relationship between existing OPE coefficients, the existence of one OPE coefficient does not automatically imply the existence of another one with permuted indices. This problem can be solved if one knows the scaling dimensions of the operators involved, because they can be used to calculate the degree of the divergence. So if one knows the

scaling dimension of the three operators related by an OPE coefficient, one can always check whether there can indeed be a associated diverging term in the OPE.

The relationship (4.43) actually takes its simplest form if one normalizes all the scaling operators such that  $c_i = 1$  for all operators. In that case the OPE coefficients are simply symmetric in all their indices. The reason we do not choose to do that is that we want the operators to be defined independently of  $K_s$  and  $K_c$ . We will consider several different values of  $K_s$  and  $K_c$  and we want the perturbations to be defined independently of the fixed point in question. This will be important in the next subsection where we will illustrate how to combine the flow equations for the different fixed points.

### 4.3.2 Combining Flow Equations for Different Fixed Points

The OPE coefficients, which we calculated above are actually enough to calculate the flow equations for the well-known Kosterlitz-Thouless(KT) model [37]. Applying equation (4.36) yields

$$\begin{aligned}\dot{g}_3 &= (2 - 2K_s)g_3 + 4\pi K_s^2 g_3 g_4, \\ \dot{g}_4 &= 2\pi g_3^2,\end{aligned}\tag{4.44}$$

where we abbreviated derivatives with respect to  $\ell$  with a dot. We will now discuss the meaning of this equation and its parameters in detail.  $K_s$  is a parameter in the fixed-point action. Therefore equations (4.44) describe the flow in the vicinity of the fixed point for which  $K_s$  has its given value. The parameters  $g_3$  and  $g_4$  are then perturbations away from this fixed point. There seems to be an unfortunate redundancy in this description, because  $g_4$  actually couples to a term that has the same structure as the fixed point action. A perturbation consisting only of  $g_4$  with  $g_3 = 0$  will simply place the system at a fixed point with a different value of  $K_s$ . This can also be seen in the flow equations (4.44), which vanish identically if  $g_3$  vanishes implying that all points on the  $g_3 = 0$  line are fixed points. The problem with the equation is that they are only perturbative in  $g_4$ , even though  $g_4$  simply places the system at another fixed point. We will now describe how to improve on that.

The idea of how to improve the flow equations is very simple, and is best understood when one thinks of a discretized solution of the flow equations. For a certain value of  $K_s$  we start at a point with  $g_4 = 0$  and  $g_3$  finite. There we calculate the change in constants  $g_3$  and  $g_4$  during the first renormalization group step. At the new point in parameter space with finite  $g_3$  and finite  $g_4$  we then want to calculate the next changes again. But now  $g_4$  is finite and that means that flow equations around the original  $K_s$  point are not the best approximation we have. In particular we get the best approximation if we choose a new  $K_s$  such that the new  $g_4$  vanishes again. This means that we simply put  $g_4 = 0$  on the right hand side of the flow equations. Simultaneously  $K_s$  becomes an  $\ell$  dependent parameter. Its change will be given directly by the change in  $g_4$ . The

situation is illustrated in figure 4.3. The flow equations are now given by

$$\begin{aligned}\dot{g}_3 &= (2 - 2K_s)g_3, \\ \dot{K}_s &= \frac{\partial K_s}{\partial g_4} \dot{g}_4.\end{aligned}\tag{4.45}$$

All that remains is to calculate the change of  $K_s$  when  $g_4$  changes. For that we have to compare the free action (4.9) with the perturbation

$$g_4 \iint dx d\tau O_4 = g_4 \iint dx d\tau ((\partial_x \varphi_s)^2 + (\partial_\tau \varphi_s)^2).\tag{4.46}$$

The change in the prefactor of (4.9) and (4.46) now has to be the same. Therefore we have

$$\begin{aligned}d\left(\frac{1}{2\pi K_s}\right) &= -\frac{dK_s}{2\pi K_s^2} \\ &\stackrel{!}{=} dg_4,\end{aligned}$$

which implies

$$\frac{\partial K_s}{\partial g_4} = -2\pi K_s^2.\tag{4.47}$$

Combining equation (4.44), (4.45) and (4.47) we arrive at the flow equations

$$\begin{aligned}\dot{g}_3 &= (2 - 2K_s)g_3, \\ \dot{K}_s &= -4\pi^2 K_s^2 g_3^2,\end{aligned}\tag{4.48}$$

which are the well-known flow equations for this problem [21]<sup>1</sup>.

To summarize this subsection, we illustrated how to combine a family of quadratic flow equations into a single system of flow equations. The resulting system no longer needs to be quadratic and in our example it was quartic.

## 4.4 Flow Equations and their Solutions

We will now state the flow equations which have been calculated using the methods described above. We will once state the flow equations around the non-interacting fixed point  $K_s = K_c = 1$ , because they take a particularly simple form and allow for analytic solutions. Afterwards we will state the flow equations more generally using the method described above to combine flow equations at different  $K_s$  and  $K_c$  values.

---

<sup>1</sup>In order to get the same result as in the reference one has to perform the substitution  $g_3 \rightarrow \frac{1}{\sqrt{8\pi}}g$ .

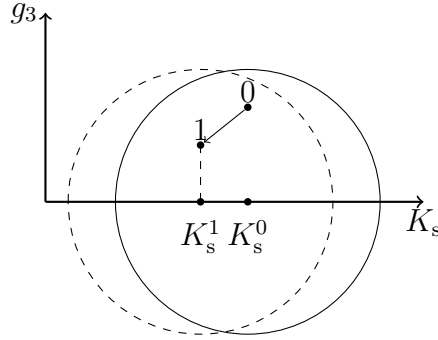


Fig. 4.3: The figure illustrates a situation where we start the flow at point 0, for which we have the starting fixed point at a value  $K_s^0$ . Consequently  $g_4^0$  is zero. A circle indicates the range of validity of the RG equations around  $K_s^0$ . After an RG step we are at the parameter point 1. Even though we might still use the RG equations around the point  $K_s^0$ , the fixed point with a value of  $K_s^1$  is closer and one obtains a better approximation by using the RG equations around this point.

#### 4.4.1 Flow Equations Close to $K_s = K_c = 1$

Close to the non-interacting point the flow equations are

$$\dot{g}_1 = (1 + \pi g_4 - \sqrt{2}\pi g_3)g_1, \quad (4.49)$$

$$\dot{g}_2 = (1 + \pi g_4 + \sqrt{2}\pi g_3)g_2, \quad (4.50)$$

$$\dot{g}_3 = 4\pi g_4 g_3, \quad (4.51)$$

$$\dot{g}_4 = 2\pi g_3^2. \quad (4.52)$$

In principle the interaction terms  $g_6$  and  $g_7$  would also enter the flow equations, but they do not flow themselves and are assumed to be initially zero. We have therefore omitted them from the flow equations. Note that the equations for  $g_3$  and  $g_4$  are simply the KT flow equations. They can therefore be solved independently of the rest of the equations. Furthermore the equations for  $g_1$  and  $g_2$  are completely decoupled from each other. It is therefore possible to insert the solutions of the KT equation in the differential equations for  $g_1$  and  $g_2$  and then integrate them directly.

Before solving all four flow equations, we will review the solutions of the KT flow equations, in particular with respect to the initial conditions. The KT flow equations have the well know constant of motion

$$g_3^2 - 2g_4^2 = I, \quad (4.53)$$

which can straightforwardly be verified. The parameter space can be divided into several sectors depending on whether this constant is positive or negative. The solutions to the KT flow equations that lie inside the different sectors behave qualitatively different. Therefore

we discuss the solutions in the different sectors separately. From the assumption that we have repulsive interaction, we know that  $g_3^0 > 0$  and  $K_s^0 > 1$ . From the relationship (4.46) we know

$$\frac{1}{2\pi} + g_4 = \frac{1}{2\pi K_s}$$

it follows that  $g_4^0 < 0$ .

We can now state the relevant solutions to the KT flow equations. For the case when  $I = A^2$ , with a real  $A$ , we have

$$g_3(\ell) = A \sec \left( \frac{4\pi A}{\sqrt{2}} \ell + \arctan \left( \frac{\sqrt{2}g_4^0}{A} \right) \right), \quad (4.54)$$

$$g_4(\ell) = \frac{A}{\sqrt{2}} \tan \left( \frac{4\pi A}{\sqrt{2}} \ell + \arctan \left( \frac{\sqrt{2}g_4^0}{A} \right) \right). \quad (4.55)$$

For the case  $I = 0$  we have

$$g_3(\ell) = \frac{\sqrt{2}}{4\pi\ell - (g_4^0)^{-1}}, \quad (4.56)$$

$$g_4(\ell) = \frac{1}{(g_4^0)^{-1} - 4\pi\ell}. \quad (4.57)$$

The region in parameter space where  $I = 0$  is a line called the separatrix, because it separates the other two regimes. For the case  $I = -A^2$ , with a real  $A$ , we have

$$g_3(\ell) = A \operatorname{csch} \left( \frac{4\pi A}{\sqrt{2}} \ell - \operatorname{arccoth} \left( \frac{\sqrt{2}g_4^0}{A} \right) \right), \quad (4.58)$$

$$g_4(\ell) = \frac{A}{\sqrt{2}} \coth \left( -\frac{4\pi A}{\sqrt{2}} \ell + \operatorname{arccoth} \left( \frac{\sqrt{2}g_4^0}{A} \right) \right). \quad (4.59)$$

With the help of the above solutions, the equations for  $\dot{g}_1$  and  $\dot{g}_2$  can readily be integrated. The general form of the solutions are

$$g_1(\ell) = g_1^0 \exp \left( \ell + \pi \int_0^\ell d\ell' \left( g_4(\ell') - \sqrt{2}g_3(\ell') \right) \right), \quad (4.60)$$

$$g_2(\ell) = g_2^0 \exp \left( \ell + \pi \int_0^\ell d\ell' \left( g_4(\ell') + \sqrt{2}g_3(\ell') \right) \right). \quad (4.61)$$

Evaluation of the remaining integrals yields for  $I = A^2$

$$\int_0^\ell d\ell' g_3(\ell') = \frac{\sqrt{2}}{4\pi} \ln \frac{\left| \sec \left( \frac{4\pi A}{\sqrt{2}} \ell + B \right) + \tan \left( \frac{4\pi A}{\sqrt{2}} \ell + B \right) \right|}{|\sec B + \tan B|}, \quad (4.62)$$

$$\int_0^\ell d\ell' g_4(\ell') = -\frac{1}{4\pi} \ln \frac{\left| \cos \left( \frac{4\pi A}{\sqrt{2}} \ell + B \right) \right|}{|\cos B|}. \quad (4.63)$$

For  $I = 0$  it yields

$$\int_0^\ell d\ell' g_3(\ell') = \frac{\sqrt{2}}{4\pi} \ln |4\pi g_4^0 \ell - 1|, \quad (4.64)$$

$$\int_0^\ell d\ell' g_4(\ell') = \frac{1}{4\pi} \ln |1 - 4\pi g_4^0 \ell|. \quad (4.65)$$

Finally for  $I = -A^2$  it yields

$$\int_0^\ell d\ell' g_3(\ell') = \frac{\sqrt{2}}{4\pi} \ln \frac{\left| \tanh \left( \frac{2\pi A}{\sqrt{2}} \ell - \frac{B}{2} \right) \right|}{\left| \tanh \frac{B}{2} \right|} \quad (4.66)$$

$$\int_0^\ell d\ell' g_4(\ell') = \frac{1}{4\pi} \ln \frac{\left| \sinh \left( -\frac{4\pi A}{\sqrt{2}} \ell + B \right) \right|}{\left| \sinh B \right|} \quad (4.67)$$

In order to investigate the topological phase transition it is helpful to look at the ratio between triplet and singlet pairing. During the RG flow the ratio changes according to

$$\frac{g_2(\ell)}{g_1(\ell)} = \frac{g_2^0}{g_1^0} \exp \left( \sqrt{8}\pi \int_0^\ell d\ell' g_3(\ell') \right). \quad (4.68)$$

For the further discussion it is helpful to look at the maximum change in the ratio between singlet and triplet pairing. This corresponds to the  $\ell \rightarrow \infty$  limit in equation (4.68). This limit is only finite below the separatrix and with (4.66) we find

$$\begin{aligned} \lim_{\ell \rightarrow \infty} \frac{g_2(\ell)}{g_1(\ell)} &= \frac{g_2^0}{g_1^0} \exp \left( \sqrt{8}\pi \int_0^\infty d\ell' g_3(\ell') \right) \\ &= \frac{g_2^0}{g_1^0} \frac{1}{\left| \tanh \frac{B}{2} \right|} \\ &= \frac{g_2^0}{g_1^0} \left( \frac{g_3^0 - \sqrt{2}g_4^0}{-g_3^0 - \sqrt{2}g_4^0} \right)^{\frac{1}{2}}. \end{aligned} \quad (4.69)$$

If we stop the RG flow at some RG time  $\ell^*$  which is long enough, we can approximate the ratio at this point by the ratio in the limit  $\ell \rightarrow \infty$ . The precise condition on this approximation is  $\ell \gg \frac{\sqrt{2}}{2\pi A}$ , which can be seen from equation (4.66). Additionally we have to require that our perturbative flow equations are still valid for RG times as long as  $\ell^*$ . This is the case if the relevant superconducting pairing terms are still small enough to fall into the perturbative regime. If we neglect the effect of  $g_4$  on the flow of the superconducting pairing terms, compared to their scaling dimension, we find the condition

$$g_{1/2}^0 \ll C \exp \left( -\frac{\sqrt{2}}{4\pi A} \right), \quad (4.70)$$

where  $C$  is a constant that corresponds to the maximum value of  $g_{1/2}$  for which one trusts the perturbative results.

For given initial values  $g_1^0$  and  $g_2^0$  we can now discuss the phase boundary between the topological and the trivial phase. As a condition for the phase boundary we use that the ratio between  $g_2$  and  $g_1$  is 1 when we stop the flow. Later we will comment more on why this is reasonable. From equation (4.69) we see that this corresponds to a straight line through the origin in the  $g_3g_4$ -plane. One is therefore in the topological phase when equation (4.69) is bigger than 1. We can solve this inequality for  $g_3^0$  and find the condition

$$g_3^0 \geq \sqrt{2} \frac{(g_2^0)^2 - (g_1^0)^2}{(g_2^0)^2 + (g_1^0)^2} g_4^0. \quad (4.71)$$

The closer the boundary line, where equality holds, is to the separatrix, the bigger the factor in equation (4.69) is. Building on the discussion from the previous paragraph, equality only holds when the long RG-time approximation is valid. For initial values of  $g_3$  and  $g_4$ , which are closer to the origin, this condition will eventually be violated and the maximum ratio (4.69) will not be reached. In this case the phase boundary has to move closer to the separatrix, where the maximum value is larger and a value below the maximum is still sufficient to bring the system into the topological phase. The exact shape of the curve in this regime is hard to calculate analytically. On the separatrix and above it the integral in (4.68) does not converge for large  $\ell$ . The ratio between triplet and singlet pairing is therefore only limited by the RG time for which we leave the perturbative regime. Lets presume the perturbative regime is valid until the pairing coupling constants reach some value  $C$  which is of order unity. We then have a stopping time which is given by

$$\ell^* = \ln \frac{C}{g_1^0}. \quad (4.72)$$

There is then a minimum value of  $g_3^0$  for which (4.68) evaluated at  $\ell^*$  takes a value greater than 1. These are the points of the phase boundary on and above the separatrix. These points can then be continuously connected to the line from the large RG-time regime.

The question remains whether it is justified to use the non-interacting criterion  $g_2 > g_1$  to identify the topological phase, even though the problem is still interacting when we stop the flow. This is indeed the case because the superconducting pairing operators are relevant close to the non-interacting fixed point. In order for non-trivial KT-like physics to happen between the superconducting pairing terms and the interaction terms, we would need to be close to the parameter point where the superconducting pairing terms are marginal. This is the case when  $K_s + K_c^{-1} = 4$ , which is in the strongly interacting regime. It is therefore justified to exclude this kind of physics close to the non-interacting point. In the next section we will study more general flow equations numerically and this will further support this claim.

Temperature imposes another constraint on the validity of the above discussion. When the energy cutoff reaches temperature we have to stop the RG flow. This imposes a

maximum on  $\ell^*$  of the form

$$\ell^* \leq \ln \frac{A_0}{T}. \quad (4.73)$$

The above discussion is only valid as long as the stopping times stay below the temperature-imposed limit.

#### 4.4.2 General Flow Equations

In this section we study more general flow equations, which were obtained according to the scheme presented above, where we did not keep terms where the scaling dimension was too high. There are equations for every  $g_i$  with the exception of  $g_4$  and  $g_5$ . Instead we will have flow equations for  $K_s$  and  $K_c$  as described above. The equations are

$$\dot{g}_1 = \left(2 - \frac{1}{2}K_s - \frac{1}{2K_c}\right)g_1 - \sqrt{2}\pi(H(K_s))g_3 - H(K_c^{-1})g_7g_1 + \sqrt{2}\pi\frac{K_s}{K_c}g_2g_6 \quad (4.74)$$

$$\dot{g}_2 = \left(2 - \frac{1}{2}K_s - \frac{1}{2K_c}\right)g_2 + \sqrt{2}\pi(H(K_s))g_3 - H(K_c^{-1})g_7g_2 + \sqrt{2}\pi\frac{K_s}{K_c}g_1g_6, \quad (4.75)$$

$$\dot{g}_3 = (2 - 2K_s)g_3 - \frac{\pi}{\sqrt{2}}H(K_c^{-1} - K_s)(g_1^2 - g_2^2), \quad (4.76)$$

$$\dot{g}_6 = \sqrt{2}\pi H(K_s + K_c^{-1} - 2)g_1g_2, \quad (4.77)$$

$$\dot{g}_7 = (2 - 2K_c^{-1})g_7 + \frac{\pi}{\sqrt{2}}H(K_c^{-1} - K_s)(g_1^2 - g_2^2), \quad (4.78)$$

$$\dot{K}_s = -2\pi K_s^2 \left(\frac{\pi}{2}H(K_c^{-1} + K_s - 2)(g_1^2 + g_2^2) + 2\pi H(2K_s)g_3^2\right), \quad (4.79)$$

$$\dot{K}_c = 2\pi \left(\frac{\pi}{2}H(K_c^{-1} + K_s - 2)(g_1^2 + g_2^2) + 2\pi H(2K_c^{-1})g_7^2\right). \quad (4.80)$$

Here  $H$  denotes the Heaviside function, which is zero for negative arguments and 1 for positive ones.

We will use these equations to numerically support the claims made in the previous subsection. We will integrate the flow numerically until either singlet or triplet pairing reaches a constant value at which the validity of the perturbation calculation breaks down. Depending on whether singlet or triplet pairing reaches this value first, we will call the phase trivial or topological. The results are plotted in figure 4.4 together with the long RG-time result. We see that the long RG-time result indeed agrees with the numerical calculation in the appropriate regime. Furthermore we see that the phase boundary has the qualitative shape that that we argued in the previous section. This supports our claim that close to the non-interacting fixed point the additional KT physics associated with the superconducting pairing terms is not relevant, because this of KT physics is included in the full flow equations.

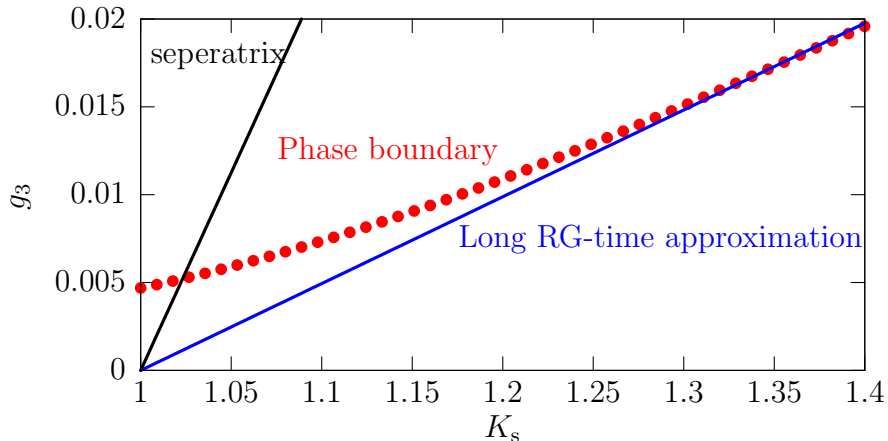


Fig. 4.4: The plot shows the numerically computed phase boundary (dots) between the topological and trivial phase. The topological phase is above the dots. The plot also shows our theoretical long RG-time result. We argued from our analytical results that the phase boundary should lie above the long RG-time limit. For small  $K_s$  values this is the case. For larger  $K_s$  values this does not seem to be the case anymore in this plot. This is an indication that we leave the perturbative regime for which the analytical results were computed. The numerical results were computed for an initial ratio of  $g_2^0/g_1^0 = 0.8$ .

## 4.5 Summary

In this chapter we have investigated the effect of repulsive interaction on the one dimensional DIII phase. We first reviewed why such a system can still be thought of as being topological and has edge states even in the presence of interaction. We then performed an RG analysis, which confirmed the previously known result that interactions support the topological phase. Previously this result was only known for mean field treatments and attractive interactions. We presented a general RG analysis for repulsive interactions. We derived analytical results for the case of weak interactions and solved the flow equations for the more general case numerically.

### 4.A Conformal Spin

There are several references that explain how to obtain the formula (4.36) [10, 16, 46]. One issue that is often mentioned but not explained in detail is regarding the absence of OPE coefficients that relate to terms with conformal spin. In particular there is the important statement that terms with conformal spin do not contribute to the RG flow. We will show that this is true for terms with integer conformal spin and we will argue that this is the relevant situation for most calculations, in particular our one. We will not derive (4.36) here, because the derivation that can be found in the references which

we mentioned above. Nevertheless we sketch very vaguely where the term appears about which we are going to reason in this section.

In deriving (4.36) one has to expand the partition function close to the fixed point in a power series in terms of the perturbations. This is proportional to an expansion of the expectation value  $\langle \exp(-S_{\text{pert}}) \rangle$ . Comparing this to the general form of the perturbations (4.13) we see that the individual terms in the expansion will consist out of expectation values of  $n$  operators at different coordinates, together with  $2n$  integrals over the different coordinates. The second-order correction in the flow equations is obtained when one considers two operators with coordinates that are very close together. The hard short scale cutoff  $a$  implies that their coordinates cannot be closer than  $a$ . It is then important for the RG flow equations to calculate the change in the integral when the short scale cutoff is increased. This can then be computed with the help of the OPE, which is valid for operators with close arguments inside an expectation value. The relevant quantity to look at is therefore

$$\iint_{a^2 < |x^2 + \tau^2| < (a(1+d\ell))^2} dx d\tau \langle \dots O_i(x_1, \tau_1) O_j(x_2, \tau_2) \dots \rangle, \quad (4.81)$$

where  $x = x_2 - x_1$  and  $\tau_2 - \tau_1$ . After applying the OPE only the divergent prefactor will depend on  $x$  and  $\tau$  and therefore the integral can be computed analytically. We will now argue that it vanishes for terms in the OPE that have conformal spin.

In order to understand why terms with conformal spin do not contribute to the RG flow we have to take a look at integrals in terms of complex coordinates. We generally write

$$\iint dx d\tau = \frac{i}{2} \iint dz d\bar{z}. \quad (4.82)$$

A generic term after inserting an OPE into (4.81) will have the form

$$\frac{i}{2} \iint_{a^2 < z\bar{z} < (a(1+d\ell))^2} dz d\bar{z} \frac{c_{ijk}}{z^h \bar{z}^{\bar{h}}} \langle \dots O_k(z_2, \bar{z}_2) \dots \rangle, \quad (4.83)$$

where we introduced the shorthand notations  $h = h_i + h_j - h_k$  and  $\bar{h} = \bar{h}_i + \bar{h}_j - \bar{h}_k$ . The important thing to keep in mind is that we do not integrate over all of the two-dimensional complex space. Instead we integrate over a two-dimensional real subspace that correspond to the initial  $x\tau$ -plane. This means that the integral is only over points for which  $\bar{z} = z^*$ . It is therefore enough to parameterize  $z$  as

$$z = r e^{i\varphi}, \quad (4.84)$$

$\bar{z}$  as

$$\bar{z} = r e^{-i\varphi}, \quad (4.85)$$

and integrate over  $r$  and  $\varphi$ . If we now look at the integral, which we have to perform we find

$$\begin{aligned} \frac{i}{2} \iint_{a^2 < z\bar{z} < (a(1+d\ell))^2} \frac{1}{z^h \bar{z}^{\bar{h}}} &= \int_{a < r < (a(1+d\ell))} dr \int_0^{2\pi} d\varphi \frac{e^{-i(h-\bar{h})\varphi}}{r^{h+\bar{h}-1}} \\ &= 2\pi \delta_{h,\bar{h}} \int_{a < r < (a(1+d\ell))} dr \frac{1}{r^{2h-1}}. \end{aligned} \quad (4.86)$$

This shows that the integral vanishes for integer conformal spin. For this argument it is very important that the short distance cutoff is chosen to be rotationally symmetric, but since we expect that the long-distance physics is not dependent on the details of the short distance cutoff we assume that we can always choose a rotationally symmetric cutoff scheme.

We will now argue why for our purpose only integer conformal spin is relevant. This is the relevant situation for the OPEs which we are dealing with, because the terms with conformal spin appear as a result of a Taylor expansion in  $z$  and  $\bar{z}$ . Terms with different powers of  $z$  and  $\bar{z}$  will have finite integer conformal spin, i.e. an integer difference in  $h$  and  $\bar{h}$ . This is independent of whether  $h$  and  $\bar{h}$  are integers themselves.



## 5 Environmental Coulomb Blockade

In contrast to the previous chapters, in this chapter we will study Majorana bound states in class D systems. One of the most relevant questions about Majorana bound states is how they influence observables or to put it differently, which measurable quantities indicate their presence. The most common method for probing Majorana bound states is via a tunnel probe. Such a measurement ideally yields a zero-bias tunneling conductance of  $\frac{2e^2}{h}$  at zero temperature. We want to study how certain electric environments influence this result. In order to do this we will first review related results regarding interactions in the tunnel probe, which is modeled as a Luttinger liquid. We will then derive an effective action for tunnel probes that are coupled to general electric environments. Thereafter we will discuss some specific examples motivated by the general result. The reason to study electronic environments is that they are described by macroscopic quantities that are easily measurable in practice. This is opposed to the Luttinger-liquid parameters which are hard to determine experimentally.

### 5.1 Superconductor-Luttinger Liquid Junction

In this section we will review some of the results from Fidkowski et al. [13]<sup>1</sup>. The system of interest is one that is commonly used in experiments, where a topological phase is obtained in a heterostructure by proximitizing a helical wire with an s-wave superconductor. The wire itself is helical through a combination of external magnetic field and spin-orbit coupling, but this will not be of particular relevance to us. The important thing to note is that usually only a part of the wire is proximitized and therefore brought into the topological phase. The rest of the wire therefore naturally forms a helical lead, which is used as a tunnel probe. The situation is illustrated in figure 5.1. The superconductor itself is grounded and the question is what conductance one observes when measuring a current from the helical lead into the superconductor. In particular we are interested in the zero-bias conductance, which contains information about the Majorana bound state which is at zero energy.

As we are only interested in low bias and therefore low-energy physics, we will focus on the low energy degrees of freedom in the helical lead and in the topological superconductor. For the helical lead this means that we can use the linearized approximation of the dispersion and treat it as a Luttinger liquid. For the topological superconductor it means that we only consider the Majorana bound state and no other (gapped) degrees of

---

<sup>1</sup>Note that the notation and conventions in this thesis differ compared to the reference. In particular the Luttinger liquid field names  $\varphi$  and  $\theta$  are interchanged.

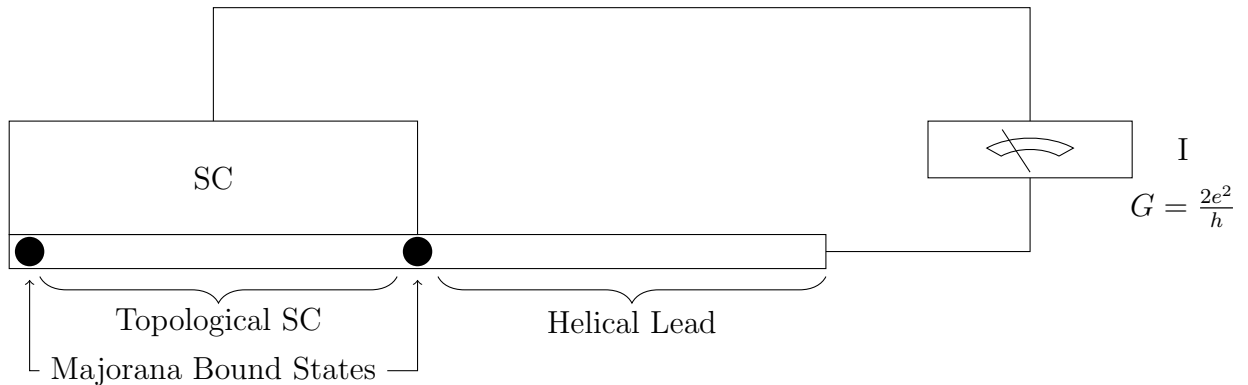


Fig. 5.1: This figure shows a typical experimental system for tunnel probing Majorana bound states. Part of a helical wire is proximitized by an s-wave superconductor (SC) such that it is in a topological phase with Majorana bound states. The remaining part of the helical wire acts as a lead, which is used for tunnel probing one of the Majorana bound states. The zero-bias conductance is measured from the lead into the superconductor and ideally reaches a value of  $\frac{2e^2}{h}$ .

freedom. This assumes that there are no other subgap states additional to the Majorana bound state at the end of the wire.

In the absence of interactions one expects a zero-bias conductance of  $\frac{2e^2}{h}$ . This can be understood in the following way. For an ideal metallic non-interacting lead the states inside the lead are delocalized throughout the whole lead. This is also true for the Majorana bound state, which couples to the metallic lead. Therefore there will be an extended zero energy state in the lead, which is an equal superposition of electrons and holes. This means that there has to be perfect Andreev reflection at zero energy, and all electrons get reflected as a hole and vice versa. The system therefore exhibits perfect Andreev reflection at zero energy. It is well known from mesoscopic scattering theory that perfect Andreev reflection corresponds to a conductance of  $\frac{2e^2}{h}$  [4, 39, 47]. Backscattering that takes place at the interface between the lead and the topological superconductor will yield corrections to this. As we often work with units in which  $\hbar = e = 1$ , the conductance  $\frac{2e^2}{h}$  becomes  $\frac{1}{\pi}$  in these units.

In the presence of interactions the picture of the extended Majorana bound states may no longer be right. In this case an adequate description is to treat the coupling between the Majorana bound state and the lead perturbatively. We will call this case the normal-reflection fixed point and the previous case the Andreev-reflection fixed point. Figure 5.2 illustrates the physics behind both fixed points.

We will now discuss each of the fixed points individually and state their corresponding effective actions. The starting point for modeling the half-infinite Luttinger liquid is the

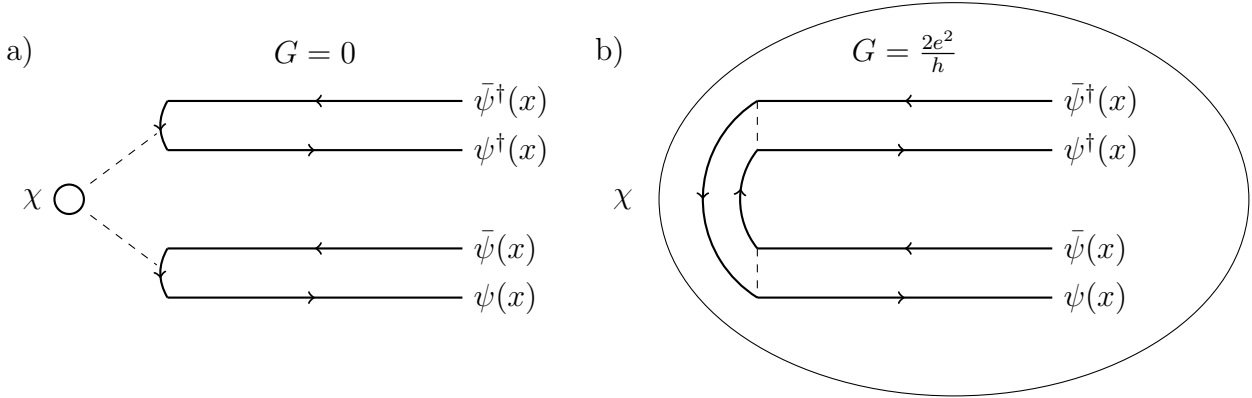


Fig. 5.2: The figure shows the physical picture behind the two fixed points that are studied. The extended directed lines describe electrons/holes in the lead and the circle/ellipse describes the Majorana bound state  $\chi$ . In a) the starting point is electrons that get normal reflected at the interface (solid lines) and the perturbation (dashed lines) is tunnel coupling to the Majorana bound state. In b) the Majorana bound state extends throughout the lead such that the electrons get Andreev reflected (solid lines). The perturbation is normal reflection at the interface (dashed lines).

Hamiltonian (2.15) with the integral over space going from zero to infinity:

$$H = iv_F \int_0^\infty dx [-\psi^\dagger(x)\partial_x\psi(x) + \bar{\psi}^\dagger(x)\partial_x\bar{\psi}(x)]. \quad (5.1)$$

This Hamiltonian is only fully meaningful if a boundary condition at zero is specified and we are going to do that in the following subsections. The general idea is to map the semi-infinite system with left- and right-moving excitations onto an infinite system with only right-moving excitations. This is sketched in figure 5.3. Thereafter one integrates out all degrees of freedom not at  $x = 0$ , in order to get an effective action for the interface between the topological superconductor and the lead.

### 5.1.1 Normal-Reflection Fixed Point

At the normal-reflection fixed point we start with the Hamiltonian (5.1) together with the boundary condition that all electrons get normal-reflected at zero. This implies that  $\psi(x=0) = e^{i\beta}\bar{\psi}(x=0)$ , where  $\beta$  is an arbitrary phase, which we set to zero at this point. For the bosonized theory this boundary condition implies that

$$\varphi(x=0) = 0 \text{ mod } \pi. \quad (5.2)$$

In the bosonized theory the Hamiltonian takes the form

$$H = \int_0^\infty dx \frac{u}{2\pi} [K(\partial_x\theta)^2 + K^{-1}(\partial_x\varphi)^2], \quad (5.3)$$

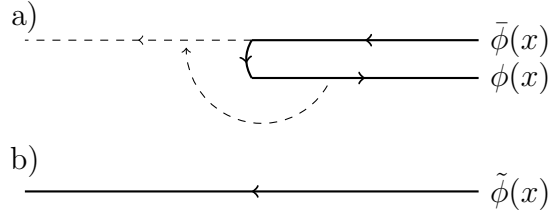


Fig. 5.3: The picture illustrates the basic idea behind the unfolding technique, where one maps a semi-infinite system into a infinite chiral one. For this technique to be useful, one has to start with non-interacting left- and right-moving modes. Otherwise unfolding will introduce complicated non-local interactions.

where we included interactions in the form of the Luttinger-liquid parameter  $K$ . Because  $\varphi(x=0)$  is pinned by the boundary condition, the only remaining degree of freedom at the boundary is  $\theta(x=0)$ . After integrating out the rest of the wire one obtains an effective boundary action [13] for  $\Theta = \theta(x=0)$  of the form

$$S_n^0[\Theta] = \frac{K}{2\pi} \int \frac{d\omega}{2\pi} |\omega| |\Theta|^2. \quad (5.4)$$

This is the action for the normal reflection fixed point. The zero-bias conductance associated with this fixed point is zero because the lead is not coupled to the Majorana bound state at all.

The action describing the tunneling between the Majorana bound state and the lead is

$$S_t = it \int d\tau [\psi^\dagger(x=0) + \psi(x=0)] \chi, \quad (5.5)$$

in terms of fermions. Here  $\chi$  describes the Majorana bound state at the end of the topological superconductor. When bosonizing this action we have to remember to insert a Klein factor  $\eta$ , because we have two different species of fermions (the ones in the lead and the Majorana bound states). We will then combine the Majorana bound state operator  $\chi$  and the Klein factor  $\eta$  into an operator  $\sigma_x = i\eta\chi$ . The bosonized action becomes

$$S_t[\Theta] = t \sqrt{\frac{2}{\pi}} \int d\tau \sigma_x \cos \Theta. \quad (5.6)$$

The operator  $\sigma_x$  flips the parity in both the lead and the topological superconductor, but since it commutes with all the other operators in the action we can simply replace  $\sigma_x$  by its eigenvalues for the following renormalization-group analysis. To simplify the analysis even more we can actually replace  $\sigma_x$  with 1 because the sign of  $t$  is irrelevant to first order in the analysis.

We will now carry out the first order perturbative renormalization group analysis explicitly for the action (5.4) and (5.6). This is a well known problem and it was first

investigated in the context of Luttinger liquids by Kane and Fisher [30]. Since a lot of the following analysis can be reduced to this model, we will present it explicitly. According to the general renormalization group theory outlined in chapter 2, we have to calculate

$$\begin{aligned} \int \mathcal{D}\Theta_{>} e^{-S_n^0[\Theta_{<}+\Theta_{>}] - S_t[\Theta_{<}+\Theta_{>}]} &= e^{-S_n^0[\Theta_{<}]} \int \mathcal{D}\Theta_{>} e^{-S_n^0[\Theta_{>}] - S_t[\Theta_{<}+\Theta_{>}]} \\ &= e^{-S_n^0[\Theta_{<}]} Z_{>}^0 \langle e^{-S_t[\Theta_{<}+\Theta_{>}]} \rangle_{>}. \end{aligned} \quad (5.7)$$

Here  $Z_{>}^0$  denotes the partition function of the quadratic  $\Theta_{>}$  part. It does not depend on any fields and therefore represents just a shift of  $-\ln Z_{>}^0$  in the free energy. As already discussed in chapter 2 this shift is not important for the renormalization group analysis, and we will therefore ignore it. The expectation value  $\langle \dots \rangle_{>}$  is defined as

$$\langle \dots \rangle_{>} = \frac{1}{Z_{>}^0} \int \mathcal{D}\Theta_{>} \dots e^{-S_n^0[\Theta_{>}]}. \quad (5.8)$$

We will now evaluate the expectation value perturbatively assuming that  $S_t$  is small. In that case one can approximate the expectation value as

$$\begin{aligned} \langle e^{-S_t[\Theta_{<}+\Theta_{>}]} \rangle_{>} &\approx 1 - \langle S_t[\Theta_{<} + \Theta_{>}] \rangle_{>} \\ &\approx e^{-\langle S_t[\Theta_{<}+\Theta_{>}] \rangle_{>}}. \end{aligned} \quad (5.9)$$

Therefore we have to calculate  $\langle S_t[\Theta_{<} + \Theta_{>}] \rangle_{>}$ . This yields

$$\begin{aligned} \langle S_t[\Theta_{<} + \Theta_{>}] \rangle_{>} &= \frac{t}{2} \sqrt{\frac{2}{\pi}} \int d\tau \langle e^{i(\Theta_{<}(\tau) + \Theta_{>}(\tau))} + \text{c.c.} \rangle_{>} \\ &= \frac{t}{2} \sqrt{\frac{2}{\pi}} \int d\tau \left[ e^{i\Theta_{<}(\tau)} \exp\left(-\frac{1}{4} \int_{b^{-1}\Lambda < |\omega| < \Lambda} \frac{d\omega}{2\pi} \frac{2\pi}{K} \frac{1}{|\omega|}\right) + \text{c.c.} \right] \\ &= \frac{tb^{-(2K)^{-1}}}{2} \sqrt{\frac{2}{\pi}} \int d\tau [e^{i\Theta_{<}(\tau)} + \text{c.c.}] \\ &= tb^{-(2K)^{-1}} \sqrt{\frac{2}{\pi}} \int d\tau \cos \Theta_{<}(\tau). \end{aligned} \quad (5.10)$$

This readily maps back to the original action. We still have to rescale  $\tau \rightarrow b\tau$ , which ensures that the cutoff of the low energy theory is again  $\Lambda$ . This way the only parameter that changes is the strength of the tunnel coupling, which makes it easier to compare to its previous value. One obtains a scaling dimension of the tunneling term of  $1 - (2K)^{-1}$ . This means that the normal-reflection fixed point is stable for  $K < \frac{1}{2}$  and unstable for  $K > \frac{1}{2}$ .

### 5.1.2 Andreev-Reflection Fixed Point

For the Andreev-reflection fixed point, the bulk Hamiltonian is the same as (5.1) and (5.3), but the boundary condition is different. At low energies all incident electrons are reflected

as holes and vice versa. This yields the boundary condition  $\psi^\dagger(x=0) = e^{i\beta}\bar{\psi}(x=0)$ , where  $\beta$  is again an arbitrary phase which we set to zero. In terms of the bosonized operators this implies

$$\theta(x=0) = 0 \bmod \pi. \quad (5.11)$$

With this boundary condition one can again derive an effective action for the remaining degree of freedom at the boundary  $\Phi = \varphi(x=0)$ . One finds [13]

$$S_a^0[\Phi] = \frac{1}{2\pi K} \int \frac{d\omega}{2\pi} |\omega| |\Phi|^2. \quad (5.12)$$

Because of the perfect Andreev reflection (which is incorporated in the boundary conditions) there is a conductance of  $\frac{2e^2}{h}$  associated with this fixed point.

Normal reflections occurring at the junction are treated as a perturbation. It is described by an action of the form

$$S_r \propto \int d\tau [\psi^\dagger(x=0)\bar{\psi}(x=0) + \text{h.c.}]. \quad (5.13)$$

This translates into a bosonic action of the form

$$S_r[\Phi] = 2\lambda \int d\tau \cos(2\Phi). \quad (5.14)$$

The translation is a little subtle, because strictly speaking it only makes sense for a regularized action with a short distance cutoff  $a$ . This is contained in the fact that  $\lambda$  has units  $(\text{length})^{-1}$  such that it implicitly contains  $a$ , which is the only scale.

A similar analysis to the one above yields a scaling dimension of  $1 - 2K$  for the normal-reflection perturbation. Therefore the Andreev-reflection fixed point is stable for  $K > \frac{1}{2}$  and unstable for  $K < \frac{1}{2}$ . This complements the results for the normal-reflection fixed point and is also consistent with the result for the non-interacting case ( $K=1$ ) where one expects perfect Andreev reflection. We will now proceed and study electric environments instead of Luttinger liquids.

## 5.2 Coupling to an Electric Environment

We now want to study a Majorana bound state coupled to an electric environment. This allows for one immediate generalization of the previously presented results to the case of a metallic lead with both spin direction, as opposed to a helical lead with only one spin direction. This generalization follows because Majorana bound states only couple to a particular spin direction in the lead [15]. If we then assume that all the effects of the electrons in the other spin direction can be effectively modeled as part of the electric environment, we arrive at a model identical to the one above plus the electric environment, where  $\psi$  and  $\bar{\psi}$  describe the spin direction to which the Majorana bound state couples.

In order to see how to include the environment, we have to revisit the coupling between the lead and the Majorana bound state, namely equation (5.5). The problem with this action is that it does not conserve charge. The reason is that the electrons that are created and annihilated by  $\psi^\dagger$  and  $\psi$  have a charge of  $e$ , but the Majorana bound state does not have any charge associated with it because it is an equal superposition of electrons and holes. In order to account for the changing total charge in the topological superconductor, we introduce the macroscopic charge operator  $Q$  for the topological superconductor and its canonically conjugate operator  $\alpha$ . Those operators fulfill  $[\alpha, Q] = i$ . Therefore  $e^{\pm i\alpha}$  creates/annihilates a charge in the topological superconductor respectively. The complete tunneling action then reads

$$S_t = it \int d\tau [\psi^\dagger(x=0)e^{-i\alpha} + \psi(x=0)e^{+i\alpha}] \chi \quad (5.15)$$

and its bosonized form is

$$S_t[\Theta, \alpha] = t \sqrt{\frac{2}{\pi}} \int d\tau \sigma_x \cos(\Theta + \alpha). \quad (5.16)$$

The electric environment itself is described by an action for  $\alpha$  of the general form

$$S_{\text{env}}[\alpha] = \frac{1}{2} \int \frac{d\omega}{2\pi} G_{\alpha\alpha}^{-1}(\omega) |\alpha|^2, \quad (5.17)$$

where  $G_{\alpha\alpha}$  is the Green function for  $\alpha$  which we will determine below. Since the non-quadratic tunneling term (5.16) only couples to the linear combination  $\Theta_+ = \Theta + \alpha$ , we can integrate out the combination  $\Theta - \alpha$  and obtain an effective action for  $\Theta_+$ . This effective action has the form

$$S[\Theta_+] = \frac{1}{2} \int \frac{d\omega}{2\pi} G_+^{-1}(\omega) |\Theta_+|^2, \quad (5.18)$$

where the Green function is given by

$$G_+(\omega) = \frac{\pi}{|\omega|} + G_{\alpha\alpha}(\omega). \quad (5.19)$$

We will now derive the coupling of the Andreev-reflection fixed point to the environment. Contrary to the normal-reflection fixed point, we will not include the charge in the tunneling Hamiltonian. The motivation for this is to get a purely additive change to the action. Since a change in electron number in the lead necessarily means that the charge in the topological superconductor has to change, we will include a capacitive coupling term of the form

$$\begin{aligned} H &= \frac{(Q + N_{\text{lead}})^2}{2C} \\ &= \frac{(Q + \Phi/\pi)^2}{2C}, \end{aligned} \quad (5.20)$$

where  $C$  is the capacitance of our tunnel junction. The Lagrangian for  $\alpha$  is obtained by Legendre transforming the environment Hamiltonian from  $Q$  to  $-\dot{\alpha}$ . If we now denote the Legendre transform of a function  $f(x)$  with  $f^*(p)$  then there exists the general rule that for  $f(x) = g(x + y)$  we have  $f^*(p) = g^*(p) - py$ . In our case  $x = Q$ ,  $p = -\dot{\alpha}$  and  $y = \Phi/\pi$ . Therefore the capacitive coupling leads to an additional term in the Lagrangian of the form

$$L[\alpha, \Phi] = \dot{\alpha} \frac{\Phi}{\pi}. \quad (5.21)$$

In imaginary time this has the form

$$L[\alpha, \Phi] = -i\partial_\tau \alpha \frac{\Phi}{\pi}. \quad (5.22)$$

Therefore the corresponding action is

$$\begin{aligned} S[\alpha, \Phi] &= \int d\tau \left( -i\partial_\tau \alpha \frac{\Phi}{\pi} \right) \\ &= \int \frac{d\omega}{2\pi} \frac{1}{2\pi} (\omega \alpha^* \Phi - \omega \alpha \Phi^*). \end{aligned} \quad (5.23)$$

This action is linear in  $\alpha$  and  $\Phi$ , therefore we can integrate out  $\alpha$  and obtain an additional quadratic term for the  $\Phi$  field. The additional quadratic term has the form

$$S_{\text{eff,env}}[\Phi] = \int \frac{d\omega}{2\pi} \left( \frac{1}{\pi^2} \frac{\omega^2}{2} G_{\alpha\alpha}(\omega) |\Phi|^2 \right). \quad (5.24)$$

The total quadratic action for the  $\Phi$  is then

$$S[\Phi] = \int \frac{d\omega}{2\pi} \left[ \left( \frac{|\omega|}{2\pi} + \frac{1}{\pi^2} \frac{\omega^2}{2} G_{\alpha\alpha}(\omega) \right) |\Phi|^2 \right]. \quad (5.25)$$

Additionally there is still the normal-reflection perturbation, which is unaffected by charging physics. Therefore it still has the form (5.14).

The missing part to study the effect of the electric environment is the action for  $\alpha$  or more precisely  $G_{\alpha\alpha}$ . General  $P(E)$  theory states that this Green function has the form [23]

$$G_{\alpha\alpha}(\omega) = \frac{Z_t^*(i\omega)}{|\omega|}, \quad (5.26)$$

where  $Z_t^*$  is the impedance of the tunnel junction and is given by

$$Z_t(\omega) = \frac{1}{i\omega C + (Z_{\text{env}}(\omega))^{-1}}. \quad (5.27)$$

Here  $C$  is the capacitance of the tunnel junction and  $Z_{\text{env}}$  is the impedance of the environment. The tunnel junction impedance is therefore given by a capacitor in parallel

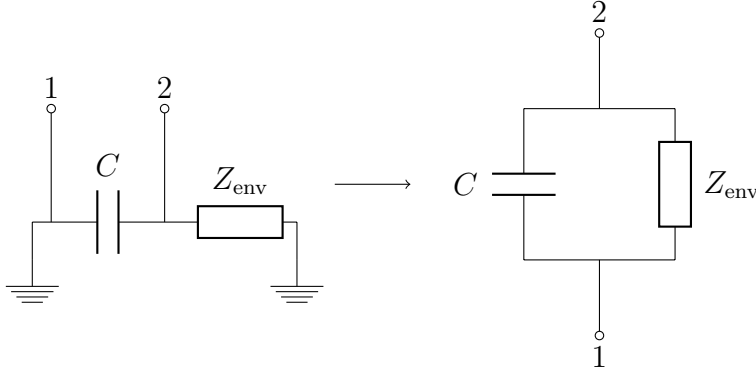


Fig. 5.4: The figure displays the circuit associated with a tunnel junction. Tunnel events charge the tunnel junction capacitively by moving charge from 1 to 2. Sequential tunnel events become therefore energetically unfavorable for the duration it takes to discharge the capacitor through the environment impedance  $Z_{\text{env}}$ . By associating the grounds of the original circuit with each other one sees that this physics is described by the correlations between the point 1 and 2 is given by the response of a circuit with a capacitor and an impedance in parallel.

with the environment impedance. We will now briefly describe the physical picture behind this. In the absence of tunneling, the tunnel junction constitutes a capacitor with capacitance  $C$ . Tunneling events now charge this capacitor and therefore make further tunneling events energetically less favorable until the capacitor is discharged again. In order to discharge the capacitor the charge has to flow to a ground through the environment which has an impedance  $Z_{\text{env}}$ . Since we are interested in whether tunnel events are favorable, we are therefore interested in electric correlations between both sides of the capacitor. Therefore the circuit for those correlations has the capacitor and the environmental impedance in parallel with respect to the tunnel junction. The situation is illustrated in figure 5.4.

For small frequencies one can approximate the environmental impedance by a constant real resistance  $R$  and if  $\omega RC \ll 1$  we can approximate the tunneling impedance by  $R$  as well, such that the Green function  $G_{\alpha\alpha}$  takes the simple form

$$G_{\alpha\alpha}(\omega) = \frac{R}{|\omega|}. \quad (5.28)$$

We can now analyze the stability of the fixed points as a function of  $R$ . In particular we will map the non-interacting fermions coupled to an environment to a model with an effective Luttinger-liquid parameter  $K_{\text{eff}}$  and then apply the results which we reviewed earlier.

### 5.2.1 Normal-Reflection Fixed Point

Starting from (5.19) we find that

$$G_+(\omega) = \frac{\pi + R}{|\omega|}.$$

If we now bring (5.18) to the form

$$S_n^0[\Theta_+] = \frac{K_{\text{eff}}}{2\pi} \int \frac{d\omega}{2\pi} |\omega| |\Theta_+|^2,$$

we find

$$K_{\text{eff}} = \left(1 + \frac{R}{\pi}\right)^{-1}. \quad (5.29)$$

We know that the critical  $K$  value is at  $\frac{1}{2}$ . It follows that the critical value for  $R$  is  $\pi$ . In proper units this is  $\frac{h}{2e^2}$ . For higher resistances the coupling to the Majorana bound state is irrelevant and the normal reflection fixed point is stable. For smaller resistances the coupling is relevant and the normal reflection fixed point is unstable. This was first found by [38].

### 5.2.2 Andreev-Reflection Fixed Point

A similar analysis can be performed for the Andreev-reflection fixed point. Inserting (5.28) into (5.25) yields

$$S[\Phi] = \frac{1}{2\pi K_{\text{eff}}} \int \frac{d\omega}{2\pi} |\omega| |\Phi|^2,$$

with the same  $K_{\text{eff}}$  as above. Therefore the Andreev-reflection fixed point is stable for resistances smaller than  $\pi$  and unstable for resistances larger than  $\pi$ .

## 5.3 Special Environments

Motivated by the result that there is a crossover depending on how the resistance of the environment compares to  $\frac{h}{2e^2}$  we now study two particular environments that fall into that regime. First we briefly demonstrate how the crossover appears if the Majorana bound state is coupled to a metallic quantum dot with quantum point contact drain, which is shown in figure 5.5b. The idea is that a conductance of  $\frac{e^2}{h}$  is associated with each fully open channel in the quantum point contact. So one might expect a crossover for exactly two channels, depending on the effect of the dot itself. More interestingly we will study two Majorana bound states that are coupled through a metallic quantum dot, which is shown in figure 5.5c. The motivation here is that the conductance of  $\frac{2e^2}{h}$ , which is associated with a Majorana bound state, is exactly the critical resistance value for the other Majorana bound state.

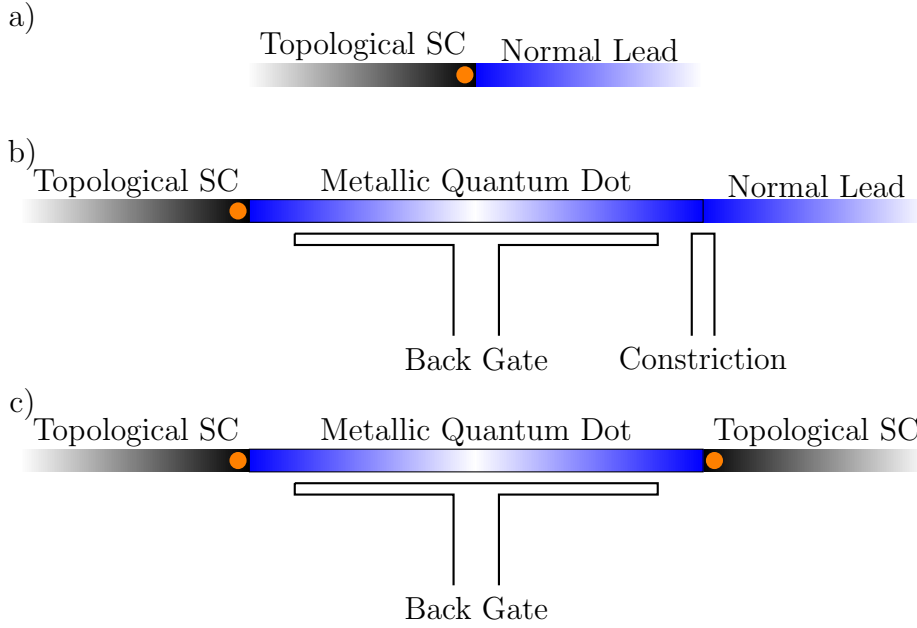


Fig. 5.5: In a) the basic system, which consists of a semi-infinite topological superconductor and a semi-infinite metallic lead, is depicted. The circle denotes a Majorana bound state at the boundary and the fading illustrates that the wires are approximated to be semi-infinite. In b) we consider a topological superconductor coupled to a metallic quantum dot, which itself is coupled to a lead via a quantum point contact. Note that the metallic quantum dot is modeled as two independent semi-infinite ends, which are coupled by charging. In c) we have a system where two topological superconductors are coupled via a metallic quantum dot. The dot is again modeled as two independent semi-infinite wires, that are coupled by charging.

### 5.3.1 Metallic Dot with a Quantum Point Contact Drain

The action for the environment of a metallic dot with a quantum point contact drain is

$$S_{\text{env}}[\alpha, Q, \Phi_i] = \int d\tau \left[ iQ\partial_\tau\alpha + E_C \left( Q + \frac{1}{\pi} \sum_{i=1}^N \Phi_i - N_g \right)^2 \right] + \sum_{i=1}^N \frac{1}{\pi} \int \frac{d\omega}{2\pi} |\omega| |\Phi_i|^2, \quad (5.30)$$

where  $Q$  is the charge operator for the dot and  $N_g$  is an offset by a gate voltage. The operators  $\Phi_i$  are the fields that describe the charge passing through the quantum point contact through channel  $i$ , similar to the action (5.12) with  $K = 1$ , except for the crucial difference of a factor of  $\frac{1}{2}$ . This factor is different, because the effective action describes the middle of an infinite wire, see 5.5b, instead of the edge of a semi-infinite one as in 5.5a. The zero-dimensional actions for the point contacts are derived in [14]. We further

assume that all channels in the point contact are either completely open (and therefore included in the action) or completely blocked (and therefore omitted from the action). Consequently the action does not contain any backscattering at the point contacts. The action for  $\alpha$  can be obtained using the following steps. First we note that the offset due to a gate  $N_g$  can be removed by trivially shifting  $Q$ . Furthermore the coupling between the fields  $\Phi_i$  and  $Q$  is only through the sum of all the  $\Phi_i$ . It is therefore advantageous to perform a change of variables for the  $\Phi_i$ . We choose to do that by means of a unitary transformation, such that the last part of the action does not change. We transform the fields  $\Phi_i \rightarrow U_{ij}\Phi_j$ . We require that one of the transformed fields, which we call  $\Phi_a$ , is the average of all the initial fields, i.e. field  $\Phi_a = \frac{1}{\sqrt{N}} \sum_i \Phi_i$ , where the prefactor follows from the requirement that the transformation is unitary. All the other transformed fields will not couple to  $Q$  and we therefore omit them from the action. The part of the unitary transformation corresponding to them is therefore arbitrary (as long as they are orthogonal to  $\Phi_a$ ) and unimportant and we will not specify it. Our simplified action now has the form

$$S_{\text{env}}[\alpha, Q, \Phi_a] = \int d\tau \left[ iQ\partial_\tau\alpha + E_C \left( Q + \frac{\sqrt{N}}{\pi}\Phi_a \right)^2 \right] + \frac{1}{\pi} \int \frac{d\omega}{2\pi} |\omega| |\Phi_a|^2. \quad (5.31)$$

We now integrate out  $\Phi_a$  and obtain

$$S_{\text{env}}[\alpha, Q] = \int \frac{d\omega}{2\pi} \frac{E_C|\omega|}{|\omega| + NE_C/\pi} |Q|^2 + i \int d\tau Q\partial_\tau\alpha. \quad (5.32)$$

Finally we integrate out  $Q$  to obtain

$$S_{\text{env}}[\alpha] = \int \frac{d\omega}{2\pi} \left( \frac{1}{4} \frac{\omega^2(|\omega| + NE_C/\pi)}{E_C|\omega|} \right) |\alpha|^2, \quad (5.33)$$

which we can compare with (5.17) to find

$$\begin{aligned} G_{\alpha\alpha} &= \frac{2E_C|\omega|}{\omega^2(|\omega| + NE_C/\pi)} \\ &\approx \frac{2\pi}{N|\omega|} \\ &= \frac{h/e^2}{N} \frac{1}{|\omega|}, \end{aligned} \quad (5.34)$$

where we approximated the result for small frequencies compared to the charging energy and restored units in the last line. Compared with (5.28) we find that the system at low frequencies behaves as a resistor with a resistance  $R = \frac{h/e^2}{N}$ , such that one should see a crossover in the conductance at two open channels as speculated above.

### 5.3.2 Two Majorana Bound States Coupled via a Metallic Dot

We now consider a metallic Coulomb blocked island coupled to two Majorana bound states. This is an inverse version of the system studied by Fu [19] and later Hutzen et al. [28], as they studied a Coulomb blocked topological-superconductor island with two Majorana bound states coupled to normal leads. The situation where more than two Majorana bound states are on the superconducting island and coupled to leads was also studied by several authors [2, 6] and is known as the topological Kondo effect. This will not be relevant to us as we only consider systems with coupling to two Majorana bound states.

Because we assume that we have a big metallic dot such that there is no coherent transport from one end to the other, the Majorana bound states are decoupled from each other and each one couples to its own dot degrees of freedom in the same way a single Majorana bound state coupled to a lead previously. We therefore introduce a new index  $r$  which is either L or R describing the degrees of freedom on the left side or the right side of the dot respectively. The total Hamiltonian describing the system consists of three parts:

$$H = \sum_r [H_{\text{el},r} + H_{\text{t},r}] + H_C. \quad (5.35)$$

The individual parts are

$$H_{\text{el},r} = \sum_k \xi_k c_{k,r}^\dagger c_{k,r}, \quad (5.36)$$

$$H_{\text{t},r} = t_r \sum_k (c_{k,r}^\dagger - c_{k,r}) \chi_r \quad (5.37)$$

$$H_C = E_C (N_L + N_R - N_g)^2, \quad (5.38)$$

where  $N_g$  is again a gate offset in the charging energy. The charging energy part  $H_C$  is particularly important because it is the only interaction between the left and the right side. The current operator for the two contacts are

$$I_r = iet_r \sum_k (c_{k,r} + c_{k,r}^\dagger) \chi_r. \quad (5.39)$$

For weak tunneling and away from  $N_g$  being a half integer, the dot is in Coulomb blockade. The largest correction to the current comes from cotunneling via virtual states which differ by one unit of charge. A second order Fermi's golden rule calculation gives a conductance

$$G_{\text{cotun}} = \frac{e^2}{h} \Gamma_R \Gamma_L \left( \frac{1}{E_C^+} + \frac{1}{E_C^-} \right)^2. \quad (5.40)$$

for  $T \ll E_C$ , where  $\Gamma_r = 2\pi v_F |t_r|^2$  and  $E_C^\pm = E_C(1 \mp 2N_g)$ , where we assumed without loss of generality that  $N_g \in (-\frac{1}{2}, \frac{1}{2})$ . The cotunneling conductance diverges near the charge degeneracy points  $N_g = \pm\frac{1}{2}$ . In order to understand the behavior near these

points we follow the discussion by Fu [19]. For large charging energies we can restrict the analysis to the two degenerate charge sectors at  $N_g = \frac{1}{2}$ . This means that the total number of electrons  $N_L + N_R$  can either be 0 or 1. We can therefore represent this charge by a fermion  $f$ , such that  $N_L + N_R = f^\dagger f$ . This way the charging Hamiltonian becomes

$$\begin{aligned} H_C &= E_C (N_L + N_R - N_g)^2 \\ &= E_C (f^\dagger f (1 - 2N_g) - N_g^2). \end{aligned} \quad (5.41)$$

One can also express the tunneling Hamiltonian in terms of the fermion  $f$ . First of all we observe that  $[c_{k,r}^\dagger \chi_r, N_L + N_R] = c_{k,r}^\dagger \chi_r$ . The same kind of commutation relation, and therefore the same dynamics in the Schrödinger equation, can be obtained if we replace  $c_{k,r}^\dagger \chi_r$  by  $c_{k,r}^\dagger f$  and treat  $c_{k,r}^\dagger$  and  $f$  as independent fermions. We then have  $[c_{k,r}^\dagger f, f^\dagger f] = c_{k,r}^\dagger f$ . From this it follows that we also have to perform the replacement  $c_{k,r} \chi_r \rightarrow -f^\dagger c_{k,r}$ . This way the tunneling Hamiltonian projected on the charge states 0 and 1 is

$$H_{t,r} = t_r \sum_k \left( f^\dagger c_{k,r} + c_{k,r}^\dagger f \right), \quad (5.42)$$

and associated current operators become

$$I_r = -iet_r \sum_k \left( f^\dagger c_{k,r} - c_{k,r}^\dagger f \right). \quad (5.43)$$

With the approximations made, the conductance is given by the conductance of a resonant level [12]

$$G = \frac{e^2}{h} \frac{4\Gamma_L \Gamma_R}{4E_C^2 (1 - 2N_g)^2 + \Gamma^2 + 2\Gamma_L \Gamma_R}, \quad (5.44)$$

where  $\Gamma = \Gamma_L^2 + \Gamma_R^2$ . Equation (5.44) agrees with the perturbative cotunneling result (5.40), if only the cotunneling via the  $N = 1$  charge state is included, i.e. keeping only the  $E_C^+$  term in equation (5.40). Even though the result was derived for  $N_g \approx \frac{1}{2}$ , it can easily be generalized by simply replacing  $(1 - 2N_g)$  by twice the distance of  $N_g$  to the closest charge degeneracy point (half integer value). We define an asymmetry angle  $\sin \theta = (\Gamma_L/\Gamma)$  with which the result takes the form

$$G = \frac{e^2}{h} \frac{2 \sin 2\theta}{(2E_C(1 - 2N_g)/\Gamma)^2 + 1 + \sin 2\theta}. \quad (5.45)$$

The reason for parameterizing the conductance with an asymmetry angle is to make the result easier to compare with the following approximation which will be derived in a different limit.

The non-perturbative result (5.44) was derived under the assumption that  $\Gamma_r \ll E_C$ , such that we reduce the analysis to only two charge states. The opposite limit in which

the contacts have large transparency can be studied best starting from the effective action close to the Andreev-reflection fixed point. The action is

$$S[\Phi_L, \Phi_R] = \sum_r \left[ \frac{1}{2\pi} \int \frac{d\omega}{2\pi} |\omega| |\Phi_r|^2 + 2\lambda_{r,\text{bs}} \int d\tau \cos(2\Phi_r) \right] + S_C[\Phi_L, \Phi_R], \quad (5.46)$$

with

$$S_C[\Phi_L, \Phi_R] = E_C \int d\tau \left( \frac{\Phi_L}{\pi} + \frac{\Phi_R}{\pi} - N_g \right)^2, \quad (5.47)$$

where  $\lambda_{r,\text{bs}}$  are the backscattering amplitudes. Because only the combination  $\Phi_L + \Phi_R$  appears in the charging term, it is natural to introduce the total charge field  $\Phi_+ = \Phi_L + \Phi_R$  and the difference charge field  $\Phi_- = \Phi_R - \Phi_L$ , which is related to the current via  $I = -i \frac{\partial \tau \Phi_-}{2\pi}$ . For  $\lambda_{r,\text{bs}} \ll E_C$  and at low energies  $|\omega| \ll E_C$  the mode  $\Phi_+$  gets pinned at  $\pi N_g$ . We can therefore integrate it out by replacing the cosine terms in the action (5.46) by their averages over  $\Phi_+$ . This is valid when  $\lambda_{r,\text{bs}} \ll E_C, \Lambda$ . Here  $\Lambda$  denotes the high energy cutoff again. This results in the following effective low-energy action for  $\Phi_-$

$$S[\Phi_-] = \frac{1}{4\pi} \int \frac{d\omega}{2\pi} |\omega| |\Phi_-|^2 + \int d\tau \left( \tilde{\lambda}_{\text{bs}} e^{i\Phi_-} + \text{c.c.} \right), \quad (5.48)$$

where

$$\tilde{\lambda}_{\text{bs}} = (\lambda_{L,\text{bs}} e^{i\pi N_g} + \lambda_{R,\text{bs}} e^{-i\pi N_g}) \langle e^{i\Phi_+} \rangle_0. \quad (5.49)$$

We evaluate the expectation value as

$$\begin{aligned} \langle e^{i\Phi_+} \rangle_0 &= \exp \left( -\frac{\pi}{2} \int \frac{d\omega}{2\pi} \frac{1}{\pi|\omega| + 4E_C} \right) \\ &\approx \frac{4E_C}{\pi\Lambda}. \end{aligned} \quad (5.50)$$

The model is now solvable because it maps to a single non-interacting quantum point contact [14]. The backscattering matrix element needed in the quantum point contact model is given by  $V_{\text{bs}} = 2\pi a \tilde{\lambda}_{\text{bs}}$ , where  $a$  is the short-distance cutoff associated with the high-energy cutoff  $\Lambda$ :  $a = \frac{v_F}{\Lambda}$ . Moreover the current operator is  $I = -i \frac{\partial \tau \Phi_-}{2\pi}$  for the original and the quantum point contact model. Therefore we find for the conductance

$$G = \frac{e^2}{h} \frac{1}{1 + \left| \frac{V_{\text{bs}}}{2v_F} \right|^2} \quad (5.51)$$

and in terms of the parameters of our original model

$$G = \frac{e^2}{h} \frac{1}{1 + \left( \frac{8E_C}{\Lambda^2} \right)^2 (\lambda_{\text{bs}}^2 + 2\lambda_{L,\text{bs}}\lambda_{R,\text{bs}} \cos(2\pi N_g))}, \quad (5.52)$$

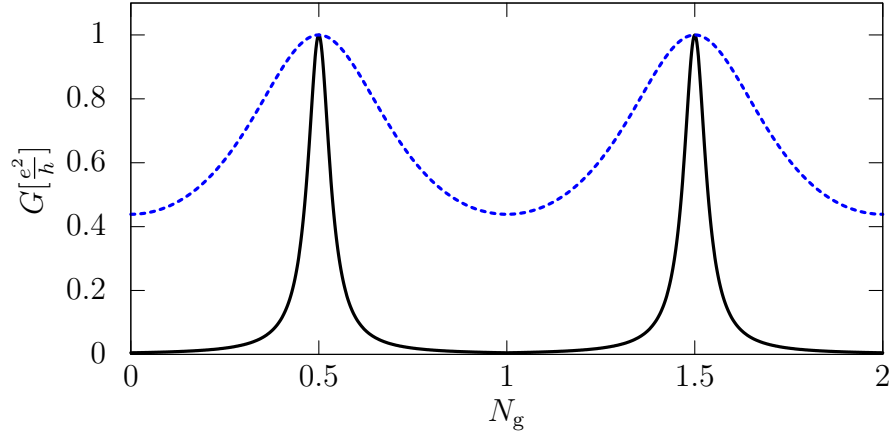


Fig. 5.6: The plot shows the conductance of two Majorana bound states coupled to a metallic dot as a function of gate voltage on the dot. The dashed blue line illustrates the weak backscattering limit (5.53), whereas the solid black line illustrates the weak tunneling limit (5.45). In both cases the plot is for symmetric coupling. For half-integer values of gate voltage, the conductance reaches its maximum of  $\frac{e^2}{h}$  corresponding to two Majorana bound state-metal lead junctions in series, each of which has a resistance of  $\frac{h}{2e^2}$ .

where  $\lambda_{\text{bs}}^2 = \lambda_{\text{L,bs}}^2 + \lambda_{\text{R,bs}}^2$ . We will again introduce an asymmetry angle as  $\sin \theta = (\lambda_{\text{R,bs}}/\lambda_{\text{bs}})$ . The result then reads

$$G = \frac{e^2}{h} \frac{1}{1 + \left(\frac{8\lambda_{\text{bs}}EC}{A^2}\right)^2 (1 + \sin 2\theta \cos(2\pi N_g))}. \quad (5.53)$$

In both the weak-tunneling and the weak-backscattering limit conductance is maximal at the charge neutrality point and reaches  $\frac{e^2}{h}$  for symmetric coupling. This agrees with the result for two resistors in series with a resistance of  $\frac{h}{2e^2}$ , each corresponding to the two coupled Majorana bound states. An example of the line shapes for symmetric coupling is shown in figure 5.6.

## 5.4 Summary

In this chapter we studied aspects of tunnel probing Majorana bound states in class D systems. Tunnel probing ideally exhibits a zero-bias conductance of  $\frac{2e^2}{h}$  if a Majorana bound state is present. Building on the results from Fidkowski et al. [13] we studied this result in the presence of a general electric environment. At low frequencies there is a crossover at an environment resistance of  $\frac{h}{2e^2}$ . Motivated by that we studied two particular systems that exhibit this crossover. In particular we showed how the crossover

can be controlled by a quantum point contact. Furthermore we studied a system of two Majorana bound states coupled to a metallic dot. For the latter case we derived the line shape of the system in certain limits.



## 6 Conclusion

To summarize this thesis we will briefly summarize the ideas of the main chapters 3, 4 and 5 and discuss to what extent important question could be answered and where there is potential for expanding upon the work in this thesis.

In chapter 3 we investigated whether topological one-dimensional superconducting systems with time-reversal symmetry, class DIII, can be used for topological quantum computation similar to the analogous systems with broken time-reversal symmetry, class D. We found that it is generally not possible to use class DIII systems for topological quantum computation, because their edge excitations contain a local degree of freedom that can be manipulated adiabatically, which we called local mixing. This generally makes adiabatic manipulations path dependent and does therefore not allow for topological quantum computation. Furthermore we analyzed which symmetry conditions are sufficient to prevent local mixing. Finally we showed that the absence of local mixing is enough to ensure that the braiding transformations in such systems are path independent. Our results give a full qualitative account of the adiabatic transformations that can occur during an adiabatic manipulation of a DIII system. Further work in this area could focus on more detailed quantitative calculations. This might be very interesting, because we identified adverse effects to topological quantum computation and we identified sufficient symmetry conditions to suppress these effect, but we did not quantify adverse effects as a result of such a symmetry breaking. This could be done in the context of studying concrete systems with clearly defined qubits and gates and calculating coherence times and fidelities as a result of local mixing.

In chapter 4 we investigate how repulsive interactions may help to induce a topological DIII phase. This has been studied before, mostly in the context of mean-field theory and we presented a fairly general renormalization-group treatment of this problem. Our treatment is not model specific but relies on a general low-energy theory, which form is mostly determined by symmetries. For weak interaction strengths we were able to solve the renormalization-group flow analytically and make some statements about when the system is in the topological phase and when it is not. We supported those results by a numerical solution of flow equations, which are valid beyond weak interaction strengths. Our results support the general conclusion that interactions can drive a system into a topological phase. Even though our results are already quite general they could be generalized in a particular way. In our calculations we always assumed that we at least approximately have spin-charge separation. From a computational point of view this is not a necessary assumption and one could calculate renormalization group equations even without this assumption. In particular this would mean that one can include inversion asymmetric interactions and differences in Fermi velocities analytically. Another more

technical point that presents itself for further studies is how to obtain information about the topological phase from renormalization group equations. A general approach, which we used as well, consists of studying an unstable fixed point and investigate it with respect to which perturbation it is most unstable. This is usually done with perturbative renormalization group techniques and involves some ambiguity with respect to the validity of this perturbative regime. It would be desirable to find less ambiguous methods. One possibility could be to study boundary conformal field theories describing the gapless edge excitations of the topological phases.

In chapter 5 we studied one of the most common ways to probe Majorana bound states by means of a conductance measurement. Based on existing theories we studied how the zero-bias conductance of such measurements is affected by the electric environment. We derived low-energy effective theories for coupling a general electric environment to the system. This is of practical interest because the electric properties of a system, namely its impedance, can easily be measured experimentally. In the low-frequency regime the impedance can be approximated by a real resistance. This way one obtains the well known result of a qualitative crossover in the zero-bias conductance as a function of the environment resistance. Motivated by this crossover we studied two particular systems. One where a quantum point contact is used to tune the system through the crossover, another where two Majorana bound states are coupled to a metallic quantum dot. The latter system is right in the crossover regime and we studied its conductance in the weak and strong coupling regime. We found a strong gate voltage dependence which reflects that the system is indeed at a crossover point. Building on the work which we presented here in this thesis it would be interesting to have conductance calculations for general electric environments. Those are analytically challenging beyond the constant impedance approximation. It might therefore be helpful to perform numerical calculations of the conductance in the case of a general electric environment. Another apparent generalization of the results in this thesis would be a similar analysis for systems in class DIII.

In conclusion, in this thesis we have studied several aspects relevant for one-dimensional topological superconductors. These aspects were related to obtaining a one-dimensional topological phase in class DIII and manipulating the Kramers pairs of Majorana bound states which it hosts. Furthermore we studied aspects of probing Majorana bound states in a topological phase in class D.

## Bibliography

- [1] J. Alicea, Y. Oreg, G. Refael, F. von Oppen, and M. P. A. Fisher. Non-Abelian statistics and topological quantum information processing in 1d wire networks. *Nature Physics*, 7(5):412–417, May 2011.
- [2] A. Altland and R. Egger. Multiterminal coulomb-majorana junction. *Physical Review Letters*, 110:196401, May 2013.
- [3] A. Altland and M. R. Zirnbauer. Nonstandard symmetry classes in mesoscopic normal-superconducting hybrid structures. *Physical Review B*, 55(2):1142–1161, January 1997.
- [4] C. W. J. Beenakker. Quantum transport in semiconductor-superconductor micro-junctions. *Physical Review B*, 46(19):12841–12844, November 1992.
- [5] C. W. J. Beenakker. Search for Majorana Fermions in Superconductors. *Annual Review of Condensed Matter Physics*, 4(1):113–136, 2013.
- [6] B. Béri and N. R. Cooper. Topological kondo effect with majorana fermions. *Physical Review Letters*, 109:156803, Oct 2012.
- [7] B. A. Bernevig and T. L. Hughes. *Topological Insulators and Topological Superconductors*. Princeton University Press, 2013.
- [8] M. V. Berry. Quantal Phase Factors Accompanying Adiabatic Changes. *Proceedings of the Royal Society of London A: Mathematical, Physical and Engineering Sciences*, 392(1802):45–57, March 1984.
- [9] M. Born and V. Fock. Beweis des Adiabatenatzes. *Zeitschrift fur Physik*, 51:165–180, March 1928.
- [10] J. Cardy. *Scaling and Renormalization in Statistical Physics*. Cambridge University Press, Cambridge; New York, edition: new. edition, April 1996.
- [11] J. Danon and K. Flensberg. Interaction effects on proximity-induced superconductivity in semiconducting nanowires. *Physical Review B*, 91(16):165425, April 2015.
- [12] S. Datta. *Electronic Transport in Mesoscopic Systems*. Cambridge University Press, May 1997.

- [13] L. Fidkowski, J. Alicea, N. Lindner, R. M. Lutchyn, and M. P. A. Fisher. Universal transport signatures of Majorana fermions in superconductor-Luttinger liquid junctions. *Physical Review B*, 85(24):245121, June 2012.
- [14] K. Flensberg. Capacitance and conductance of mesoscopic systems connected by quantum point contacts. *Physical Review B*, 48(15):11156–11166, October 1993.
- [15] K. Flensberg. Tunneling characteristics of a chain of Majorana bound states. *Physical Review B*, 82(18):180516, November 2010.
- [16] E. Fradkin. *Field Theories of Condensed Matter Physics*. Cambridge University Press, February 2013.
- [17] P. Di Francesco, P. Mathieu, and D. Sénéchal. *Conformal Field Theory*. Springer, New York, edition: 1st ed. 1997. corr. 2nd printing 1999 edition, 1999.
- [18] M. H. Freedman, A. Kitaev, M. J. Larsen, and Z. Wang. Topological Quantum Computation. *arXiv:quant-ph/0101025*, January 2001.
- [19] L. Fu. Electron Teleportation via Majorana Bound States in a Mesoscopic Superconductor. *Physical Review Letters*, 104(5):056402, February 2010.
- [20] Erikas Gaidamauskas, Jens Paaske, and Karsten Flensberg. Majorana Bound States in Two-Channel Time-Reversal-Symmetric Nanowire Systems. *Physical Review Letters*, 112(12):126402, March 2014.
- [21] T. Giamarchi. *Quantum Physics in One Dimension*. Clarendon Press, December 2003.
- [22] S. M. Girvin, L. I. Glazman, M. Jonson, D. R. Penn, and M. D. Stiles. Quantum fluctuations and the single-junction Coulomb blockade. *Physical Review Letters*, 64(26):3183–3186, June 1990.
- [23] H. Grabert and M. H. Devoret. *Single Charge Tunneling: Coulomb Blockade Phenomena In Nanostructures*. Springer Science & Business Media, November 2013.
- [24] A. Haim, A. Keselman, E. Berg, and Y. Oreg. Time-reversal-invariant topological superconductivity induced by repulsive interactions in quantum wires. *Physical Review B*, 89(22):220504, June 2014.
- [25] B. I. Halperin, Y. Oreg, A. Stern, G. Refael, J. Alicea, and F. von Oppen. Adiabatic manipulations of Majorana fermions in a three-dimensional network of quantum wires. *arXiv:1112.5333 [cond-mat]*, December 2011.
- [26] G. Huang, M. Leijnse, K. Flensberg, and H. Q. Xu. Tunnel spectroscopy of Majorana bound states in topological superconductor/quantum dot Josephson junctions. *Physical Review B*, 90(21):214507, December 2014.

- 
- [27] T. Hyart, B. van Heck, I. C. Fulga, M. Burrello, A. R. Akhmerov, and C. W. J. Beenakker. Flux-controlled quantum computation with Majorana fermions. *Physical Review B*, 88(3):035121, July 2013.
- [28] R. Hütten, A. Zazunov, B. Braunecker, A. Levy Yeyati, and R. Egger. Majorana Single-Charge Transistor. *Physical Review Letters*, 109(16):166403, October 2012.
- [29] D. A. Ivanov. Non-Abelian Statistics of Half-Quantum Vortices in  $p$ -Wave Superconductors. *Physical Review Letters*, 86(2):268–271, January 2001.
- [30] C. L. Kane and M. P. A. Fisher. Transport in a one-channel Luttinger liquid. *Physical Review Letters*, 68(8):11156, February 1992.
- [31] T. Kato. On the Adiabatic Theorem of Quantum Mechanics. *Journal of the Physical Society of Japan*, 5:435, November 1950.
- [32] A. Keselman and E. Berg. Gapless symmetry-protected topological phase of fermions in one dimension. *Physical Review B*, 91(23):235309, June 2015.
- [33] A. Keselman, L. Fu, A. Stern, and E. Berg. Inducing Time-Reversal-Invariant Topological Superconductivity and Fermion Parity Pumping in Quantum Wires. *Physical Review Letters*, 111(11):116402, September 2013.
- [34] A. Kitaev. Unpaired Majorana fermions in quantum wires. *cond-mat/0010440*, October 2000.
- [35] A. Kitaev. Fault-tolerant quantum computation by anyons. *Annals of Physics*, 303(1):2–30, January 2003.
- [36] A. Kitaev. Periodic table for topological insulators and superconductors. *arXiv:0901.2686 [cond-mat, physics:hep-th, physics:math-ph]*, pages 22–30, 2009.
- [37] J. M. Kosterlitz and D. J. Thouless. Ordering, metastability and phase transitions in two-dimensional systems. *Journal of Physics C: Solid State Physics*, 6(7):1181, April 1973.
- [38] Dong E. L. Proposed Method for Tunneling Spectroscopy with Ohmic Dissipation Using Resistive Electrodes: A Possible Majorana Filter. *Physical Review Letters*, 111(20):207003, November 2013.
- [39] C. J. Lambert. Generalized Landauer formulae for quasi-particle transport in disordered superconductors. *Journal of Physics: Condensed Matter*, 3(34):6579, August 1991.
- [40] V. Mourik, K. Zuo, S. M. Frolov, S. R. Plissard, E. P. a. M. Bakkers, and L. P. Kouwenhoven. Signatures of Majorana Fermions in Hybrid Superconductor-Semiconductor Nanowire Devices. *Science*, 336(6084):1003–1007, May 2012.

- [41] Stevan Nadj-Perge, Ilya K. Drozdov, Jian Li, Hua Chen, Sangjun Jeon, Jungpil Seo, Allan H. MacDonald, B. Andrei Bernevig, and Ali Yazdani. Observation of Majorana fermions in ferromagnetic atomic chains on a superconductor. *Science*, 346(6209):602–607, October 2014.
- [42] C. Nayak, S. H. Simon, A. Stern, M. Freedman, and S. Das Sarma. Non-Abelian anyons and topological quantum computation. *Reviews of Modern Physics*, 80(3):1083–1159, September 2008.
- [43] J. D. Sau, D. J. Clarke, and S. Tewari. Controlling non-Abelian statistics of Majorana fermions in semiconductor nanowires. *Physical Review B*, 84(9):094505, September 2011.
- [44] A. P. Schnyder, S. Ryu, A. Furusaki, and A. W. W. Ludwig. Classification of topological insulators and superconductors in three spatial dimensions. *Physical Review B*, 78(19):195125, November 2008.
- [45] R. Slager, A. Mesaros, V. Juričić, and J. Zaanen. The space group classification of topological band-insulators. *Nature Physics*, 9(2):98–102, February 2013.
- [46] D. Sénéchal. An introduction to bosonization. *arXiv:cond-mat/9908262*, August 1999.
- [47] Y. Takane and H. Ebisawa. Conductance Formula for Mesoscopic Systems with a Superconducting Segment. *Journal of the Physical Society of Japan*, 61(5):1685–1690, May 1992.
- [48] D. J. Thouless, M. Kohmoto, M. P. Nightingale, and M. den Nijs. Quantized Hall Conductance in a Two-Dimensional Periodic Potential. *Physical Review Letters*, 49(6):405–408, August 1982.
- [49] X. Wen. Topological order: from long-range entangled quantum matter to an unification of light and electrons. *ISRN Condensed Matter Physics*, 2013:198710, 2013.
- [50] F. Wilczek and A. Zee. Appearance of Gauge Structure in Simple Dynamical Systems. *Physical Review Letters*, 52(24):2111–2114, June 1984.
- [51] F. Zhang, C. L. Kane, and E. J. Mele. Time-Reversal-Invariant Topological Superconductivity and Majorana Kramers Pairs. *Physical Review Letters*, 111(5):056402, August 2013.